MATERIALS AND BIOLOGICAL APPROACH TO GENE DELIVERY IN HUMAN EMBRYONIC STEM CELLS

BY

JONATHAN S Y YEN

DISSERTATION

Submitted in partial fulfillment of the requirements
for the degree of Doctor of Philosophy in Bioengineering
in the Graduate College of the
University of Illinois at Urbana-Champaign, 2015

Urbana, Illinois

Doctoral Committee:

Associate Professor Jianjun Cheng, Chair
Professor Ning Wang
Assistant Professor Kristopher Kilian
Assistant Professor Jian Ma
Assistant Professor Gregory Underhill

Abstract

Gene delivery is an important tool used in the study and manipulation of human pluripotent stem cells for regenerative medicine purposes. However current methods of transient gene delivery are still highly inefficient. Using materials and biologically based concepts, I aim to develop new methods and protocols to enhance the efficiency of gene delivery. For the materials aspect, diblock copolymers consisting of poly(ethylene glycol)-*block*-poly(γ-4-(((2-(piperidin-1-yl)ethyl)amino)methyl)benzyl-L-glutamate) (PEG-*b*-PVBLG-8) were synthesized and evaluated for their ability to mediate gene delivery in hard-to-transfect cells, such as IMR-90 human fetal lung fibroblasts and human embryonic stem cells (hESCs). The PEG-*b*-PVBLG-8 contained a membrane-disruptive, cationic, helical polypeptide block (PVBLG-8) for complexing with DNA and a hydrophilic PEG block to improve the biocompatibility of the gene delivery vehicle. PEG-*b*-PVBLG-8 diblock polymers with a high degree of polymerization have a greater transfection efficiency and lower toxicity in IMR-90 cells than the commercial reagent Lipofectamine 2000. The usefulness of PEG-*b*-PVBLG-8 was further demonstrated via the successful transfection of hESCs without a measured loss in cell pluripotency markers. This system proved to be inefficient for hESCs, thus I designed a system that uses the combination of a cell specific and materials approach. Plasmid DNA was condensed with PVBLG-8 to form nanocomplexes, which were further coated with hyaluronic acid. PVBLG-8 has proven to be an effective gene delivery material in certain cell lines, due to its membrane disruptive properties. Yet in more sensitive cell lines, like hESCs, it proves to be toxic and

thus ineffective. Hyaluronic acid not only shields the positive charges from the helical peptides, but also acts as a targeting moiety for cell surface receptor CD44, which binds and facilitates the internalization of hyaluronan for degradation. Despite the negative charged surface, the gene transfection of the cells increased by 1.5 fold with reduced toxicity. I demonstrated that the increased transfection efficiency is due to the CD44 mediated targeting delivery of DNA by HA coating nanocomplex. In addition, this nanocomplex system can be further activated through the endosomal specific degradation of HA by hyaluronidase to expose PVBLG-8. From the biological aspect, a small molecule that selectively inhibits the Rho-associated kinase inhibitor (Y-27632) was discovered to transiently alter the hESC morphology to induce spreading and reduced membrane tension. These morphological changes allowed the increase of plasmid transfection, siRNA transfection and nanoparticle uptake to increase substantially. Cells were also able to recover after treatment back to normal pluripotent stem cell morphology and express important pluripotency markers. These new methods expands the field of gene delivery in human pluripotent stem cells, which can be further applied to other biomedical applications.

For my family, who have always been there for me.

ACKNOWLEDGEMENTS

I would like to thank my advisor, Professor Jianjun Cheng for giving me the opportunity to complete my PhD training in his lab and for all the guidance and support. Thank you for your patience, as I was able to explore a whole new field. I am inspired by the high standards that you set for yourself and of those around you, your attention to detail, and dedication and commitment to science. Thank you for always encouraging me to be better and not give up.

I would also like to thank the other members of my thesis committee, Dr. Kris Kilian, Dr. Jian Ma, Dr. Gregory Underhill, and Dr. Ning Wang for contributing their valuable experience, intelligence, and time.

I would like to thank former and current Cheng lab members for all their support, intellectual discussions, and great memories. Special thanks to Dr. Li Tang, Dr. Fei Wang, Dr. Yanfeng Zhang, Dr. Menghua Xiong and Dr, Lichen Yin for your mentorship, friendship, and advice. I would also like to thank, Hanze Ying, for reading through my dissertation, Qian Yin, Ryan Baumgartner, and Ziyuan Song for your friendship, great discussions, support, and great memories. I would also like to thank Linna Guan, who worked closely with me during her undergraduate studies, for her hard work and friendship.

I would like to acknowledge my training grant under the National Science Foundation Integrative Graduate Education and Research Traineeship in Cellular and Molecular Mechanics and BioNanotechnology (Grant: 0965918). Special thanks to Laura Miller for all your help during the program.

I would also like to thank Professor Prashant Mali and Sarah Dowey for their inspiration in the stem cell field, their friendship, advice, and support whenever I need it. Finally, I would like to give special thanks to my parents, who have always fostered my interest in the sciences, and my sister for being there for me and supporting me in everything I have done. Baruch Hashem for giving me the opportunity to pursue my love for science, medicine, and stem cells.

Table of Contents

CHAPTER 1

Introduction and Background

Human embryonic stem cells (hESCs) hold tremendous potential in the field of regeneration due in particular to two characteristics: pluripotency and self-renewal. The former allows these cells to differentiate into either the endoderm, mesoderm or ectoderm lineages and therefore can transform into virtually any of the cells found in the human body. The latter allows the cells to proliferate almost endlessly. This is unlike many of the other cells in the human body, which are limited in their growth and expansion. This has been a major hindrance in regenerative medicine thus far. In order for research in the lab to be an applicable technique for biomedical purposes, it is necessary to obtain enough of a certain type of cell in order to encapsulate it into three-dimensional scaffold for tissue engineering uses. This second main property of embryonic stem cells solves this issue of the source of the cells and allows one to grow a large quantity of the cells. The ability of human pluripotent stem cells to differentiate into virtually any cell in the body is a double edged- sword, where although it holds much promise, the control of the differentiation is a major hurdle to be solved. Once accurate control is held over pluripotency as well as growth, tissue engineering could hold much promise.

Despite the tremendous potential in the application of tissue engineering, there are still many caveats and ethical issues in the use of embryonic stem cells. Embryonic stem

cells are derived from embryos discarded during in-vitro fertilization. Upon entry into the blastocyst, the invasive procedure destroys the embryo and thus leads to the biggest ethical issue pertaining to human embryonic stem cells; many people believe that the destruction of an embryo is considered murder. Another problem that one faces with human embryonic stem cells is its direct clinical application, although not of ethical nature. Since these cells were not derived from the patient himself, the actual transplantation of the cell as well as its differentiated lineages could lead to many immunological complications. For example, due to an immunological incompatibility, the patient could contract what is known as graft-versus-host disease, (GVHD), where the implanted cells are rejected and fail to be grafted in the body.

There are various roads to pluripotency, the most obvious is when the sperm is reprogrammed by the egg upon normal fertilization resulting in a totipotent cell that gives rise to the entire embryo proper and to the extra-embryonic tissues. This is the process that nature takes and is associated with near perfect efficiency of reprogramming. For somatic cells however, this uphill ascent has classically been achieved by one of two means. For Instance, one can introduce nuclei of somatic cells into oocytes. In this process, typically only 5% of cloned embryos develop to term. Nevertheless one can get surviving off-spring, as in the remarkable case of Dolly the sheep. Alternatively, one can do a simple cell fusion of somatic cells to ES cells, but the resultant cells, although multipotent by various criterion, have tetraploid nuclei. In both scenarios, the oocytes/ES cells provide undefined

trans-acting factors that actively remodel the somatic genome back to a pluripotent state. While the former process is saddled by serious ethical and technical concerns, the latter process of cell fusion results in the formation of tetraploid cells, which have limited clinical potential. What would be ideal is an *in vitro* reprogramming approach where simple expression of few factors could directly convert somatic cells into pluripotent stem cells. Until recently this had been merely fantasy. Now, the two main problems in using embryonic stem cells can also be easily overcome with in-vitro reprogrammed induced pluripotent stem cells. These cells have been found to look and behave like human embryonic stem cells in all forms.

Viral Gene Delivery

Both viral and non-viral gene delivery have been explored extensively for basic research as well as therapeutic applications. In the pursuit of regenerative medicine, gene delivery is an important tool to manipulate and control cell fate. One of the newest applications of gene delivery is the reprogramming of terminally differentiated cells into induced pluripotent stem cells (iPSCs) or, more recently, induced neurons, blood progenitors and cardiomyocytes [3-5]. In the pioneering work of Yu et al., a recombinant lentivirus carrying the genes for *OCT4*, *SOX2*, *NANOG* and *LIN28* was used to reprogram IMR-90 fetal lung fibroblasts into iPSCs [6]. While the resulting iPSCs were characteristically and functionally pluripotent, they nonetheless retained remnants of viral DNA as a result of lentiviral integration. This could have serious implications if tissue

derived from such iPSCs was used therapeutically. Non-viral approaches to achieve safe, virus-free reprogramming of IMR-90 cells using synthetic polymers and lipids have been fruitless as existing gene delivery materials have proven to be inefficient at mediating effective gene delivery in these cells.

The genetic manipulation of hESCs is also an important tool in regenerative medicine. The control and overexpression of specific genes afforded by gene delivery is valuable not only in efforts to control stem cell fate, but also to study cell behavior in differentiation and gene targeting studies [7]. Lentiviral transduction has been established as an effective method for gene delivery to hESCs because of their consistently high transfection efficiency and capability to maintain stable transgene expression[8].

Viral gene delivery is typically more efficient than its non-viral counterpart but poses increased risks of immunogenicity, insertional mutagenesis, and viral integration into the host genome [9]. While the integration event results in permanent transgene expression—which may not be desirable for all applications—it also provides a route for the prolonged expression of undesired viral components in host cells. As non-viral gene delivery relies on synthetic polymers or lipids and DNA that are explicitly free from viral components, it is generally considered a safer alternative than viral gene therapy. Therefore, there is a push to develop non-viral gene delivery materials to match the efficiency of viral vectors [10-19].

Non-Viral Gene Delivery

Non-viral gene delivery, often characterized by its desired biocompatibility and minimal immunogenicity, provides an ideal alternative to viral gene delivery [10-13,16-24]. Nevertheless, non-viral systems applied to human embryonic stem cell colonies are hindered by low transfection efficiency, which limits their applications [22,24-26]. There have been several materials developed for non-viral gene delivery into a variety of cells, such as poly-beta amino esters [25] and cationic helical peptides, like PVBLG-8 [27,28], but very few are effective in hESCs. But, there are many issues that plague non-viral gene delivery in hESCs, such as low efficiency and high cytotoxicity. Due to the physiology of hESCs, non-viral gene delivery nanoparticles have low uptake efficiency. After the nanoparticles are taken up, the DNA/plasmid needs to reach the nucleus for transcription, but can be trapped in the endosomes and thus tagged for degradation. Active targeting of various cell surface receptors has been found to be quite effective for nanoparticle uptake, due to receptor mediated endocytosis. After the nanoparticles are endocytosed, they need to quickly escape the endosome and release their DNA cargo. Therefore, it will be very practical to develop a smart delivery system with active targeting motif coated on the complex, which can enhance the uptake of the gene delivery vehicles and shield the cationic polymers to reduce cytotoxicity, and also can quickly escape from the endosome after rapid deshelling of the charge shielding moiety in the endosome.

Polypeptides were among the first set of materials examined as non-viral gene delivery agents [29-31]. Given the simplicity in synthesis and formulation with anionic DNA, cationic poly($_L$-Lysine) (PLL) was one of the most intensively studied gene delivery polypeptides. However, as a DNA delivery vector, unmodified PLL suffered from low transfection efficiency. Even following modification with functional moieties like saccharide [32,33], imidazole [34], and guanidinium groups [35], PLL has proven to be a largely ineffective gene delivery vector. Nonetheless, there have been numerous attempts to create novel gene delivery vehicles with modified polypeptides, like poly(glycoamidoamine)s [36] and HPMA-oligolysines [37].

Many biologically active peptides share facially amphipathic helical domains as a common structural motif [38,39]. Peptides that possess this structure are often able to interact with and destabilize the lipid bilayers of cell membranes. In terms of gene delivery, cell membrane destabilization can facilitate cell internalization and escape from endocytic vesicles [40,41]. PLL and modified PLL, however, adopt random coil structures because strong intramolecular side-chain charge repulsion prohibits α-helix formation. As such, PLL functions as a conventional polyelectrolyte in gene delivery studies and exhibits limited membrane activity.

Cell Morphology

Low transfection efficiency can be largely attributed to the distinct physiology of hESCs. hESCs are mildly intrinsically stiff in structure due to the fact that they grow in tight colonies and in rounded up shapes [42]. Because of such tight two-dimensional colonies, cells in the center are often compressed by the surrounding cells [43] and exposure of centered cells to exogenous materials is greatly limited, which prevents effective internalization of gene delivery materials and thus leads to low transfection efficiency. Such cases have been widely noted in previous gene delivery studies by [24] and [44-46], which demonstrates that the outer edge of the hESCs have notably higher uptake efficiency. These physical properties of the hESC colony growth pose a large limitation in gene delivery that may not be able to be solved through the material design of the delivery vector. To this end, I am seeking alternative strategies to increase the gene delivery efficiency by manipulating the cellular state and physiology of hESCs.

It has been discovered that pluripotent stem cells have two main states, naïve and primed states [1]. Mouse embryonic stem cells (mESC) derived from the inner cell mass of developing blastocysts are capable of indefinite maintenance in the pluripotent state. These mESCs are termed naïve cells, in which they are capable of chimeric embryo contribution. There is another type of pluripotent cell lineage that is derived from postimplantation epiblast of mouse embryos termed epiblast stem cells (mEpiSCs), which are distinct molecularly and epigenetically from mESCs. These mEpiSCs are incapable of chimeric contribution, but able to generate teratomas, demonstrating their pluripotent

potential, thus termed primed cells. Naïve cells and primed cells demonstrate tremendous difference in their growth condition and morphology. Naïve mESCs depend on LIF/Stat3 signaling and grow in a packed dome colony, while primed mEpiSCs depend on bFGF and TGFb/Activin signaling and grow in a flattened 2D morphology. In addition, it has been found that in contrast to naïve mESCs, primed EpiSCs are intolerant to single cell passaging. Gene delivery into naïve ESCs have been found to be highly efficient in contrast to the primed EpiSCs. It is possible for the primed mEpiSCs to revert back to the naïve mESC state with specific overexpression and growth factor treatments. It has been shown that human pluripotent stem cells, both hESCs and hiPSCs behave identically to the primed mEpiSCs. In a recent report, it was demonstrated that naïve human embryonic stem cells could be rewired to behave like mESCs through gene over expression and controlled growth factors. In addition, they were able to produce naïve human induced pluripotent stem cells [2]. There have been supplemental studies to further efficiently convert the primed hESCs to naïve hESCs for more effective therapeutic applications due to their robustness and ease of manipulation. Currently, the process is complex and inefficient.

Scope and Organization

The aim of my PhD research is to develop a new and more effective gene delivery system for hESCs through both a materials approach and a more biologically cell based approach to control cell fate. In the following four chapters, I will describe unique methods developed to overcome obstacles of non-viral gene delivery systems based on the cationic

helical peptide, PVBLG-8, and the small molecule Y-27632. The organization of my thesis is briefly described below. Chapter 2 describes the chemical modification of PVBLG-8 with PEG to reduce cytotoxicity from the charges. By establishing that reduced charges can reduce cytotoxicity, and still have some gene transfection efficiency, Chapter 3 discusses other non-chemical modifications of the PVBLG-8 system to retain the low cytotoxicity while increasing the transfection efficiency. Acknowledging the importance of the physiological state of hESC colonies, Chapter 4 explores coupling a biological approach to increasing transfection efficiency, through the transient alteration of the cells with Y-27632.

1.1 References:

[1] Nichols J, Smith A. Naive and primed pluripotent states. Cell Stem Cell 2009;4(6):487-92.

[2] Hanna J, Cheng AW, Saha K, Kim J, Lengner CJ, Soldner F, et al. Human embryonic stem cells with biological and epigenetic characteristics similar to those of mouse ESCs. Proceedings of the National Academy of Sciences 2010;107(20):9222-27.

[3] Pfisterer U, Kirkeby A, Torper O, Wood J, Nelander J, Dufour A, et al. Direct conversion of human fibroblasts to dopaminergic neurons. Proceedings of the National Academy of Sciences 2011;108(25):10343.

[4] Ambasudhan R, Talantova M, Coleman R, Yuan X, Zhu S, Lipton SA, et al. Direct reprogramming of adult human fibroblasts to functional neurons under defined conditions. Cell Stem Cell 2011.

[5] Szabo E, Rampalli S, Risueño RM, Schnerch A, Mitchell R, Fiebig-Comyn A, et al. Direct conversion of human fibroblasts to multilineage blood progenitors. Nature 2010;468(7323):521-26.

[6] Yu J, Vodyanik MA, Smuga-Otto K, Antosiewicz-Bourget J, Frane JL, Tian S, et al. Induced pluripotent stem cell lines derived from human somatic cells. Science 2007;318(5858):1917.

[7] Zou J, Maeder ML, Mali P, Pruett-Miller SM, Thibodeau-Beganny S, Chou BK, et al. Gene targeting of a disease-related gene in human induced pluripotent stem and embryonic stem cells. Cell Stem Cell 2009;5(1):97-110.

[8] Ye Z, Yu X, Cheng L. Lentiviral gene transduction of mouse and human stem cells. Methods in Molecular Biology 2008;430:243-53.

[9] Dave UP, Jenkins NA, Copeland NG. Gene therapy insertional mutagenesis insights. Science 2004;303(5656):333.

[10] Leong KW, Mao HQ, Truong-Le VL, Roy K, Walsh SM, August JT. DNA-polycation nanospheres as non-viral gene delivery vehicles. J Controlled Release 1998;53(1-3):183-93.

[11] Kizjakina K, Bryson JM, Grandinetti G, Reineke TM. Cationic glycopolymers for the delivery of pDNA to human dermal fibroblasts and rat mesenchymal stem cells. Biomaterials 2012;33(6):1851-62.

[12] McLendon PM, Fichter KM, Reineke TM. Poly(glycoamidoamine) Vehicles Promote pDNA Uptake through Multiple Routes and Efficient Gene Expression via Caveolae-Mediated Endocytosis. Mol Pharm 2010;7(3):738-50.

[13] Srinivasachari S, Reineke TM. Versatile supramolecular pDNA vehicles via "click polymerization" of beta-cyclodextrin with oligoethyleneamines. Biomaterials 2009;30(5):928-38.

[14] Bak XY, Lam DH, Yang J, Ye K, Wei EL, Lim SK, et al. Human embryonic stem cell-derived mesenchymal stem cells as cellular delivery vehicles for prodrug gene therapy of glioblastoma. Hum Gene Ther 2011;22(11):1365-77.

[15] Yang F, Green JJ, Dinio T, Keung L, Cho SW, Park H, et al. Gene delivery to human adult and embryonic cell-derived stem cells using biodegradable nanoparticulate polymeric vectors. Gene Ther 2009;16(4):533-46.

[16] Shim MS, Kwon YJ. Controlled delivery of plasmid DNA and siRNA to intracellular targets using ketalized polyethylenimine. Biomacromolecules 2008;9(2):444-55.

[17] Shim MS, Kwon YJ. Acid-transforming polypeptide micelles for targeted nonviral gene delivery. Biomaterials 2010;31(12):3404-13.

[18] Shim MS, Kwon YJ. Dual mode polyspermine with tunable degradability for plasmid DNA and siRNA delivery. Biomaterials 2011;32(16):4009-20.

[19] Jiang XA, Zheng YR, Chen HH, Leong KW, Wang TH, Mao HQ. Dual-Sensitive Micellar Nanoparticles Regulate DNA Unpacking and Enhance Gene-Delivery Efficiency. Adv Mater 2010;22(23):2556-60.

[20] Yin LC, Song ZY, Kim KH, Zheng N, Tang HY, Lu H, et al. Reconfiguring the architectures of cationic helical polypeptides to control non-viral gene delivery. Biomaterials 2013;34(9):2340-49.

[21] Yang F, Cho SW, Son SM, Bogatyrev SR, Singh D, Green JJ, et al. Genetic engineering of human stem cells for enhanced angiogenesis using biodegradable polymeric nanoparticles. Proc Natl Acad Sci USA 2010;107(8):3317-22.

[22] Yang F, Green JJ, Dinio T, Keung L, Cho SW, Park H, et al. Gene delivery to human adult and embryonic cell-derived stem cells using biodegradable nanoparticulate polymeric vectors. Gene Ther 2009;16(4):533-46.

[23] Gabrielson NP, Lu H, Yin LC, Li D, Wang F, Cheng JJ. Reactive and Bioactive Cationic a-Helical Polypeptide Template for Nonviral Gene Delivery. Angew Chem Int Ed 2012;51(5):1143-47.

[24] Yen J, Zhang YF, Gabrielson NP, Yin LC, Guan LN, Chaudhury I, et al. Cationic, helical polypeptide-based gene delivery for IMR-90 fibroblasts and human embryonic stem cells. Biomaterials Science 2013;1(7):719-27.

[25] Green JJ, Zhou BY, Mitalipova MM, Beard C, Langer R, Jaenisch R, et al. Nanoparticles for Gene Transfer to Human Embryonic Stem Cell Colonies. Nano Lett 2008;8(10):3126-30.

[26] Kobayashi N, Rivas-Carrillo JD, Soto-Gutierrez A, Fukazawa T, Chen Y, Navarro-Alvarez N, et al. Gene delivery to embryonic stem cells. Birth Defects Res C Embryo Today Rev 2005;75(1):10-8.

[27] Yen J, Zhang Y, Gabrielson NP, Yin L, Guan L, Chaudhury I, et al. Cationic, helical polypeptide-based gene delivery for IMR-90 fibroblasts and human embryonic stem cells. Biomaterials Science 2013.

[28] Gabrielson NP, Lu H, Yin LC, Li D, Wang F, Cheng JJ. Reactive and Bioactive Cationic a-Helical Polypeptide Template for Nonviral Gene Delivery. Angewandte Chemie-International Edition 2012;51(5):1143-47.

[29] Monsigny M, Roche AC, Midoux P, Mayer R. Glycoconjugates as carriers for specific delivery of therapeutic drugs and genes. Adv Drug Del Rev 1994;14(1):1-24.

[30] Wagner E, Curiel D, Cotten M. Delivery of Drugs, Proteins and Genes into Cells Using Transferrin as a Ligand for Receptor-Mediated Endocytosis. Advanced Drug Delivery Reviews 1994;14(1):113-35.

[31] Cho SK, Kwon YJ. Polyamine/DNA polyplexes with acid-degradable polymeric shell as structurally and functionally virus-mimicking nonviral vectors. Journal of Controlled Release 2011;150(3):287-97.

[32] Ferkol T, Perales JC, Mularo F, Hanson RW. Receptor-mediated gene transfer into macrophages. Proceedings of the National Academy of Sciences 1996;93(1):101-05.

[33] Erbacher P, Bousser MT, Raimond J, Monsigny M, Midoux P, Roche AC. Gene transfer by DNA/glycosylated polylysine complexes into human blood monocyte-derived macrophages. Human Gene Therapy 1996;7(6):721-29.

[34] Putnam D, Gentry CA, Pack DW, Langer R. Polymer-based gene delivery with low cytotoxicity by a unique balance of side-chain termini. Proceedings of the National Academy of Sciences 2001;98(3):1200=05.

[35] Okuda T, Sugiyama A, Niidome T, Aoyagi H. Characters of dendritic poly (-lysine) analogues with the terminal lysines replaced with arginines and histidines as gene carriers in vitro. Biomaterials 2004;25(3):537-44.

[36] Ingle NP, Malone B, Reineke TM. Poly (glycoamidoamine) s: a broad class of carbohydrate-containing polycations for nucleic acid delivery. Trends in Biotechnology 2011:443-53.

[37] Johnson RN, Chu DSH, Shi J, Schellinger JG, Carlson PM, Pun SH. HPMA-oligolysine copolymers for gene delivery: Optimization of peptide length and polymer molecular weight. Journal of Controlled Release 2011:303-11.

[38] Robertson DE, Farid RS, Moser CC, Urbauer JL, Mulholland SE, Pidikiti R, et al. Design and synthesis of multi-haem proteins. Nature 1994(368):425-32.

[39] Muñoz V, Serrano L. Elucidating the folding problem of helical peptides using empirical parameters. Nature Structural & Molecular Biology 1994;1(6):399-409.

[40] Stewart KM, Horton KL, Kelley SO. Cell-penetrating peptides as delivery vehicles for biology and medicine. Organic & biomolecular chemistry 2008;6(13):2242-55.

[41] Deshayes S, Morris M, Divita G, Heitz F. Cell-penetrating peptides: tools for intracellular delivery of therapeutics. Cellular and Molecular Life Sciences 2005;62(16):1839-49.

[42] Thomson JA, Itskovitz-Eldor J, Shapiro SS, Waknitz MA, Swiergiel JJ, Marshall VS, et al. Embryonic stem cell lines derived from human blastocysts. Science 1998;282(5391):1145-7.

[43] Hammerick KE, Huang ZB, Sun N, Lam MT, Prinz FB, Wu JC, et al. Elastic Properties of Induced Pluripotent Stem Cells. Tissue Engineering Part A 2011;17(3-4):495-502.

[44] Xiong C, Tang DQ, Xie CQ, Zhang L, Xu KF, Thompson WE, et al. Genetic engineering of human embryonic stem cells with lentiviral vectors. Stem Cells Dev 2005;14(4):367-77.

[45] Xia X, Zhang Y, Zieth CR, Zhang SC. Transgenes delivered by lentiviral vector are suppressed in human embryonic stem cells in a promoter-dependent manner. Stem Cells Dev 2007;16(1):167-76.

[46] Xia X, Zhang SC. Genetic modification of human embryonic stem cells. Biotechnol Genet Eng Rev 2007;24:297-309.

Chapter 2

Development of biocompatible, cationic, helical polypeptide for non-viral gene delivery to stem cells

Significant portions of this chapter were published as "Cationic, helical polypeptide-based gene delivery for IMR-90 fibroblasts and human embryonic stem cell" Jonathan Yen, Yanfeng Zhang, Nathan Grabrielson, Lichen Yin, Linna Guan, Isthier Chaudhury, Hua Lu, Fei Wang, and Jianjun Cheng, *Biomaterials Science*, **2013**, 1, 719 - 727.

2.1 Introduction

Viral transfections have proven to be quite effective in gene transfection, but none of the traditional polymeric gene delivery methods have proven quite as effective in hESCs. Therefore a new class of gene transfection material is required for hESCs. Recently, we reported a new cationic polypeptide possessing a pH-, ionic- and temperature-stable cationic helical structure [1]. Traditionally, charged polypeptides adopt random coil orientations because strong intramolecular side-chain charge repulsion prohibits α-helix formation. In our reported polypeptide, termed PVBLG$_n$-8 where n is the degree of polymerization, the helical structure is stabilized by increasing the distance between the charged side chain groups and the polypeptide backbone. This has the net effect of both minimizing the effect of charge repulsion while simultaneously stabilizing the helix through hydrophobic interaction between the pendent side chain groups.

Our prior characterization of PVBLG$_n$-8 peptides as non-viral gene delivery materials revealed that the helical structure facilitates strong, disruptive interactions with cell membranes which aid the endosomal escape of the endocytosed complexes of polypeptide and DNA [2]. Although gene delivery with PVBLG$_n$-8 proved to be effective in COS-7 and HEK 293 cells with comparable performance to the commercial transfection agent Lipofectamine 2000 [2], it was largely ineffective in IMR-90 fibroblasts and hESCs due to its substantial toxicity in these cells. However, I believe that the cationic helicity of PVBLG-8 is an important characteristic that can increase transfection efficiency into hard to transfect cells, though it is also responsible for the cytotoxicity in the cells. Therefore, before the material can be effectively used in IMR90s and hESCs, the charges need to be effectively reduced, while still maintaining some of the cationic helical structure. Thus, I have designed and synthesized a diblock copolymer incorporating polyethylene glycol (PEG) to the PVBLG$_n$-8 polypeptide. I demonstrated that the addition of PEG to PVBLG$_n$-8 markedly decreases the toxicity of PVBLG$_n$-8 yet preserves the biological activity and gene delivery efficiency of the polypeptide. Moreover, with its reduced toxicity, PEG-*b*-PVBLG-8 is able to effectively transfect IMR-90 fibroblasts and human embryonic stem cells (Scheme 2.1), which suggests that it may be possible to ultimately achieve higher-reprogramming efficiency of fibroblasts with a safer non-viral vector.

2.2 Materials and Methods

2.2.1 General

All chemicals were purchased from Sigma-Aldrich (St. Louis, MO, USA) and used as received unless otherwise specified. Anhydrous dimethylformamide (DMF) was dried by a column packed with 4Å molecular sieves and stored in a glovebox. Tetrahydrofuran (THF) and hexane were dried by a column packed with alumina and stored in a glove box. OptiMEM and Lipofectamine 2000 were purchased from Invitrogen (Carlsbad, CA, USA). pEGFP-N1 was obtained from Elim Biopharmaceuticals (Hayward, CA, USA). The human embryonic stem cell line H1 was cultured in mTeSR 1 medium from Stem Cell Technologies (Vancouver, Canada). Milli-Mark™ Anti-SSEA-4-PE were purchased from EMD Millipore (Billerica, MA, USA). IMR-90 fetal lung fibroblast cells were purchased from ATCC (Manassas, VA, USA) and cultured in MEM containing Earle's balanced salt solution supplemented with 10% fetal bovine serum. L-glutamic acid copper(II) complex copper(II) salt tetrahydrate[3] and γ-(4-vinylbenzyl)-L-glutamate *N*-carboxyanhydride (VB-Glu-NCA)[1,4] were prepared by following previously reported procedures.

2.2.2 Instrumentation

NMR spectra were recorded on a Varian UI400 MHz, a UI500NB MHz or a VXR-500 MHz spectrometer. Tandem gel permeation chromatography (GPC) experiments were performed on a system equipped with an isocratic pump (Model 1100, Agilent Technology,

Santa Clara, CA, USA), a DAWN HELEOS 18-angle laser light scattering detector (also known as multi-angle laser light scattering (MALLS) detector, Wyatt Technology, Santa Barbara, CA, USA) and an Optilab rEX refractive index detector (Wyatt Technology, Santa Barbara, CA, USA). The detection wavelength of HELEOS was set at 658 nm. Separations were performed using serially connected size exclusion columns (100, 500, 10^3 and 10^4 Å Phenogel columns, 5 μm, 300 × 7.8 mm, Phenomenex, Torrance, CA, USA) at 60 °C using DMF containing 0.1 M LiBr as the mobile phase. The MALLS detector was calibrated using pure toluene with no need for external polymer standards and was used for the determination of the absolute molecular weights. The molecular weights (MWs) of all polymers were determined based on the *d*n/*d*c value of each sample, calculated offline by using the internal calibration processed by the ASTRA V software (version 5.1.7.3, Wyatt Technology, Santa Barbara, CA, USA). Infrared spectra were recorded on a Perkin Elmer 100 serial FTIR spectrophotometer equipped with universal attenuated total reflectance (ATR), which enabled the analysis of polymer samples in powder form. Circular dichroism (CD) measurements were carried out on a JASCO J-700 or a JASCO J-720 CD Spectrometer. Ozone was produced by an OZV-8S ozone generator manufactured by Ozone Solutions Inc. (Hull, IA, USA). Lyophilization was performed on a FreeZone lyophilizer (Labconco, Kansas City, MO, USA). Flow cytometry analysis was conducted on a BD FACSCanto 6 color flow cytometry analyzer (Becton Dickinson, Franklin Lakes, NJ, USA). Cells were visualized with a Zeiss Axiovert 40 CFL fluorescence microscope equipped with a 20× objective (Thornwood, NY, USA). Zeta potential and particle size

were analyzed with a Malvern Zetasizer (Worcestershire, UK).

2.2.3 General procedure for the polymerization of VB-Glu-NCA

Following previously established procedure to synthesize and polymerize NCAs to prepare polypeptides [5-8]. In a glove box, VB-Glu-NCA (56 mg, 0.2 mmol) was dissolved in DMF (1 mL) followed by the addition of PEG-amine and 1,5,7-triazabicyclo[4.4.0]dec-5-ene (TBD) at various monomer:amine:TBD ratios (Table 2.1). The polymerization solutions were stirred at room temperature for 24-60 h until VB-Glu-NCA was consumed. Aliquots of the polymerization solutions were diluted to 10 mg polymer/mL using DMF containing 0.1 M LiBr and analyzed by GPC. The real-time concentration of NCA was quantified by measuring the intensity of the anhydride band at 1784 cm^{-1} by FTIR. The conversion of VB-Glu-NCA was determined by comparing the VB-Glu-NCA concentration in the polymerization solution versus the initial VB-Glu-NCA concentration. When the polymerization was complete, the majority of the DMF was removed under vacuum and the polymer was precipitated with ether (15 mL). The resulting PEG-*b*-PVBLG polymer was sonicated in ether for 5 min and centrifuged to remove remaining solvent. After the sonication-centrifugation steps were repeated two more times, PEG-*b*-PVBLG was collected and dried under vacuum (44 mg and 75% yield, and 35 mg and 68% yield for PEG_{113}-*b*-$PVBLG_{76}$ and PEG_{113}-*b*-$PVBLG_{287}$, respectively). ^{1}H NMR (TFA-*d*, 500 MHz): δ 7.53 (d, 2H, *J* =7.0 Hz, Ar<u>H</u>), 7.39 (d, 2H, *J* =7.0 Hz, Ar<u>H</u>), 6.84 (dd, 1H, J_1

=11.0 Hz, J_2 =18.0 Hz $C_6H_4C\underline{H}=CH_2$), 5.91 (d, 1H, J =18.0 Hz, $C_6H_4CH=C\underline{H_2}$), 5.43 (d, 1H, J =11.0 Hz, $C_6H_4CH=C\underline{H_2}$), 5.26 (m, 2H, $Ar\underline{CH_2}$), 4.80 (m, 1H, $C\underline{H}CH_2CH_2COOCH_2$), 4.13 (m, -$O\underline{CH_2CH_2}$- in PEG), 2.68 (m, 2H, $CHCH_2\underline{CH_2}COO$), 2.30 (m, 1H, $CH\underline{CH_2}CH_2COO$), 2.12 (m, 1H, $CH\underline{CH_2}CH_2COO$).

2.2.4 General procedure for the synthesis of poly(ethylene glycol)-block-poly(γ-(4-aldehydebenzyl)-L-glutamate) (PEG-b-PABLG)

PEG-*b*-PVBLG (40 mg) was dissolved in chloroform (30 mL) at -78°C. Oxygen was then bubbled into the solution for 1 min followed by the bubbling of ozone until the solution became blue. The ozone was then replaced by oxygen, which was bubbled into the solution for 2 min until the solution became colorless. The solution was degassed and back filled with nitrogen. Dimethyl sulfide (1 mL) was then added and the solution was stirred at room temperature overnight. Afterwards, the solvent was removed under vacuum and the resulting PEG_{113}-*b*-$PABLG_{76}$ was purified by sonicating the polymer in methanol (3 × 15 mL) and collected by centrifugation. PEG_{113}-*b*-$PABLG_{76}$ was dried under vacuum (33 mg, 82% yield). PEG_{113}-*b*-$PABLG_{287}$ was synthesized from PEG_{113}-*b*-$PVBLG_{287}$ by following the similar procedure for synthesis of PEG_{113}-*b*-$PABLG_{76}$ with 86% yield. ^{1}H NMR (TFA-*d*, 500 MHz): δ 10.31 (1H, $C\underline{H}OC_6H_4$), 8.40 (d, 2H, J =7.0 Hz, ArH), 7.96 (d, 2H, J =7.0 Hz, ArH), 5.71 (2H, $CHOC_6H_4\underline{CH_2}$), 5.21 (1H, $\underline{CH}CH_2CH_2CO_2CH_2$), 4.10 (m, -$O\underline{CH_2CH_2}$- in PEG), 3.12 (2H, $CHCH_2\underline{CH_2}$), 2.75 (1H, $CH\underline{CH_2}CH_2$), 2.56 (1H,

$CH\underline{CH_2}CH_2$).

2.2.5 General procedure for the preparation of PEG-b-PVBLG-8

PEG-*b*-PABLG (20 mg), *N*-(2-aminoethyl)piperidine (5 molar equiv relative to the Glu repeating unit of PEG-*b*-PABLG) and borane-pyridine complex (5 molar equiv) were mixed in DMF (3 mL) and stirred at 50°C for 48 h (Table 2). The mixture was poured into 3 M HCl (3 mL) and dialyzed against water for 48 h. The resulting PEG-*b*-PVBLG-8 was lyophilized. The yields of PEG-*b*-PVBLG-8 copolymers were between 60 and 70%, with grafting efficiencies greater than 95%, which was determined as previously reported [2].

2.2.6 General procedure for the analysis of polypeptide conformations by circular dichroism (CD)

Circular dichroism studies were performed on JASCO J-700 and J-720 CD spectrometers. Samples were prepared at polymer concentrations of 0.01-0.1 mg/mL unless otherwise specified. In a representative experiment, the sample solution was placed in a quartz cell with a path length of 0.5 cm and the mean residue molar ellipticity of the polymer was calculated based on the measured apparent ellipticity according to the equation: Ellipticity ([θ] in deg·cm^2·dmol^{-1}) = (millidegrees × mean residue weight)/(path length in millimeters × concentration of polypeptide in mg·mL^{-1}) [9]. For helix-

temperature dependency studies, the temperature of the sample chamber containing the quartz cell was varied from 4 to 70°C using a water bath. A minimum of 10 min was allowed for sample temperature equilibration prior to collecting CD measurements. The α-helix contents of the polypeptides were calculated using the following equation: % α-helix = $(-[\theta]_{222} + 3000)/39{,}000$ [10].

2.2.7 Agarose gel retardation

A solution of DNA (0.5 µg) was prepared in OptiMEM (50 µL). Separately, a solution of polypeptide in OptiMEM (50 µL) was prepared to achieve the desired polypeptide:DNA weight ratio. Following mixing of the two solutions, complexes were incubated at room temperature for 20 min, after which an aliquot (20 µL) was withdrawn and loading dye (4 µL) was added. The mixture was then run on a 2% agarose gel (100 V, 60 min). DNA was stained with ethidium bromide and visualized on a Gel Doc imaging system (Biorad, Hercules, CA, USA)

2.2.8 Characterization of polymer/DNA complex with zeta potential and dynamic light scattering

Solutions of DNA (25 µg) were prepared in OptiMEM (400 µL). Separately, a solution of polypeptide (1 mg) was prepared in OptiMEM (400 µL). A solution of Lipofectamine 2000 (50 µL, 1 mg/mL) in OptiMEM (400 µL) was also prepared as a

control. The DNA solution was then mixed with either the polypeptide or Lipofectamine 2000 solution and allowed to incubate at rt for 20 min. The size and surface charge of the resulting polyplexes were analyzed by dynamic light scattering (DLS) and zeta potential.

2.2.9 Transfection of IMR-90 with Lipofectamine 2000 and PVBLG-8 Polymers

IMR-90 cells were seeded at 50,000 cells per well in 24-well plates one day prior to transfection. On the day of transfection, plasmid pEGFP-N1 DNA (1 μL, 1 mg/mL) was diluted with OptiMEM (50 μL). Separately, Lipofectamine 2000 (2 μL, 1 mg/μL) or the polymer solution (10-80 μL, 1 mg/mL) was diluted with OptiMEM (50 μL). The individual solutions were then mixed gently and allowed to incubate for 5 min at rt, after which they were combined and allowed to incubate at rt for another 20 min. The cell media was then aspirated and replaced with pre-warmed (37°C) OptiMEM (500 μL). The complex solution was added dropwise to the cells. The cells were then incubated at 37°C with 5% CO_2 for 4 h, after which the cell media was replaced with normal culture media (500 μL). After incubation for a total of 48 h at 37°C with 5% CO_2, the cells were imaged with a fluorescent microscopy. The EGFP transfection efficiency was quantified by flow cytometry.

2.2.10 Sample preparation and flow cytometry analysis

Prior to analysis by flow cytometry, transfected cells on the 24-well plate were washed with 1× PBS (500 μL for each well) to remove any residual serum, dead cells and

debris. Next, trypsin (100 µL) was added and incubated for 5-10 min to detach the cells from the plate. PBS (100 µL) was then added and pipetted up and down to break up cell clumps. A solution of 4% paraformaldehyde (100 µL) was added to fix the cells. Samples were kept in covered flow cytometry tubes until analysis (BD FACSCanto, Franklin Lakes, NJ, USA).

2.2.11 MTT assay of polymers

For MTT assays, 10,000 cells were seeded in each well of a 96-well plate one day before transfection. The cells were then transfected as described above, save for an 80% reduction in volume and reagent quantity to accommodate the reduced well volume. The cells were incubated for 4 h at 37°C in the transfection mix before being returned to fresh growth media. After 48 h, the cells were washed with PBS and MTT solution was added. Following 4-h incubation at 37°C, MTT solubilization solution (10% Triton X-100 in acidic (0.1M HCl) isopropanol) was added to the cells and the absorbance of 570 nm light was quantified on a Perkins Elmer plate reader (Waltham, MA, USA).

2.2.12 hESC transfection

hESCs were seeded in Matrigel-coated 24-well plates. Plasmid DNA (1 µL, 1mg/mL) was diluted in OptiMEM (50 µL). The polymer solution (10-40 µL, 1 mg/mL)

was diluted with OptiMEM (50 µL). The two solutions were then vortexed gently and allowed to incubate for 5 min at rt, after which they were combined and allowed to incubate for another 20 min at rt. Next, the mixtures were added to the cells dropwise and allowed to incubate at 37°C for 4 h. The media was then aspirated and fresh media was added. After 48 h, the cells were stained with DAPI (250 µL, 3 nM) and SSEA-4 –PE (250 µL, 0.02 mg/mL), a pluripotency cell marker, for 30 min at 37 °C.

2.3 Results

2.3.1 Synthesis and characterization of PEG-b-PVBLG-8 (PEV)

γ-(4-Vinylbenzyl)-L-glutamate *N*-carboxyanhydride (VB-Glu-NCA) was prepared by following previously reported methods [1,2,4]. The ring-opening polymerization of VB-Glu-NCA with PEG-amine as the macroinitiator yielded PEG-*block*-poly(γ-(4-vinylbenzyl)-L-glutamate) (PEG-*b*-PVBLG) with controlled molecular weights (MWs) and narrow molecular-weight distributions (Scheme 2.2). At the VB-Glu-NCA/PEG-amine ratio of 100, the obtained M_n of 20.7×10^3 g·mol^{-1} agreed well with the theoretical M_n of 24.6×10^3 g·mol^{-1} and had a narrow molecular weight distribution of 1.21 (entry 1, Table 2.1). Two PEG-*b*-PVBLG copolymers were prepared with degrees of polymerization (DP) of 76 (PEG-*b*-PVBLG$_{76}$) and 287 (PEG-*b*-PVBLG$_{287}$) of the PVBLG block (Table 2.1). The ozonation of PEG-*b*-PVBLG yielded PEG-*b*-poly(γ-(4-aldehydebenzyl-L-glutamate) (PEG-*b*-PABLG), which served as the reactive intermediate that, through subsequent

hydroamination and reduction with *N*-(2-aminoethyl)piperidine, yielded the desired PEG-*b*-PVBLG$_{76}$-8 (PEV-L) and PEG-*b*-PVBLG$_{287}$-8 (PEV-H). Grafting efficiencies of greater than 95% were achieved for both PEV-L and PEV-H (Table 2.2).

Both PEV-L and PEV-H are highly soluble in water at pH 1-10 (> 50 mg/mL), which is drastically different from the corresponding parental (PEG-*b*-PVBLG) and intermediate polymers (PEG-*b*-PABLG) that are insoluble in water. The excellent water solubility of PEV-L and PEV-H is clearly related to their charged side groups, which make it possible for the applications of PEV at physiological pH. Both PEV-L and PEV-H showed the characteristic CD spectra of an α-helix with two minima at 208 and 222 nm (Fig. 2.1a), consistent with our previously reported α-helical conformation of PVBLG-8 [2,11]. Helical contents of greater than 90% were observed for both PEV-L and PEV-H at pH 3 when the side chain amine groups are protonated (Table 2.2). As expected, the charge repulsion of the side groups had minimal effect on helix stability because the charged amine groups were placed far away from the polypeptide backbone. Furthermore, the helicity—as measured by the value of -[θ]$_{222}$—was shown to be stable against pH and salt changes in the surrounding environment. For example, the -[θ]$_{222}$ values of PEV-L and PEV-H remained unchanged when the solution pH was increased from 1 to 9 (Fig. 2.1b). The helices of PEV-L and PEV-H were also fairly stable in concentrated denaturing conditions, such as in 1M NaCl (Fig. 2.1c) and 2M urea (Fig. 2.1d) aqueous solutions. These observations suggested that PEVs would maintain their helical conformation in

various extracellular and intracellular environments with well-preserved properties throughout the gene transfection processes.

2.3.2 Complex formation with PEG-b-PVBLG-8 with DNA

The ability of PEG-*b*-PVBLG-8 to bind and complex with DNA was examined using a gel retardation assay. Polymer was mixed with plasmid DNA at DNA:polymer weight ratios between 1:1 and 1:60 and run on an agarose gel. The results for PEV-L can be seen in Fig. 2.2. The addition of polymer in excess of a 1:2 (DNA:polymer weight ratio) resulted in the formation of stable complexes which prohibited the migration of DNA under an electrophoretic force. Interestingly, at a 1:2 DNA:polymer weight ratio, the DNA could still be seen in the loading well, indicating incomplete condensation. However, the DNA was no longer visible when sufficient polymer was added to achieve a 1:10 DNA:polymer weight ratio, indicating complete condensation. As can be seen in Fig. 2.1a, DNA binding does not affect the α-helicity of the peptide.

2.3.3 Dynamic light scattering

Dynamic light scattering revealed complexes formed between DNA and Lipofectamine 2000 at a 1:2 DNA:Lipofectamine 2000 weight ratio to be approximately 574 nm in diameter. Meanwhile, the hydrodynamic diameter of complexes of PEV-L and PEV-H at a 1:40 DNA:polymer weight ratio were substantially smaller—about 107 nm

and 246 nm for PEV-L and PEV-H, respectively (Fig. 2.3). Testing of DNA:polymer weight ratios less than and greater than 1:40 did not dramatically change the measured diameter—provided a minimum amount of polymer was added to achieve complexation. For example, the diameter of complexes made with DNA:PEV-L weight ratios of 1:10, 1:20, 1:40 and 1:80 were 117 nm, 115 nm, 107 nm, and 84 nm, respectively. This suggests that once a minimum amount of polypeptide is present—presumably enough to achieve a 1:10 DNA:polymer weigh ratio based on Fig. 2.2—the excess polymer is not incorporated into the complex and exists freely in the solution. Furthermore, despite the rod-like structure of the helical polypeptide, complexes formed between DNA and PEG-PVBLG-8 possessed a globular structure under TEM (Fig. 2.4). Zeta potential measurements were performed to ensure that the complex formed between PEV-L (or PEV-H) and DNA were overall positively charged. PEV/DNA complexes formed possessed zeta potentials between 2 and 10 mV (Fig. 2.5), while PVBLG-8/DNA complexes possessed zeta potentials between 20 and 30 mV (data not shown). The addition of PEG block to the polypeptide shielded the cationic charge of the PVBLG-8 block.

2.3.4 Toxicity

The toxicity of the PEV-H was compared with PVBLG-8 homopolymer (P0) and Lipofectamine 2000 via MTT assays in IMR-90 cells. PVBLG-8 (P0) was found to be notably toxic to IMR-90 cells. At 1:40 DNA:polymer weight ratio, a viability of 6% was

observed. The new diblock polymers of both low (PEV-L) and high (PEV-H) molecular weight showed substantially reduced toxicity to IMR-90 cells (Fig. 2.6). Increasing DNA:polymer ratio resulted in increased toxicity for both PEV-L and PEV-H polymers. PEV-H/DNA complexes showed slightly reduced toxicity compared to PEV-L/DNA complex, but both PEV-L- and PEV-H polymers were less toxic than Lipofectamine 2000 under similar condition.

2.3.5 Transfection

Transfection experiments were performed with the diblock co-polymers to determine if their reduced toxicity impacted their ability to effectively delivery genes to IMR-90 cells. As shown in Fig. 2.7, the commercial reagent Lipofectamine 2000 resulted in approximately 19% of treated cells expressing the delivered GFP transgene. Unmodified PVBLG-8 (P0), on the other hand, had a transfection efficiency of only 1.4% with low cell viability. While PVBLG-8 performed comparable to Lipofectamine 2000 in COS-7 and HeLa cells in previous studies, its poor performance as shown in Fig. 7 is likely due to the excessive toxicity of the polypeptide in IMR-90 cells. Reducing the toxicity of PVBLG-8 through the addition of PEG blocks resulted in an increased IMR-90 transfection efficiency to 9.4% and 21.4% for PEV-L and PEV-H, respectively. Because of the reduced toxicity of PEV-L and PEV-H, the DNA dosage could be increased from 1 μg to 2 μg, which resulted in slightly higher transfection efficiencies, 13% and 27%, for PEV-L and PEV-H

formulations, respectively (data not shown). Although this increase in efficiency was modest, it should be highlighted that the diblock polymers appeared to have reduced toxicity. For example, even though both Lipofectamine 2000- and PEV-H-transfected cells expressed similar amount of GFP in Figure 2.8, the cells transfected with PEV-H possessed an overall healthier phenotype with flat and elongated shapes as opposed to cells transfected with Lipofectamine 2000 that appeared to be sparse and rounded.

To further demonstrate the application of PEG-*b*-PVBLG-8, I next evaluated the gene delivery efficiency to the H1 hESCs. PEV-H transfection in separated H1 cells resulted in higher transfection efficiency than in cells plated as colonies (Fig. 2.9, 2.10). Moreover, the polymer was shown to have no impact on hESC pluripotency 48 h post-transfection. This was evidenced by the similar expression of stage specific embryonic antigen-4 (SSEA-4) both before and after transfection in colonies and single cells (Fig. 2.11). Further evidence of pluripotency was shown through a western blot of the *OCT4* pluripotency transcription factor before and after transfection with PEV-H (Fig. 2.12). Combined with its efficiency, the mild cell impact of the PEV-H made it a promising reagent to manipulate the gene expression of human stem cells.

2.4 Discussion

Transfection efficiency is often limited due to the toxicity of vectors. Generally, the more efficient the transfection material, the greater impact it may have on cell health. This

is largely due to the requirements of effective gene delivery—namely, a high polycationic charge to condense DNA and enable cell surface binding and membrane-lytic properties to facilitate intracellular escape from endocytic vesicles. While good for the delivery of nucleic acids, highly cationic materials can also bind and interfere with the function of necessary proteins within the cell. Moreover, the membrane lytic effect of materials can be unspecific and may act in desirable as well as undesirable manners. Effective gene delivery materials are able to balance their positive and negative tendencies so that they are efficient enough to allow macromolecules like DNA to enter the cells but safe enough that the cells are not irreparably damaged during the process. In my dissertation, I focus on the previously described PVBLG-8 materials and try to reduce their overall toxicity while maintaining their effective gene delivery performance.

Previous characterization of the helical polypeptide PVBLG-8 revealed that it can operate as an effective delivery vector for both DNA and siRNA [2]. In both cases, its performance was demonstrated to be tied to its ability to form stable helices that cause pore formation within membranes. In the case of DNA delivery, the membrane lytic potential was essential to the escape of DNA-polypeptide complexes from endocytic vesicles. In the case of siRNA delivery, the helical PVBLG-8 caused pore formation within cells membranes to allow the non-endocytic diffusion of siRNA into the cell cytosol. Therefore, in our desire to reduce the toxicity of the PVBLG-8 materials, it was also essential to retain their helical structure. Unfortunately, just as helicity makes the materials effective delivery

agents, it is also a contributing factor to overall toxicity. As such, I sought a strategy to append charge-shielding materials to the helical PVBLG-8. By shielding the positive charge, the toxicity of the material should be minimized by reducing its electrostatic attraction with negatively charged cell membranes. At the same time, since the helicity of the PVBLG-8 block was maintained (Fig. 2.1a), I believed that the material would retain its ability to effectively escape the endosome and mediate effective gene delivery (Scheme 2.1).

To test the feasibility of incorporation of charge shielding groups, PEG was covalently conjugated with PVBLG-8 to yield the diblock polymer PEG-*b*-PVBLG-8. The PEG used had a MW of 5000 Da (DP of 113) and was conjugated to helical PVBLG-8 with DPs of 76 and 287 to yield the diblock materials PEV-L and PEV-H, respectively (Scheme 2.2). Circular dichroism experiments revealed that the incorporation of PEG did not alter the presence and stability of the helices even after the DNA is bound and condensed by the peptide (Fig. 2.1a). Moreover, the materials were also able to bind and condense plasmid DNA into spherical particles with diameters on the order of 100 nm (Fig. 2.2–2.4). Despite the inclusion of PEG, these particles were demonstrated to retain an overall positive surface charge similar to commercial materials like Lipofectamine 2000 by analyzing their surface zeta potential (Fig. 2.5).

Toxicity measurements with the diblock materials revealed that the inclusion of a

PEG block substantially increased the biocompatibility of the materials in IMR-90 cells. For example, treatment with the unmodified PVBLG-8 left only approximately 5% of IMR-90 cells viability. However, with the addition of a PEG block, cell viability increased dramatically and was less toxic than Lipofectamine 2000 (Fig. 2.6). With its improved toxicity profile, PEG-*b*-PVBLG-8 was able to mediate effective transfection in IMR-90 cells. Previously, the toxicity of the materials was so extreme that only 1.4% of cells were successfully transfected. With the reduced toxicity, that number was increased to approximately 20%—an increase of approximately 14-fold. With its improved safety profile, PEG-*b*-PVBLG-8 was mild enough to transfect H1 human embryonic stem cells without affecting the expression of cell pluripotency markers (Fig. 2.9-2.12).

2.5 Conclusion

I prepared diblock copolymers consisting of poly(ethylene glycol)-*block*-poly(γ-4-(((2-(piperidin-1-yl)ethyl)amino)methyl)-benzyl-L-glutamate) (PEG-*b*-PVBLG-8) and evaluated their capability to mediate gene delivery in IMR-90 human fetal lung fibroblasts and human embryonic stem cells (hESCs). The PEG-*b*-PVBLG-8 contained a membrane-disruptive, cationic, helical polypeptide block (PVBLG-8) for complexing with DNA and a hydrophilic PEG block to improve the biocompatibility of the gene delivery vehicle. PEG-*b*-PVBLG-8 copolymers with low (n = 76) and high (n = 287) degrees of polymerization (n) of the PVBLG-8 block were synthesized. I found that the incorporation of PEG effectively reduced the toxicity of the helical PVBLG-8 block without dramatically

compromising the complexation of copolymers with DNA and their transfection efficiencies. PEG-*b*-PVBLG-8 diblock polymer with a high degree of polymerization had a greater transfection efficiency and lower toxicity in IMR-90 cells than the commercial reagent Lipofectamine 2000. The usefulness of PEG-*b*-PVBLG-8 was further demonstrated via the successful transfection of hESCs without a measured loss in cell pluripotency markers. In contrast to many other polymer- and lipid-based transfection systems which utilize the proton sponge mechanism (e.g. polyethylenimine) or lipid mixing (e.g. DOTAP, DOPE, etc.) to facilitate endosomal escape, the peptides described here make use of a novel pore formation mechanism. As endocytic escape is generally considered one of the most challenging aspects of gene delivery, this alternative endosomolytic mechanism may prove useful when working with cell lines not readily amenable to transfection by current methods (i.e. IMR-90 and hES cells). This method of the PEG modification onto the PVBLG-8 backbone proved to be quite tedious and hard to control, to scale up the diblock polypeptide is quite costly and difficult. Therefore, an alternative gene delivery system that uses the cationic helical peptide was developed to take advantage of the endosomal escape of the nanocomplexes.

2.6 Figures

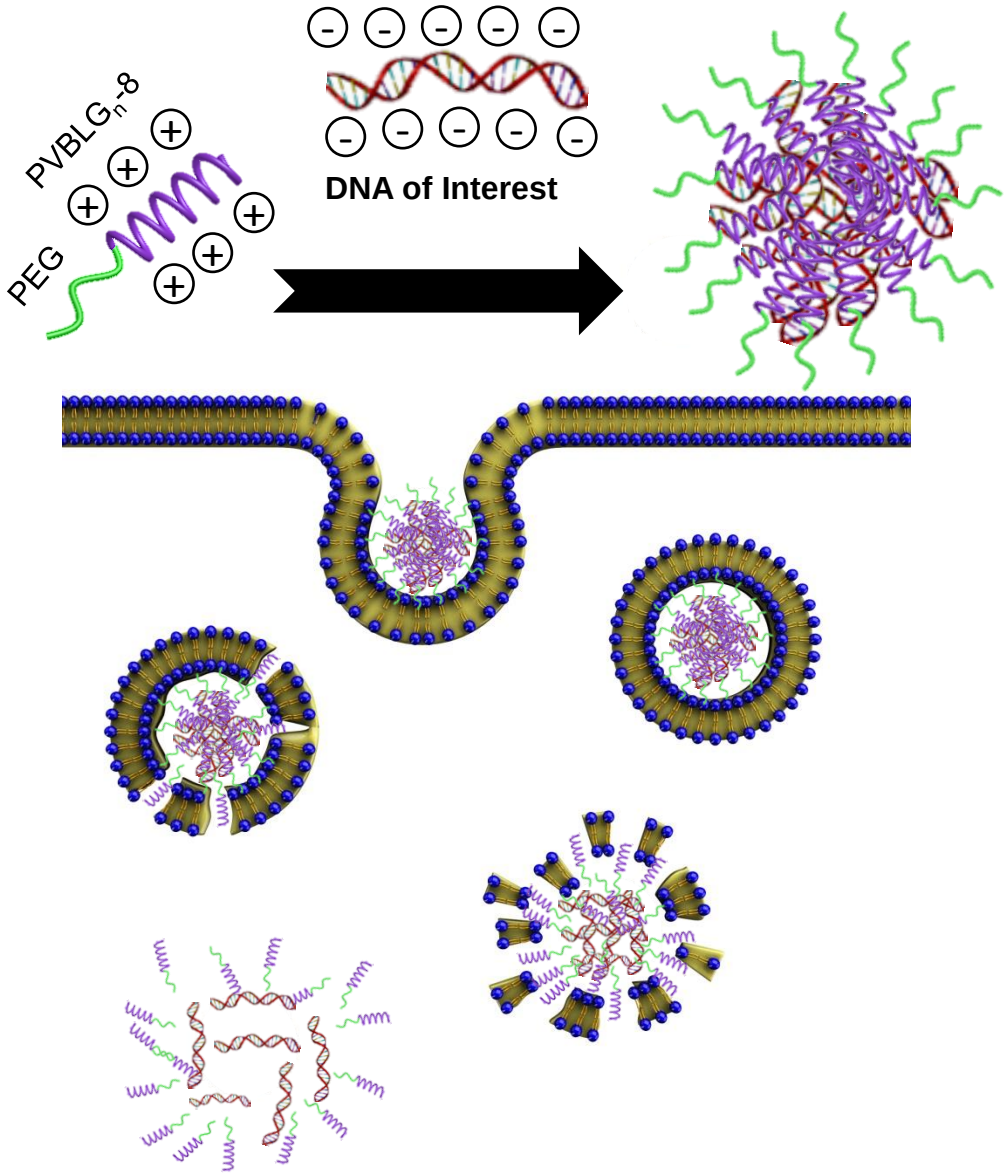

Scheme 2.1: Plasmid DNA condensation by PEG-b-PVBLG-8 and the uptake and release of DNA inside the cell.

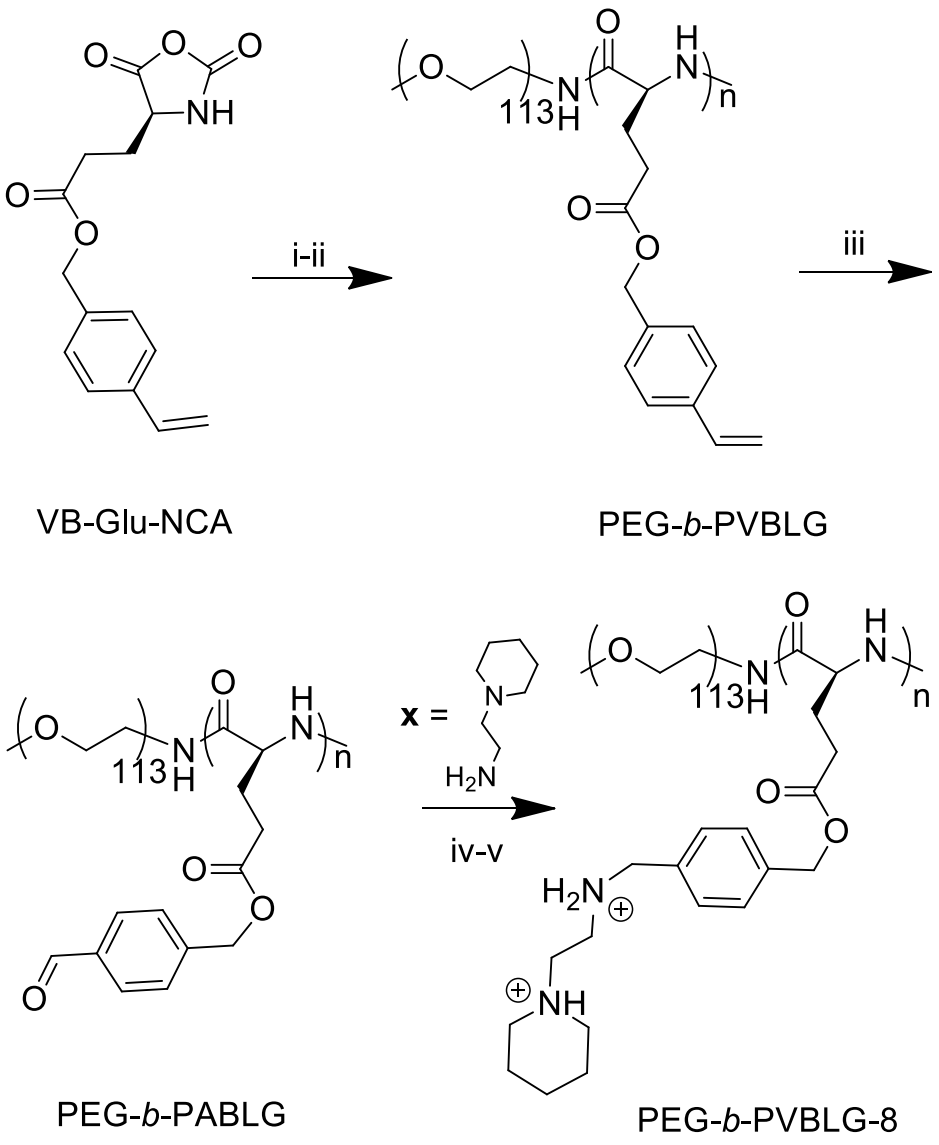

Scheme 2.2: The chemical route for preparation of PEG-b-PVBLG-8 from VB-Glu-NCA. (i) $mPEG_{113}$-NH_2, TBD, nitrobenzene; (ii) benzyl chloroformate, diisopropyl ethyl amine, tetrabutylammonium floride; (iii) O_3, $CHCl_3$, -78°C, Me_2S; (iv) **x**, Borane-pyridine; (v) HCl

Table 2.1. PEG_{113}-NH_2 Initiated Polymerization of VB-Glu-NCA.

Product	M:Amine: TBD[a]	Time (h)	Conv. (%)	M_n (M_n*) (× 10^3 g/mol)[b]	MWD
PEG_{113}-*b*-$PVBLG_{76}$	100:1:0.1	24	80	20.7 (24.6)	1.21
PEG_{113}-*b*-$PVBLG_{287}$	400:1:0.1	60	78	75.3 (81.4)	1.29

[a]TBD: 1,5,7-triazabicyclo[4.4.0]dec-5-ene; [b] the MW obtained (theoretical MW = $M_{n,PEG}$ + 245.27 × conv. × [M]/[I]).

Table 2.2. Synthesis and conformation analysis of PEG-*b*-PVBLG-8.[a]

Starting Polymer	Product	Grafting Eff. (%)[b]	$[\theta]_{222}$ (10^3deg cm^2/dmol)[c]	Helical Content (%)[d]
PEG_{113}-*b*-$PABLG_{76}$	PEG_{113}-*b*-$PVBLG_{76}$-8 (PEV-L)	> 95	32.8	91.8
PEG_{113}-*b*-$PABLG_{287}$	PEG_{113}-*b*-$PVBLG_{287}$-8 (PEV-H)	> 95	34.6	96.4

[a] Reducing reagent (5 molar equiv) was used. Reaction was carried out for 48 h at 50°C. [b]The grafting efficiency was determined by ^{1}H NMR analysis; [c]The mean residue molar ellipticity was calculated by following literature-reported formulas: Ellipticity ($[\theta]_{222}$ nm in cm^2 deg dmol−1) = (millidegrees × mean residue weight)/(path length in millimeters × concentration of polypeptide in mg mL^{-1}); [d]The α-helix contents of the polypeptides were calculated using the following equation: % α-helix = (-$[\theta]_{222}$ + 3000)/39,000 [10].

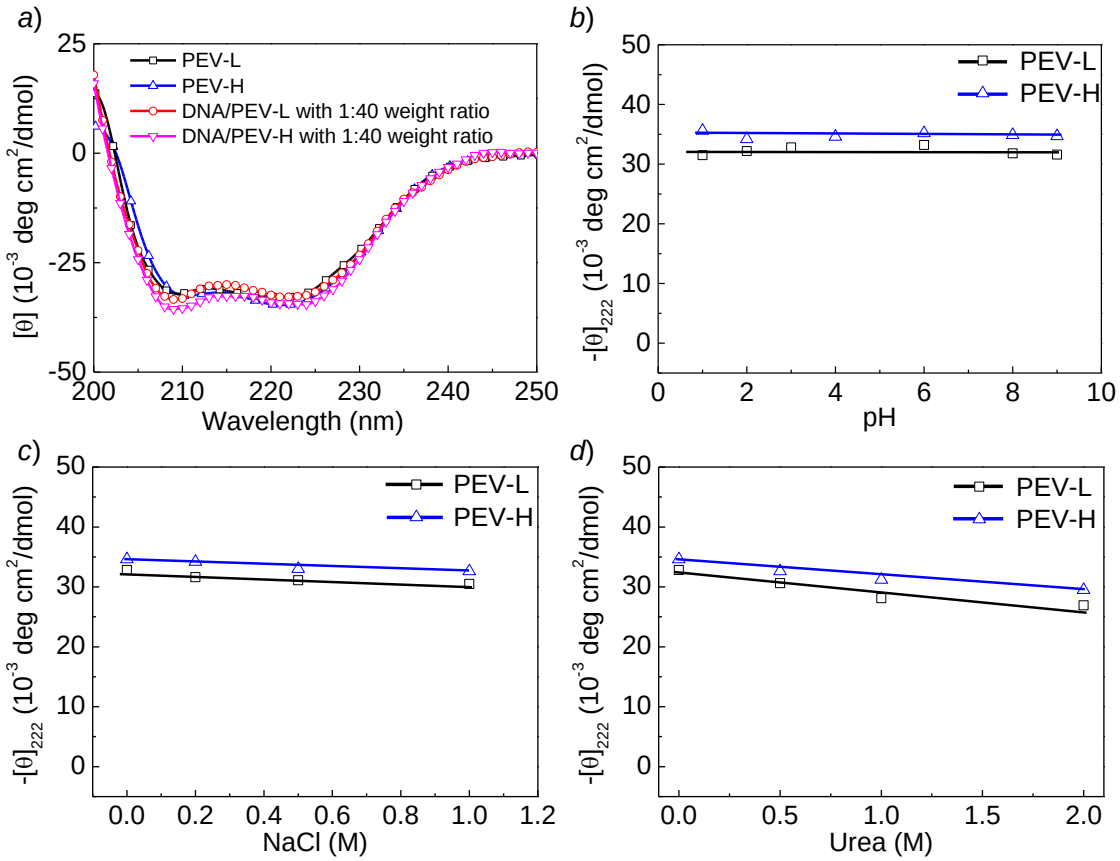

Figure 2.1: Demonstration of helicity of PEV (a) CD spectra in water of PEV-L,PEV-H, DNA/PEV-L, and DNA/PEV-H at 1:40 weight ratio at pH 3. (b) The pH dependence of the residue molar ellipticity at 222 nm for PEV-L and PEV-H at 0.05 mg/mL. (c) Salt dependence of residue ellipticity at 222 nm for PEV (d) The helical stabilities of PEV-L and PEV-H at pH 3 and 0.05 mg mL−1 in the presence of urea.

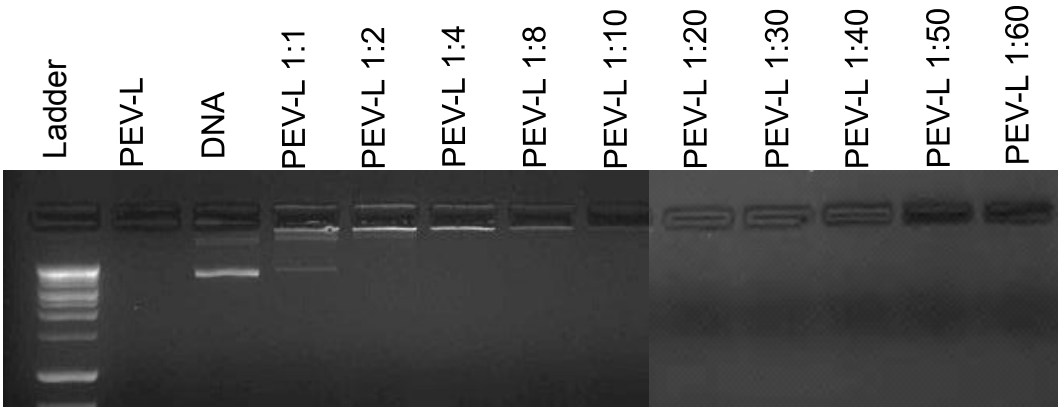

Figure 2.2: DNA/Polymer complex analysis: Gel Retardation of the PEV-L at different DNA to polymer weight ratios.

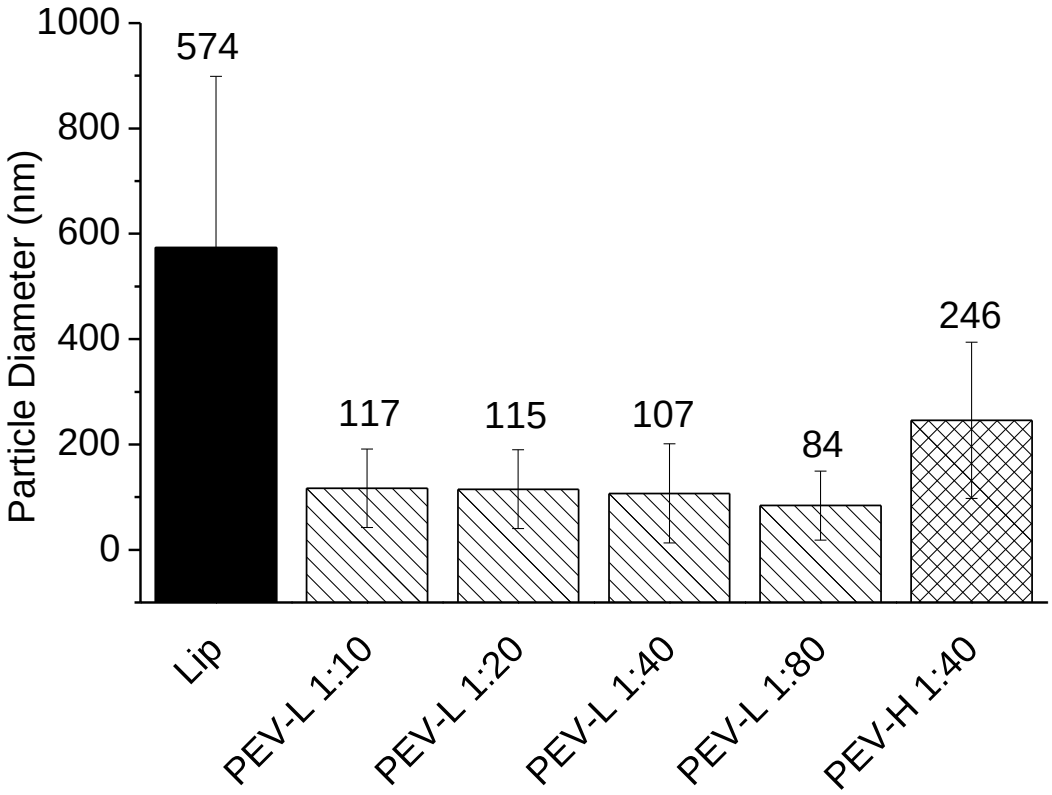

Figure 2.3: Particle size analysis of the PEV-L copolymer and DNA complex with different PVBLG-8 chain lengths and DNA to polymer weight ratios.

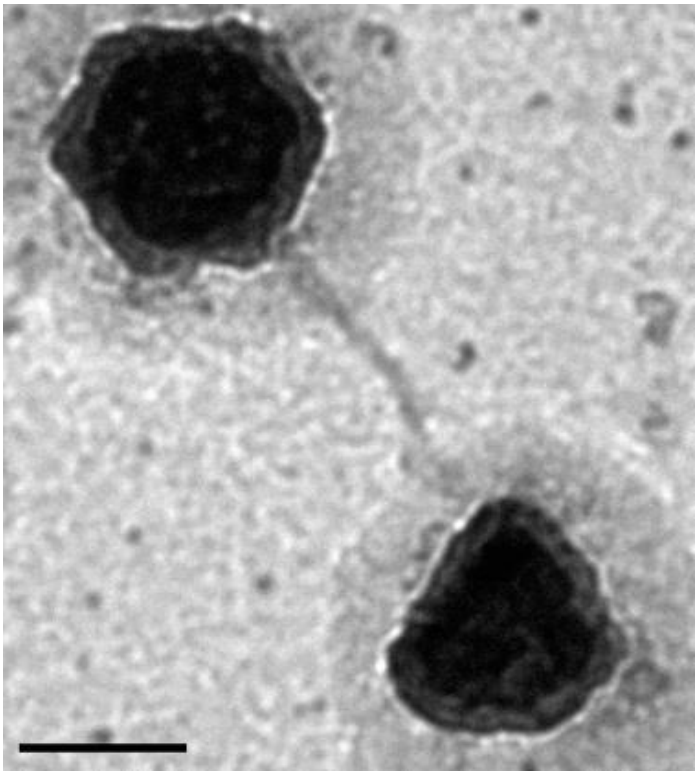

Figure 2.4: TEM image of PEV-L with DNA nanocomplex. Scale bar: 200 nm

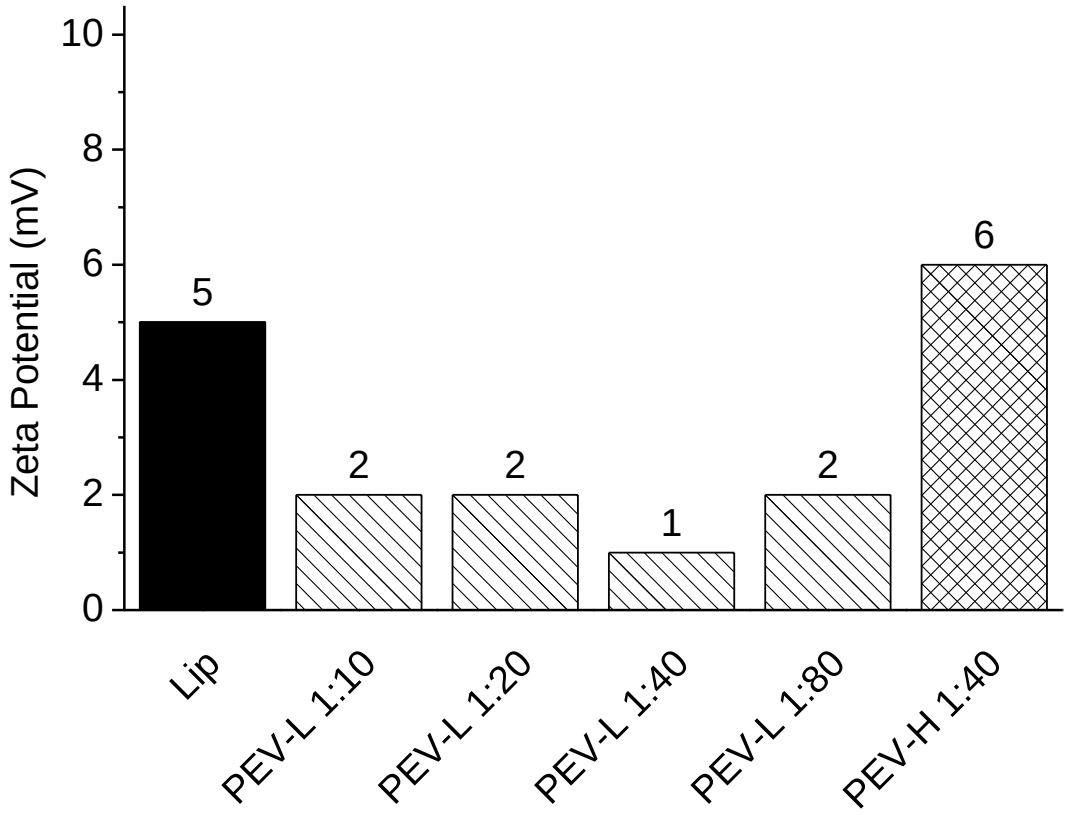

Figure 2.5: Particle zeta-potential of the PEV-L copolymer and DNA complex with different PVBLG-8 chain lengths and DNA to polymer weight ratios.

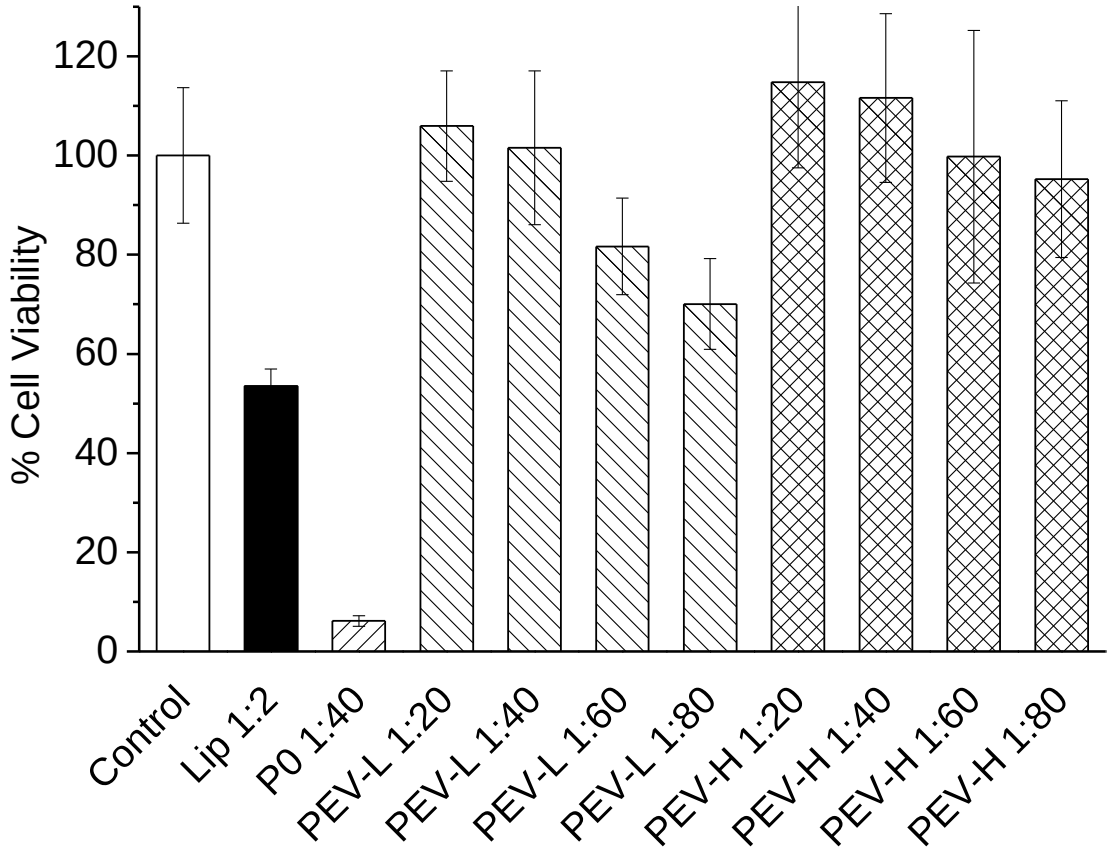

Figure 2.6: In-vitro analysis in IMR90 cells. MTT cell viability assay of the DNA/polymer nanocomplex with different polymers and at different weight ratios in IMR90.

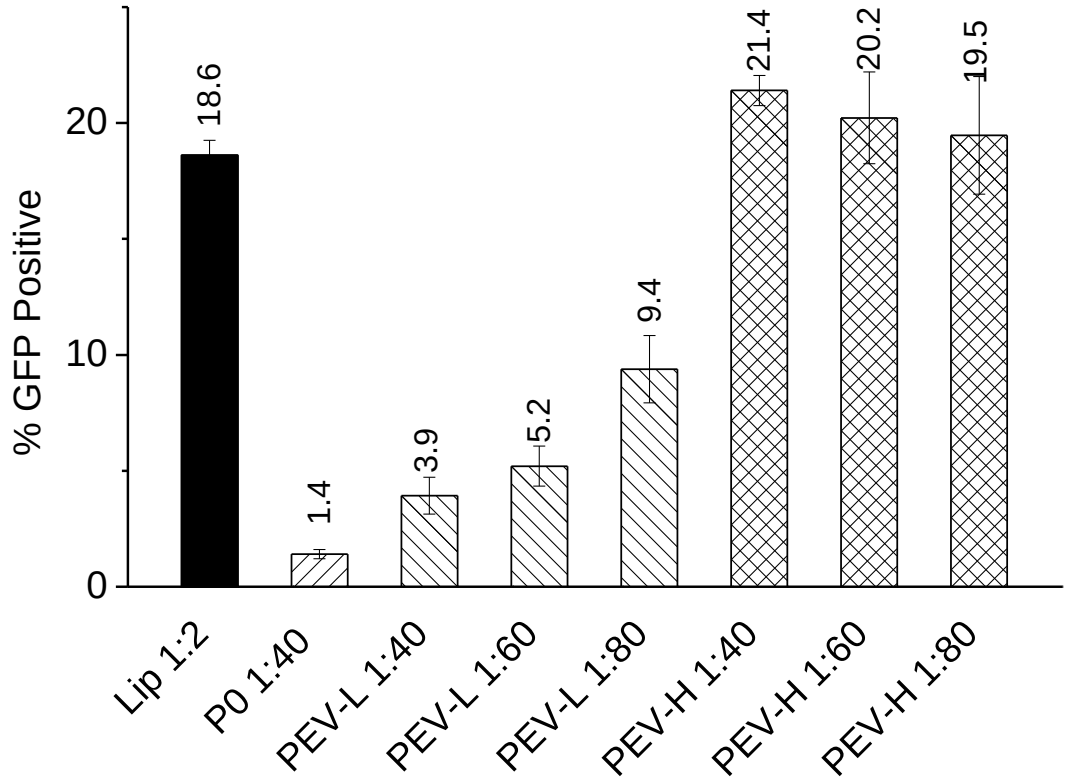

Figure 2.7: Initial testing for PEV-L along with Lipofectamine 2000 (Lip) and PVBLG-8 (P0) with varying pEGFP-N1 plasmid and polymer amount. Transfection efficiency was analyzed 48 hours post transfection with flow cytometry.

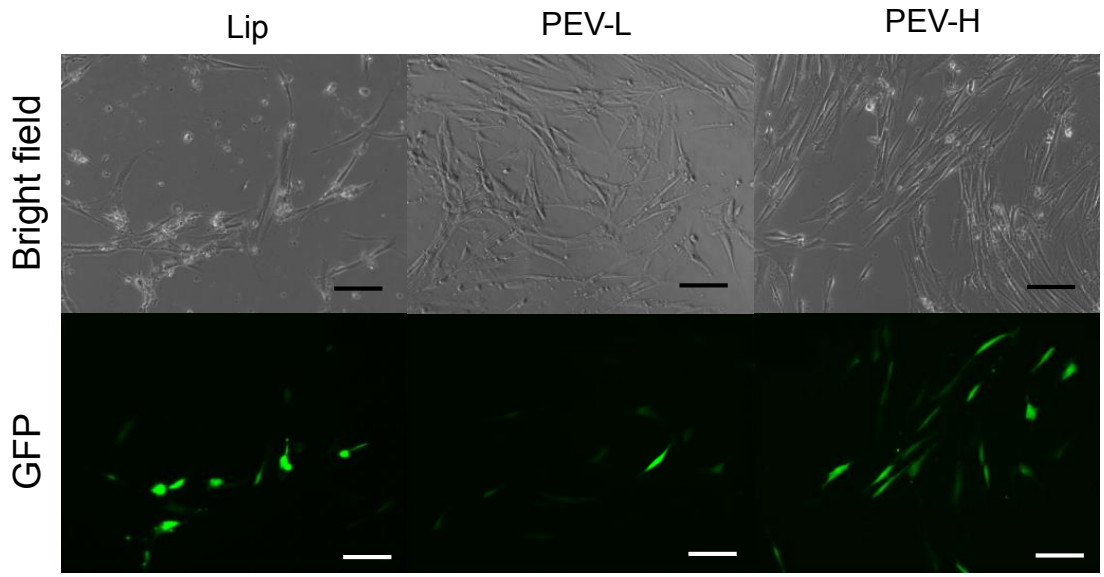

Figure 2.8: Fluorescent images of the transfection using Lipofectamine and PEV-H. Scale bar: 250 µm

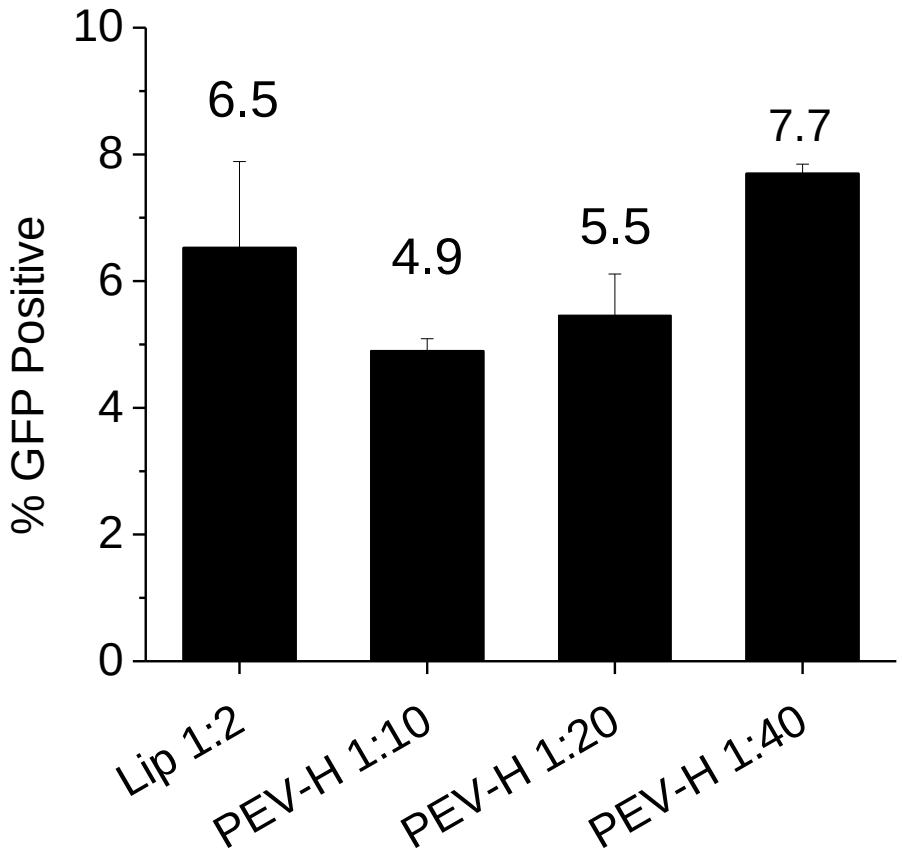

Figure 2.9: EGFP plasmid transfection efficiency using Lipofectamine 2000 and PEV-H of hESC H1 as small colonies

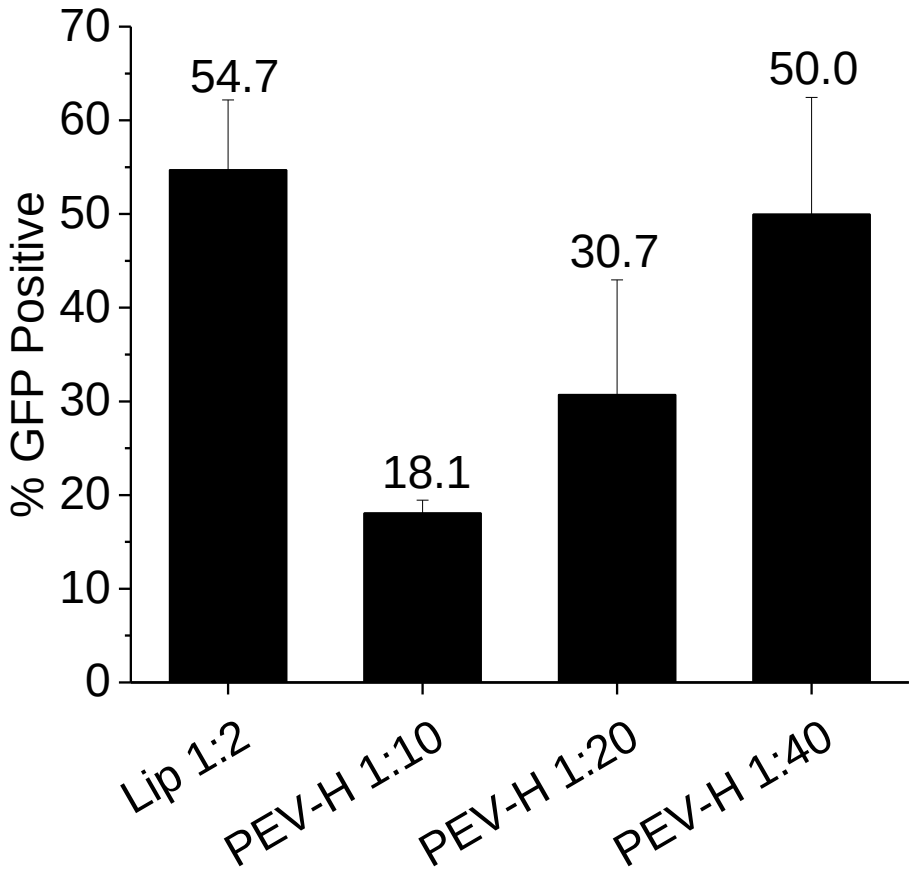

Figure 2.10: EGFP plasmid transfection efficiency using Lipofectamine 2000 and PEV-H of hESC H1 as single cells as analysed by flow cytometry.

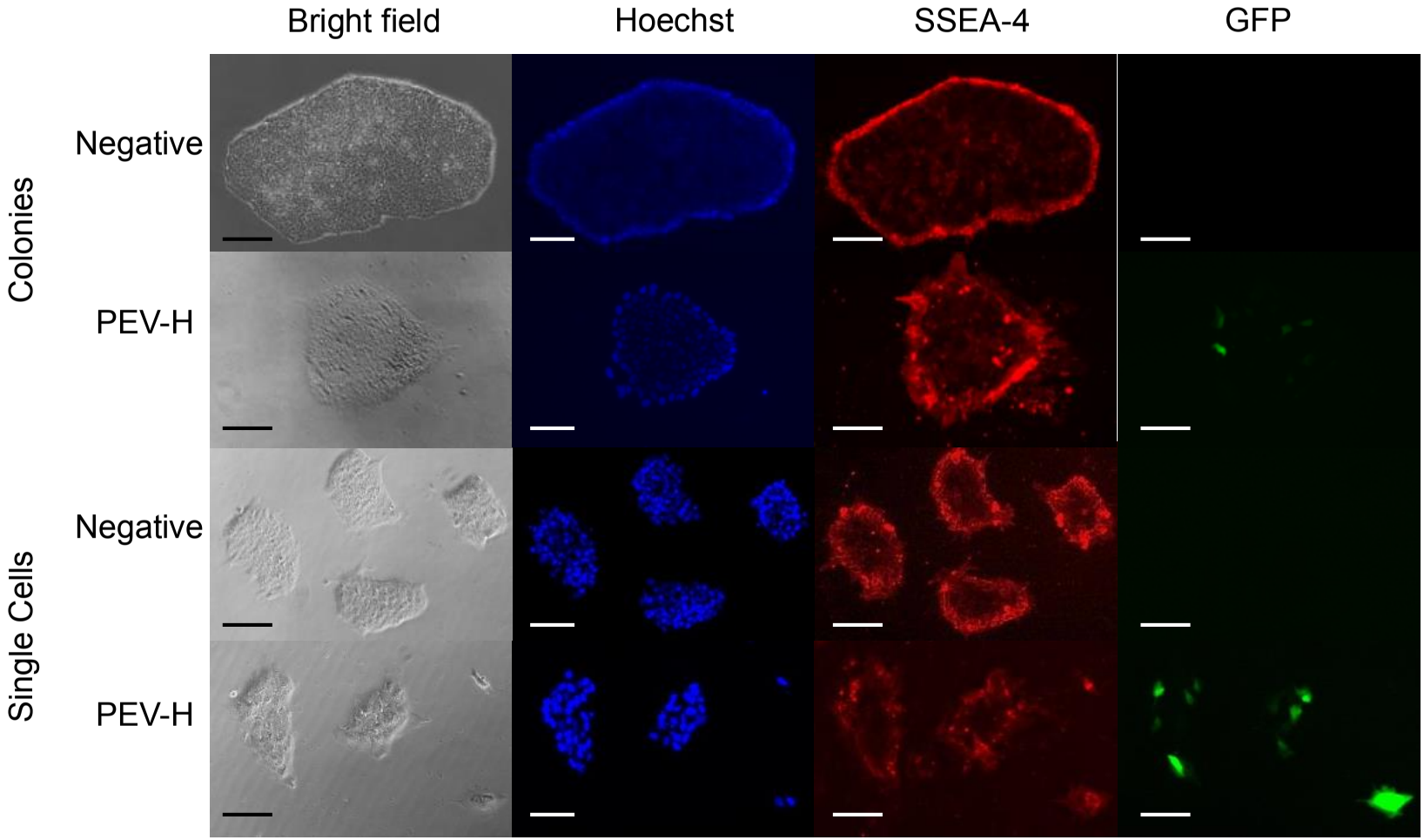

Figure 2.11: Bright field and fluorescence imaging of PEV-H transfection of EGFP plasmid into hESC as colonies and single cells. Colonies were stained with Hoechst and pluripotency marker SSEA-4 antibody conjugated with PE. Scale bar: 250 µm

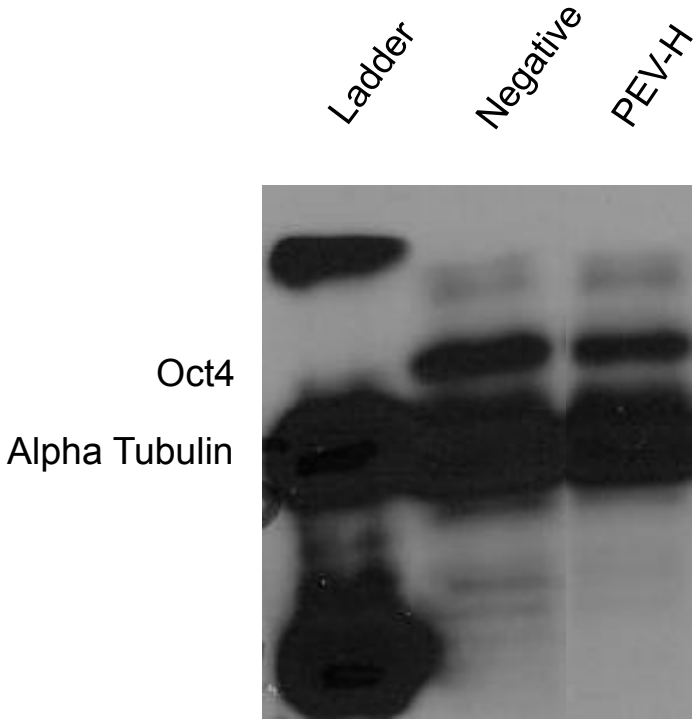

Figure 2.12: Western blot of cells isolated 72 h post transfection demonstrating the protein expression of OCT4 in hESC H1 cells.

2.7 References

[1] Lu H, Bai YG, Wang J, Gabrielson NP, Wang F, Lin Y, et al. Ring-Opening Polymerization of gamma-(4-Vinylbenzyl)-L-glutamate N-Carboxyanhydride for the Synthesis of Functional Polypeptides. Macromolecules 2011;44(16):6237-40.

[2] Gabrielson NP, Lu H, Yin LC, Li D, Wang F, Cheng JJ. Reactive and Bioactive Cationic a-Helical Polypeptide Template for Nonviral Gene Delivery. Angewandte Chemie-International Edition 2012;51(5):1143-47.

[3] Vanheeswijk WAR, Eenink MJD, Feijen J. An Improved Method for the Preparation of Gamma-Esters of Glutamic-Acid and Beta-Esters of Aspartic-Acid. Synthesis-Stuttgart 1982(9):744-47.

[4] Lu H, Wang J, Bai YG, Lang JW, Liu SY, Lin Y, et al. Ionic polypeptides with unusual helical stability. Nat Commun 2011;2:206.

[5] Lu H, Wang J, Lin Y, Cheng J. One-pot synthesis of brush-like polymers via integrated ring-opening metathesis polymerization and polymerization of amino acid N-carboxyanhydrides. J Am Chem Soc 2009;131(38):13582-83.

[6] Lu H, Cheng J. N-trimethylsilyl amines for controlled ring-opening polymerization of amino acid N-carboxyanhydrides and facile end group functionalization of polypeptides. J Am Chem Soc 2008;130(38):12562-63.

[7] Lu H, Cheng JJ. Hexamethyldisilazane-mediated controlled polymerization of alpha-Amino acid N-carboxyanhydrides. J Am Chem Soc 2007;129(46):14114-15.

[8] Bai YG, Lu H, Ponnusamy E, Cheng JJ. Synthesis of hybrid block copolymers via integrated ring-opening metathesis polymerization and polymerization of NCA. Chem Commun 2011;47(38):10830-32.

[9] Greenfield NJ. Using circular dichroism spectra to estimate protein secondary structure. Nat Protoc 2006;1(6):2876-90.

[10] Morrow JA, Segall ML, Lund-Katz S, Phillips MC, Knapp M, Rupp B, et al. Differences in stability among the human apolipoprotein E isoforms determined by the amino-terminal domain. Biochemistry-Us 2000;39(38):11657-66.

[11] Gabrielson NP, Lu H, Yin L, Kim KH, Cheng J. A Cell-penetrating Helical Polymer For siRNA Delivery to Mammalian Cells. Mol Ther 2012;20(8):1599-609.

Chapter 3:

Coating of cationic, helical peptide with hyaluronic acid for smart, safe, and targeted non-viral gene delivery

Significant portions of this chapter were published as "Enhanced Non-Viral Gene Delivery to Human Embryonic Stem Cells via Small Molecule-Mediated Transient Alteration of Cell Structure" Jonathan Yen, Lichen Yin, and Jianjun Cheng, *J. Mat. Chem. B.,* **2014**, 2, 8098-8105.

3.1 Introduction

PVBLG-8 has been demonstrated as a gene delivery system with high membrane activity and endosomal escape, which can be attributed to the cationic helicity and rigid structure[1]. Although PVBLG-8 showed some gene transfection in hESCs, it also exhibited remarkable cytotoxicity to the cells due to the cationic helical characteristics of the peptide[1]. There is a fine balance between the transfection efficiency and toxicity of cationic helical peptides. There have been chemical methods to modify the cationic helical peptide to reduce its toxicity, like structural reconfiguration[2], conjugations[3-6], and triggered degradation of the material [7].These modifications can effectively reduce the toxicity through the reduction of the cationic charge density on the peptide, while retaining its transfection efficiency. Yet, the conjugation of PEG onto PVBLG-8 as I described earlier was tedious and not easily tuneable.

Herein, I decided to take a formulative approach to develop a new gene delivery system based on self-assembled DNA/PVBLG-8 nanocomplexes coated by negatively charged hyaluronic acid (HA). HA can target and specifically bind to CD44, a known receptor specific to HA with high expression level in hESCs[8]. HA has been used in nanomedicine to target tumors, which also have high CD44 expression levels[9-14]. By coating the nanocomplexes with HA, it not only shields the charges to decrease the toxicity, but also acts as a targeting moiety for receptor-based endocytosis through HA/CD44 interactions. Furthermore, the HA can be deshielded through the pH drop and actions of endogenous hyaluronidase after internalization to expose the cationic helical peptides, allowing rapid and efficient endosomal release and expression of DNA plasmids. The HA coated nanocomplex demonstrates three important characteristics that enhance gene transfection efficacy in hESCs; an outer shell with active targeting moiety against CD44, an enzyme and pH sensitive targeting shell that can be released in the endosome exposing the cationic helical peptides, and the cationic helical peptides which can effectively allow for endosomal escape (Scheme 3.1).

3.2. Materials and Methods

3.2.1 General

hESCs H1 (hESC-H1) was cultured in E8 medium from Stem Cell Technologies (Vancouver, Canada). Y-27632 was purchased from Stemgent (Cambridge, MA, USA).

YOYO-1 was purchased from Invitrogen (Carlsbad, CA, USA). pEGFP-N1 was obtained from Elim Biopharmaceuticals (Hayward, CA, USA). Milli-Mark™ Anti-SSEA-4-PE was purchased from EMD Millipore (Billerica, MA, USA). PVBLG-8, a helical cationic polypeptide with a polymerization degree of 200, was synthesized following our reported procedures [15].

3.2.2 Instrumentation

Flow cytometry analysis was conducted on a BD LSRII flow cytometry analyzer (Becton Dickinson, Franklin Lakes, NJ). Cells were visualized with a Zeiss Axiovert 40 CFL fluorescence microscope equipped with a 10 and 20x objective (Thornwood, NY). Zeta potential and size analysis was conducted on the Malvern Zetasizer (Worcestershire, UK).

3.2.3 Nanocomplex formation and characterization

Various non-viral vectors were used for the transfection analyses. Plasmid DNA (1 µL, 1mg/mL) was diluted in water (25 µL). PVBLG-8 (7.5µL, 1 mg/mL) was diluted with water (25 µL). For the PVBLG-8 and coated nanocomplex procedures, the PVBLG-8 and plasmids were mixed at various w:w ratios and were incubated for 20 m at rt for complex formation. Hyaluronic acid (2.5-50µL,1mg/mL), dissolved in water, was added to the nanocomplex mixture and incubated for another 20 m at rt. For the mixed system, the DNA and hyaluronic acid were first mixed together at various w:w ratios and then the PVBLG-

8 was added at various ratios. The mixture was incubated at rt for 30 m for complex formation. Dynamic light scattering (DLS) and zeta potential analysis was conducted on the samples with a Malvern Zetasizer (Worcestershire, UK).

The nanocomplexes were subjected to electrophoresis in 1% agarose gel at 100 V for 45 minutes to evaluate DNA condensation by the polypeptides in terms of DNA migration.

3.2.4 In-vitro Gene Transfection

Cells were seeded in matrigel coated 24 well plates as single cells using accutase and incubated for 24 hours with rho-kinase inhibitor Y-27632 (10 μM). Using fresh low protein and serum free E8 medium, nanocomplexes as described earlier were added at 1μg DNA/well. After incubation for 4 h, the medium was replaced with fresh E8 medium and cells were cultured for 48 h. The cells were collected with accutase, fixed with paraformaldehyde and analyzed using flow cytometry to determine transfection efficiency.

3.2.5 In-vitro HA blocking

hESCs were incubated with free hyaluronic acid (300kDa, 1-5mg/mL) for 1 h prior to transfection. The cells were then washed 1x with PBS and placed back with fresh E8 media. The nanoparticles were added to the cells at 1 μg DNA/well. After incubation for 4 h, the medium was replaced with fresh E8 medium and cells were cultured for 48 h. The

cells were collected with accutase, fixed with paraformaldehyde and analyzed using flow cytometry to determine transfection efficiency.

3.2.6 pH and hyaluronidase exposure of nanocomplex

Nanocomplexes were formulated as previous described. HA coated nanocomplexes (400 µL, 100 µg/mL DNA) were incubated with hyaluronidase (100 µL, 0.5 mg/mL) in phosphate and citric acid buffer with a pH of 7.4, 6.8, 6.2 or 5.6 for 0, 30, or 120 m at 37°C. The HA coated nanocomplexes (100 µL) were then diluted in their corresponding buffer and the zeta potential of the resulting particles were analysed with the Zetasizer.

To test the membrane activity of the nanoparticles, Large Unilamellar Vesicles by Extrusion Technique (LUVETS)[16] loaded with 8-aminonaphthalene-1,3,6-trisulfonic acid (ANTS) and p-xylene-bis-pyridinium bromide (DPX) were formulated[17]. Briefly,DOPC (100 µL, 25 mg/mL $CHCl_3$) and POPC (1 mL, 10 mg/mL $CHCl_3$) were mixed in round bottom flask and evaporated with a rotary evaporator to create dry thin film. The film was allowed to dry overnight under vacuum. The lipid film was rehydrated by 5 mL of ANTS/DPX solution (12.5 mM ANTS, 45 mM DPX, 10 mM phosphate buffer, pH 7.4) for 30 m at rt. The solution was then put through 5 freeze thaw cycles in liquid nitrogen and like warm water. The solution was then extruded 15 times through 0.4 µM polycarbonate membranes. Any extravesicular components were removed through a Sephadex G-50 gel filtration column.

Nanocomplexes were formulated as previous described. HA coated nanocomplexes (400 µL, 100 µg/mL DNA) were incubated with hyaluronidase (100 µL, 0.5 mg/mL) in phosphate and citric acid buffer with a pH of 7.4 or 6.8 for 0 or 30 m at 37°C. The HA coated nanocomplexes (10 µL) and the ANTS/DPX LUVETs (5 µL) were mixed diluted in a final solution of the corresponding buffer of 100 µL. Triton x was used as the positive control. The leaked ANTS dye was measured using a plate reader at 360 nm excitation and 530 nm emission. The final leakage percentage was calculated using the ratio of fluorescence of the sample with the positive control after background subtraction.

3.2.7 Cell viability

Cells were seeded in matrigel coated 96 well plates as single cells using accutase and incubated for 24 hours with y-27632 (10 µM). Using fresh low protein and serum free E8 medium, nanocomplexes were added at 0.2µg DNA/well. After incubation for 4 h, the medium was replaced with fresh E8 medium and cells were cultured for 48 hours. Cell viability was evaluated through a MTT assay. Cells without complex treatment served as the control and results were expressed as percentage viability of control cells.

3.2.8 Intracellular Uptake Studies

DNA (1 mg/mL) was mixed and labeled with YOYO-1 (20 µM) at one dye molecule per 50bp of DNA. The HA coated nanocomplexes were then formed with

YOYO-1/DNA as discussed before at a DNA:PVBLG-8:HA weight ratio of 1:7.5:7.5. hESCs were plated on matrigel coated 24-well plate and allowed to grow to medium sized colonies. The complexes were added to the wells at 1 µg of YOYO-1-DNA per well and incubated for 4 h at 37°C. The cells were then quantified through flow cytometry to quantify YOYO-1 uptake. Results are expressed as mean fluorescence levels.

To elucidate the mechanisms regarding the cellular internalization of DNA/PVBLG-8/HA complexes, the uptake study was performed at 4 °C or in the presence of various endocytic inhibitors for 2 h. Cells were pre-treated with chlorpromazine (10 µg/mL), genistein (200 µg/mL), dynasore (80 µM), and wortmannin (50 nm) for 30 min before the complexes were added and throughout the experiment for 2 h at 37°C. Results are expressed as percentage mean GFP fluorescence level at 37 °C in control cells in the absence of endocytic inhibitors.

3.2.9 Western blot analysis and SSEA staining

After 72 h, the cells were stained with DAPI (250 µL, 3 nM) and SSEA-4–PE (250 µL, 0.02 mg/mL), a pluripotency cell marker, for 30 min at 37 °C. After 5 d, the cells were collected with RIPA buffer and mixed with Laemmli buffer supplemented with 2-Mercaptoethanol and heated for 5 m at 100°C to denature the proteins and then put on ice. The samples were ran on 10% SDS PAGE Gel at 120 V for 1.5 h, and wet transferred to the nitrocellulose membrane using the AMRESCO Rapid Western Blot Kit per

manufacturer's instructions. The membrane was stained with OCT4 and α-Tubulin primary antibodies and then with HRP-tagged secondaries.

3.3. Results

3.3.1 Characterization of DNA:PVBLG-8:HA Nanocomplexes

DNA condensation by PVBLG-8 followed by HA coating was evaluated by gel retardation assay. As shown in Fig. 3.1, DNA can be bind tightly to PVBLG-8 with a weight feed ratio at 1:7.5,and the coating of HA on the nanocomplex did not disrupt or displace the DNA in the nanocomplexes even when the feeding ratio of DNA to PVBLG-8 to HA at 1:7.5:50. This result indicated that the complexes are relatively stable through the coating method, and the negative charges on the HA does not interfere in the assembly or disassemble the nanocomplexes. Yet, when the HA was mixed directly with the DNA and PVBLG-8, the complex was unstable and some DNA leakage was detected (Fig. 3.2).

The size and zeta potential of the DNA/PVBLG-8 nanocomplexes at 1:7.5 weight ratios with varying HA weight ratio coatings were characterized using the DLS and zetasizer. Without HA coating, the nanocomplex size was 57.9 nm in diameter. After the coating of HA, at between 1:7.5:5 and 1:7.5:15 weight ratios, the effective diameters increased to around 170 nm. With further addition of HA to 1:7.5:50, the diameter increased to 270 nm. The zeta potential of the nanocomplex without HA, measured to be 19.2 mV, decreased to 11.1 mV with HA coating at 1:7.5:1 ratio indicating that the

nanocomplexes retained their positive charges. The zeta potential then decreases to between -18 and -25 mV when the ratio of HA was between 1:7.5:5 and 1:7.5:15 and then drops to -42 mv at 1:7.5:50. The increase and stabilization of the size and zeta potential demonstrates that the nanocomplexes were successfully coated with HA (Fig. 3.3).

The stability of the nanocomplexes was tested through the use of the dynamic light scattering to determine the size of the nanoparticles over time. The particles were tested at 30 min and 4 h after formulation at 37°C. As previously demonstrated, the size of the nanocomplexes with HA coating ranged from 150-180 nm and less than a hundred nm without the HA coating. Thus, if the HA coating were to come off or be destabilized, the size of the nanocomplex would become smaller. The sizes of nanocomplex remained constant in the different mediums, thus indicating that the nanocomplexes are quite stable (Fig. 3.4).

3.3.2 hESC Transfection with HA Coated DNA/PVBLG-8 Nanocomplexes

Through the optimization of various DNA:PVBLG-8 weight ratios, 1:7.5 is the optimal ratio for the highest transfection efficiency (Fig. 3.5). Thus, the 1:7.5 ratio was used with various ratios of HA coating on the nanocomplexes. Without HA coating, the nanocomplexes achieved 22% transfection efficiency, while with the increased ratio of HA coated on the nanocomplexes, the transfection efficiency went up to 28%, 27% and 30% for 7.5:2.5, 7.5:5, 7.5:7.5 of PVBLG-8:HA ratios, respectively. As the amount of HA was

increased to 15 and 30, the transfection efficiency dropped significantly to 20% and 17%, respectively (Fig. 3.6).This drop in transfection efficiency can be attributed to the excess HA in the system that did not coat the nanocomplexes, which compete for the CD44 receptors. PVBLG-8 by itself has also proven to be quite toxic to the cells, (Fig. 3.7, 3.17), where the cells are unhealthy and littered with cell debris. On the other hand, with HA coating the cells demonstrated lower toxicity and higher transfection. The HA coating not only acts as a targeting moiety, but also significantly counters the charges from the PVBLG-8 thus decreasing the overall toxicity in hESCs.

To demonstrate that the targeting of the HA coated nanocomplexes was due to the CD44 binding of the HA coated on the surface, pre-treatment of free HA was applied to the cells for 30 min and then washed off before transfection. With the treatment of 2.5 and 5 mg/mL of free HA pre-treated on the cells , a drop of transfections to 8% and 6% were shown, respectively, from 35% without pre-treatment (Fig. 3.8). This indicates that free HA has bound to the cell surface CD44 receptors and blocked them from further uptake, indicating that the CD44/HA interactions are an important aspect to the increased transfection efficacy of the nanocomplex. To further demonstrate the importance of the CD44 receptor for the system, the HA coated nanocomplexes were transfected in other CD44 positive and negative cells, human mesenchymal stem cells (hMSCs) and COS-7 cells, respectively. For CD44 positive hMSCs, HA coated nanocomplexes showed almost twice the transfection efficiency than those without HA coating. On the other hand, in

CD44 negative COS-7 cells, without the HA coating, the transfection efficiency was 36% and it dropped down to 15% after HA coating (Fig. 3.9). These trends demonstrate the important roles the CD44 receptors play in the transfection, which may due to the increased uptake of the HA coated nanocomplexes.

3.3.3 Mechanistic Studies of DNA/PVBLG-8/HA Nanocomplexes

To demonstrate that the enhanced gene transfection is due to the increased uptake through the CD44 receptor mediated pathway, the total uptake of DNA was evaluated. Using DNA tagged with YOYO-1, an uptake study was done to determine the amount of DNA/YOYO-1 uptake into the cells. It can be seen that without HA coating, the mean YOYO-1 fluorescence level measured to be about 61%, while with the HA coating at 1:7.5:7.5 ratio, the mean YOYO-1 fluorescence was significantly higher at 67% (Fig 3.10). In addition, with the treatment of free HA, the mean YOYO-1fluorescence level declined significantly to around 44%, indicating a reduced nanocomplex uptake. Alternatively, the uptake of DNA/YOYO-1 in CD44 negative COS-7 cells is reduced significantly after the coating of HA, further demonstrating that the CD44 receptor mediated the uptake of HA coating nanocomplex (Fig 3.11).

To show that the HA coated nanoparticles were indeed targeting the CD44 receptors, hESCs were stained with CD44 antibodies and incubated with HA coated DNA/YOYO-1/PVBLG-8nanocomplexes for 2 h at 4°C. Through confocal imaging, CD44

is stained uniformly across the surface of the hESCs. The DNA/YOYO-1 can be visualized on the cell surface co-localized with the CD44 receptors, indicating the importance of the roles of the CD44/HA interactions (Fig 3.12).

To elucidate the mechanisms underlying the cellular internalization of the HA coated nanocomplexes, an uptake study at 4°C or in the presence of various endocytic inhibitors was performed. Energy dependent endocytosis was blocked at 4°C; clathrin mediated endocytosis was blocked by chlorpromazine, which triggers dissociation of the clathrin lattice; caveolae was inhibited by genistein and mβCD by inhibiting tyrosine kinase and depleting cholesterol, respectively; macropinocytosis was inhibited by wortmannin by inhibiting phosphatidyl inositol-3-phosphate[18,19]. When the cells were incubated at 4°C, the uptake dropped to almost 3% of the control, while chlorpromazine dropped to 62%, genistein dropped to 22%, and wortmannin to 91% of the control (Fig. 3.13). The dramatic drop of transfection efficiency at 4°C indicates the process is energy dependent, and with the drop in uptake with the treatment of chlorpromazine and genistein, further demonstrates that the nanocomplexes enters the cells through receptor mediated endocytosis.

Due to the quick membrane disruption ability of PVBLG-8, the YOYO-1-DNA can quickly escape the endosomes and permeate into the cell cytoplasm after 2 h incubation at 37°C (Fig. 3.14). Therefore a substitute, poly-lysine, a cationic peptide with lower

membrane disruption ability was used to visualize the uptake and localization of the HA coated complexes. Through confocal imaging, there is significant co-localization of the HA coated YOYO-1-DNA/PLL complex with the lysotracker red stain as seen through CLSM confocal imaging (fig 4b). It demonstrates that HA coating helps the nanocomplex uptake through receptor mediated endosomal pathway. But it also showed that PVBLG-8 nanocomplex induces faster and more efficient endosomal escape, which is beneficial for gene transfection[1]. PVBLG-8 is exposed to allow for membrane disruption and endosomal escape once the nanocomplex reaches the endosomes.

3.3.4 Exposure of PVBLG-8 of HA Coated Nanocomplex for Endosomal Escape

To demonstrate the endosome triggerable membrane disruption of HA coated nanocomplexes for rapid endosomal escape, the nanocomplex zeta potentials and membrane disruption abilities were evaluated after treatment with hyaluronidase (HAase) at varying endosomal pH. At the initial time point of incubation of the HAase with varying pH of 7.4, 6.8, 6.2 and 5.6, the zeta potential remains negative at -21, -17.6, -16.8, and -10.3 mV, respectively. After 30 min incubation, the zeta potential at pH of 7.4 and 6.8 increased but remained negative at -18.2 and -8.32 mV, respectively. On the other hand, the zeta potential at pH of 6.2, and 5.6, all increased to the positive range of 1.34 and 9.39 mV, respectively. Finally, after 120 min the zeta potential at pH of 7.4 stays negative at -9.3 mV. But, for the pH at 6.8, 6.2 and 5.6, the zeta potential increases to positive of 1.69, 7.2 and 11.8 mV, respectively. A pH of 7.4 is representative of the cytoplasmic pH, while

early and late endosomes have a pH of 6.8 and 5.6, respectively[20] (Fig. 3.15). The shift of zeta potential towards positive indicates the exposure of the cationic helical peptides, which are then capable of membrane disruption.

But to further prove the membrane disruption ability of the HA coated nanocomplexes at an early pH endosome of 6.8, large unilamellar vesicles (LUV) were synthesized for dye leakage assay. At a pH of 7.4 and 6.8 it can be seen that the non-HA coated nanocomplexes allowed for 100% release of the dye. While with HA coating, the nanocomplexes only demonstrated slight membrane disruption at pH of 7.4, and a slight increase in membrane disruption at a pH of 6.8. Alternatively, with the addition of HAase after 30 min incubation at pH of 7.4 and 6.8, the dye leakage increased up to 46% and 76%, respectively, indicating strong membrane disruption ability (Fig. 3.16). In addition, nanocomplexes using PLL were also studied and it was found that with or without HA coating, there was no membrane disruption as expected. These studies indicate that the HA coated PVBLG-8 nanocomplex is responsive to the endosomal environment of both the pH and HAase activity, allowing for rapid endosomal escape.

3.3.5 Toxicity and Maintenance of hESCs

Cytotoxicity of the HA coated complexes was evaluated in hESCs 48 h after transfection using the MTT assay. PVBLG-8 demonstrated a cell viability of 75% (Fig.

3.17). But with the HA coated nanoparticles, the cell viability increased to approximately 90% with the HA coated at 1:7.5:7.5 weight ratios.

To ensure that the materials did not alter the cell's behavior or cause any differentiation, the cells were stained with SSEA-4 antibodies, stage specific embryonic antigen-4, 72 h after transfection, in which the cells all stained positive (Fig. 3.18). In addition, cell lysate were collected 5 days after transfection and a western blot was conducted to confirm the continued expression of the pluripotent factor, OCT4 (Fig. 3.19). The expression of SSEA-4 and OCT4 demonstrates that this system does not cause undesired differentiation or interferes with the pluripotency of the hESCs.

3.4. Discussion

Here, I developed a novel gene transfection system that contains an outer negatively charged cell targeting shell consisting of HA, with an inner core made from a cationic helical peptide that is able to condense DNA and facilitate endosomal escape. The system utilizes the charge interactions between the outer negatively charged shell and positive inner shell to be stable at neutral pH, but allows for the deshelling and exposure of the positive helical peptides when exposed to a lower pH and HAase with in the endosome. With the HA coating of the nanocomplexes, the hESC transfection efficiency of DNA/PVBLG-8 nanocomplexes increases significantly, despite the alteration of the overall charge of positive to negative. HA is a negatively charged biocompatible

polysaccharide that is found naturally in the body and has been used as the backbone of many hydrogel systems for stem cell engineering[8]. A few glycosaminoglycans, except for hyaluronic acid, have been shown to disrupt cationic polypeptide gene transfections[21]. The reversal of charge indicates the loss of the initial membrane disruption effect of the cationic helical peptide, which in theory should have decreased transfection. However, the negative nanocomplexes increased the transfection efficiency, indicating that the HA on the nanocomplexes is an integral part to the transfection efficiency, in which they target the CD44 receptors that are expressed on hESC surfaces. At up to 1:7.5:7.5 weight ratios, the transfection efficiency increases, then drops with additional HA coating. This drop is likely to be caused by the excess HA that were not coated on the nanocomplex. This can be seen by the DLS and zetapotential, that after a certain ratio, the size and zeta potential of the nanocomplex stays constant. Thus, the excess free HA could be competitively binding with the CD44 receptor against the nanoparticles, demonstrated by the drastic drop in transfection efficiency with the pre-treatment of HA. The drop demonstrates that the free HA has bound to the cell surface CD44 receptors and blocked them from further uptake, indicating that the CD44/HA interactions are an important aspect to the increased efficacy of the nanocomplex. The HA coated nanocomplexes also showed a higher efficacy in CD44 positive hMSCs, yet in CD44 negative cells, COS-7 cells dropped significantly. The drop in transfection efficiency in CD44 negative COS-7 cells with HA coated nanocomplexes, indicates that the CD44 receptor is indeed an important factor for the uptake of the HA coated nanocomplexes.

To understand the mechanism of uptake, I conducted uptake studies of DNA tagged with YOYO-1 dye and found that the cells did significantly increase the uptake of the nanoparticles with the HA coating. Through the study with various endocytosis inhibitors, the uptake was drastically inhibited at 4°C, indicating that the uptake of the particles was highly energy dependent. In addition, the decrease of the uptake due to the chlorpromazine, demonstrated that some of the particles were taken up through clathrin dependent endocytosis. On the other hand, genistein also had a large decrease in uptake of the YOYO-1/DNA, thus indicating that some of the uptake is due to clathrin independent pathways like caveolae mediated uptake. This denotes the importance of the CD44 receptor mediated endocytosis. Both CD44[22] receptors and caveolin[23] have been known to be present in lipid rafts domains, which are the sites of endocytosis in caveolae mediated endocytosis, indicating the localization of the HA nancomplexes at CD44 containing lipid rafts domains[24].

Commonly used transfection materials like polyethylenimine and polylysine have the ability to condense DNA for non-viral gene delivery, but PEI demonstrates slower endosomal release through the proton sponge effect, while polylysine demonstrates no endosomal escape[25,26]. Our nanocomplex system transforms to exhibit membrane disruptive properties in the endosomal environment of low pH and HAase activity. The exposure of PVBLG-8 in the system enhances the endosomal release of the nanocomplex

and thus the DNA. When the materials were switched to poly-L-lysine, a non-membrane disrupting polymer, there was little endosomal escape, and the nanocomplexes were mainly retained in the endosomes. In early endosomes, at a low pH and with some HAase activity, the HA coated nanocomplexes demonstrated increased LUV dye leakage due to membrane disruption. Our system is superior to other materials, due to our highly available and active membrane disruption activity that is initially shielded to reduce cytotoxicity to the cells, but is revealed when it enters the endosomes.

Not only did the HA coated nanocomplexes increase transfection efficiency, they also lowered the toxic effect of the cationic helical peptide. It also has little effect on the cells pluripotency, for the hESCs still proved to be both OCT4 and SSEA4 positive. Thus, the use of a targeting moiety for a receptor on hESCs is a step in looking at non-viral gene delivery into hESCs differently, in which a cell's specific mechanism is exploited to enhance transfection efficiency.

3.5 Conclusion

Here I report a new targeting and triggerable gene delivery system for human embryonic stem cells based on the PVBLG-8 peptide, a cationic helical peptide with high membrane disruption properties. The DNA/PVBLG-8 nanocomplex by itself proves to be toxic to the cells due to the high membrane disruption properties. Using HA as a coating for the nanocomplexes not only decreases the toxicity from the cationic helical peptides,

but allows a specific targeting moiety for hESCs that increases the uptake and release of DNA, which in turn increases the transfection efficiency. But after the material is taken up through endocytosis, the low pH and HAase are able to degrade and the HA on the nanocomplex is removed exposing the positive peptides and allowing for endosomal escape through membrane disruption. This provides a promising approach for manipulation of hESCs or pluripotent stem cells through transient gene delivery, overcoming major hurdles towards development of many biomedical applications. Increased gene transfection efficiency reduces the need for enrichment and sorting of the manipulated pluripotent stem cells. These preliminary studies lead to further possibilities of selective gene delivery to undifferentiated hESCs and potential further modification of the HA coating for PVBLG-8 based *in-vivo* gene delivery to other CD44 positive cells. The use of HA to target and enhance the non-viral gene delivery system provides an alternative method that does not just rely on the chemical characteristics of the material for gene delivery, but also targets and takes advantage of the biological properties of hESCs. Given this information, I then looked further into other physiological properties of hESCs I could use to further enhance gene transfection efficiency.

3.6 Figures

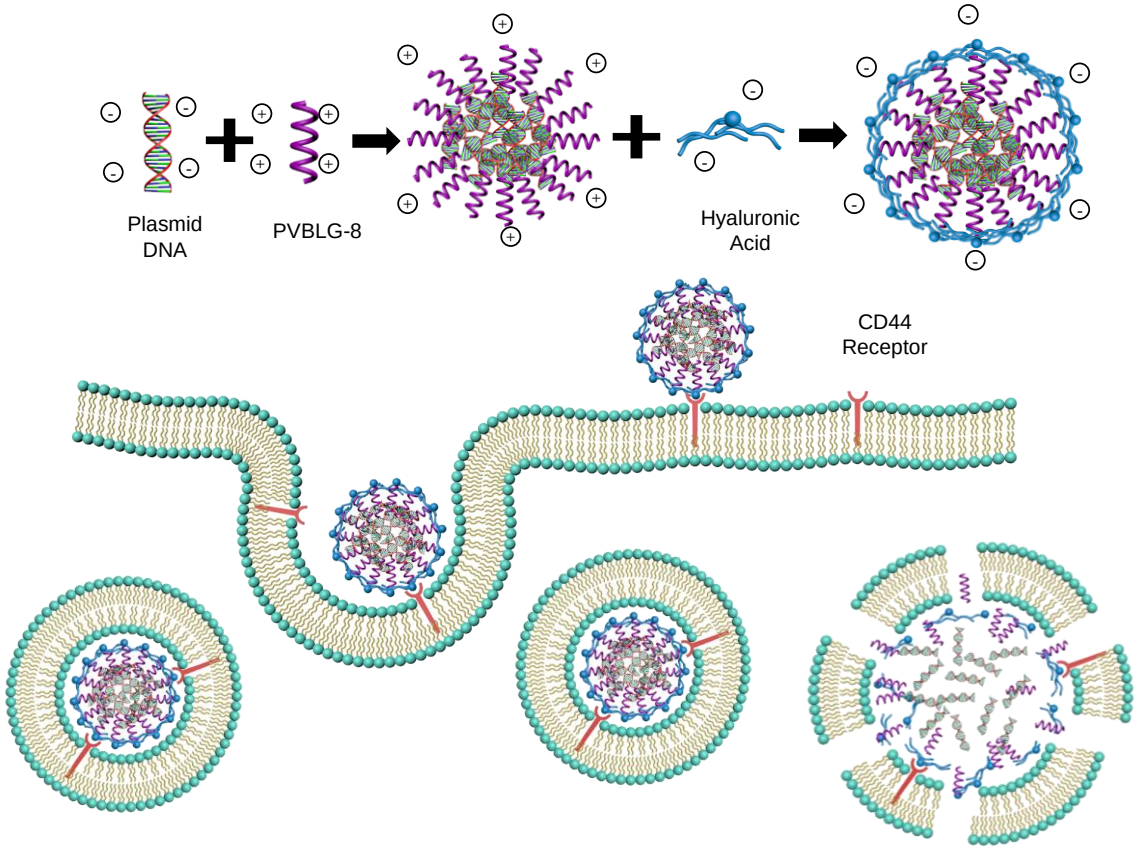

Scheme 3.1: Formulation and uptake route of the hyaluronic acid coated PVBLG-8/DNA nanocomplexes

DNA (w)	1	1	1	1	1	1	1	1	1	1
PV-BLG-8 (w)	0	7.5	7.5	7.5	7.5	7.5	7.5	7.5	7.5	7.5
HA (w)	0	0	1	2.5	5	7.5	10	15	25	50

Figure 3.1: Gel Retardation of HA coated nanocomplexes at varying DNA:PVBLG-8 weight ratios.

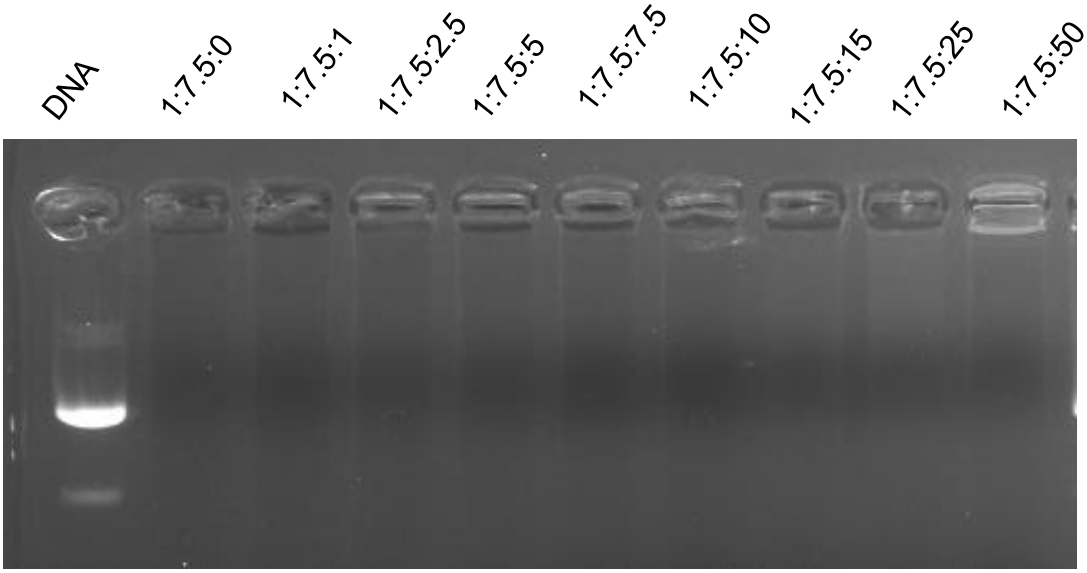

Figure 3.2: Gel Retardation of HA coated nanocomplexes at varying DNA:PVBLG-8 weight ratios.

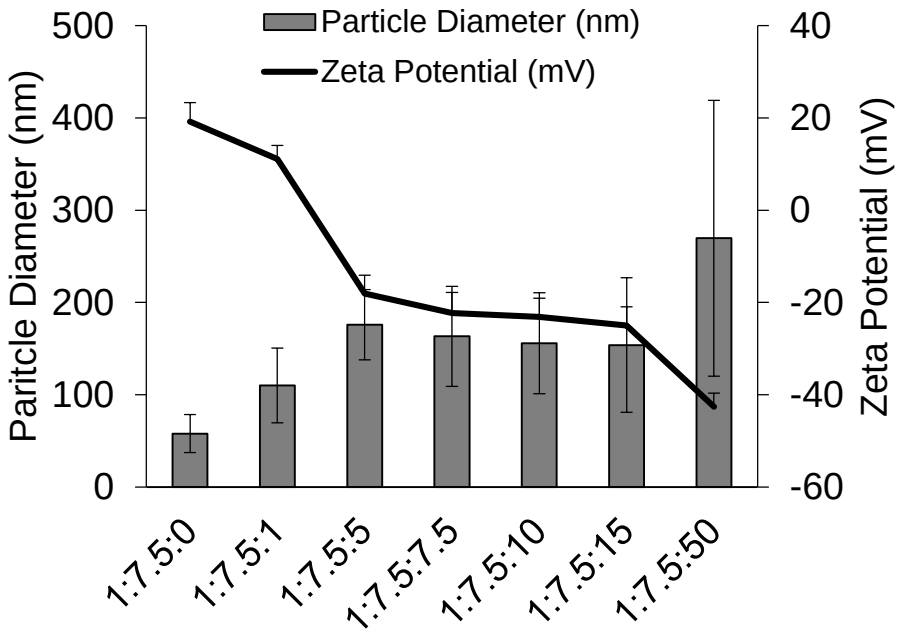

Figure 3.3: Size and zeta potential of HA coated nanocomplexes at 1:7.5 DNA:PVBLG-8 weight ratios.

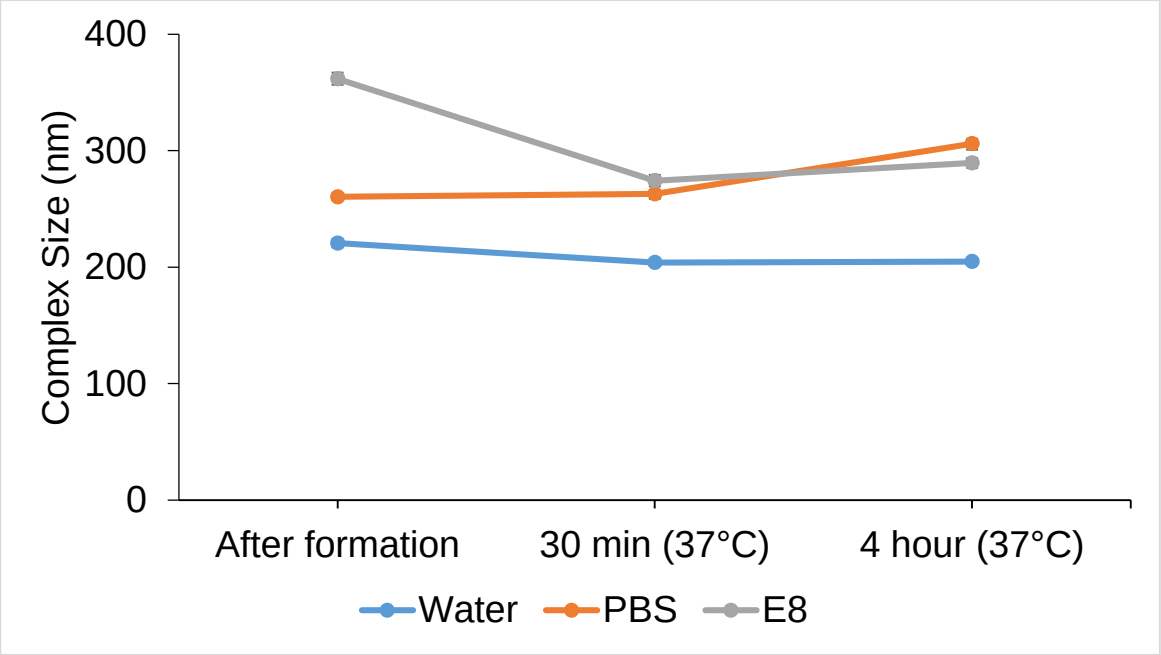

Figure 3.4: Stability of HA coated nanocomplexes at 1:7.5:7.5 DNA:PVBLG-8:HA weight ratios in water, PBS and E8 medium as determine by size change measured by DLS.

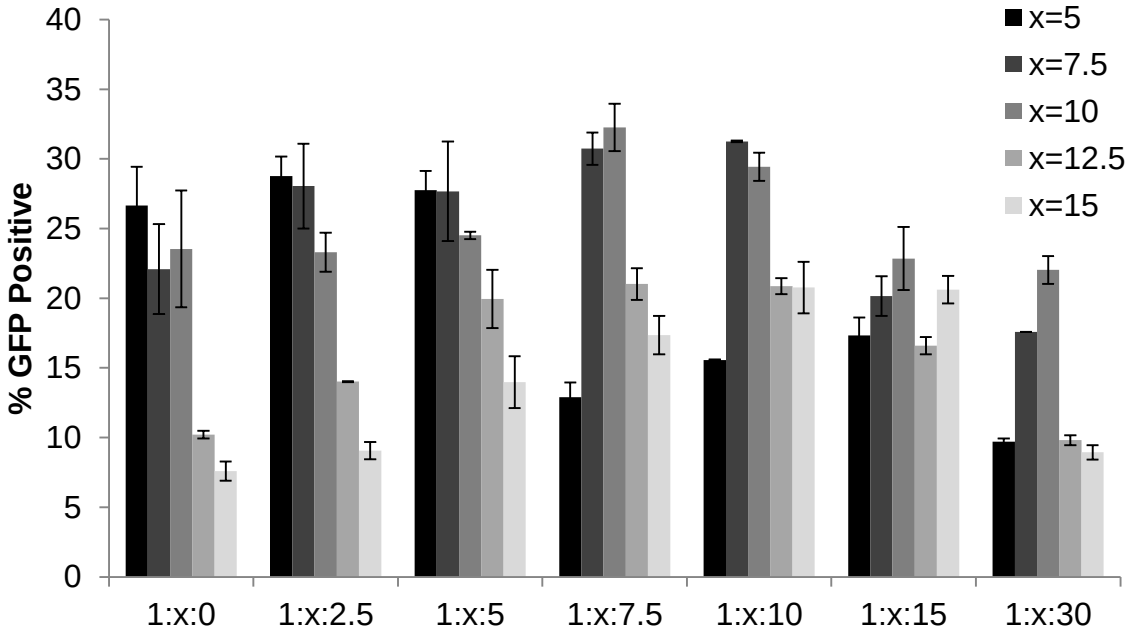

Figure 3.5: Gene transfection optimization at varying DNA:PVBLG-8:HA coating ratios (w:w:w).

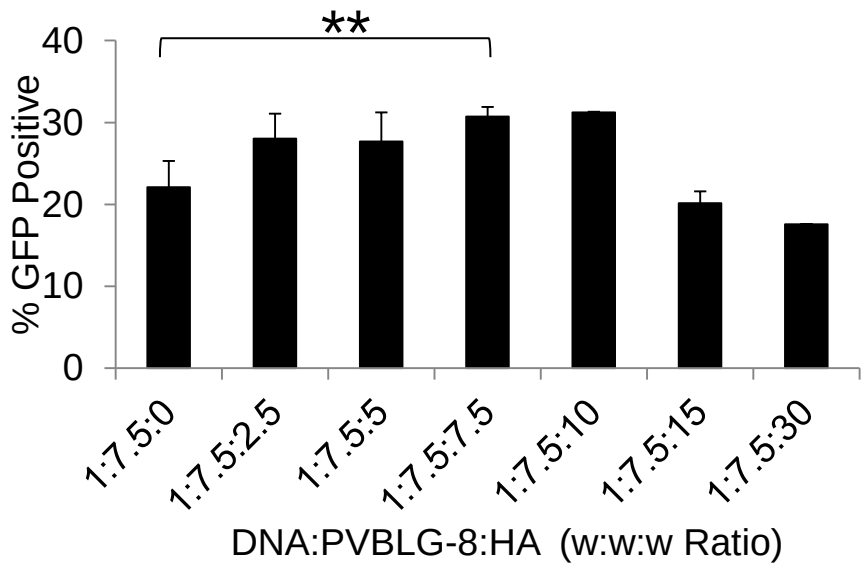

Figure 3.6: Transfection of hESCs with varying ratios of HA coating on DNA:PVBLG-8 nanocomplexes.

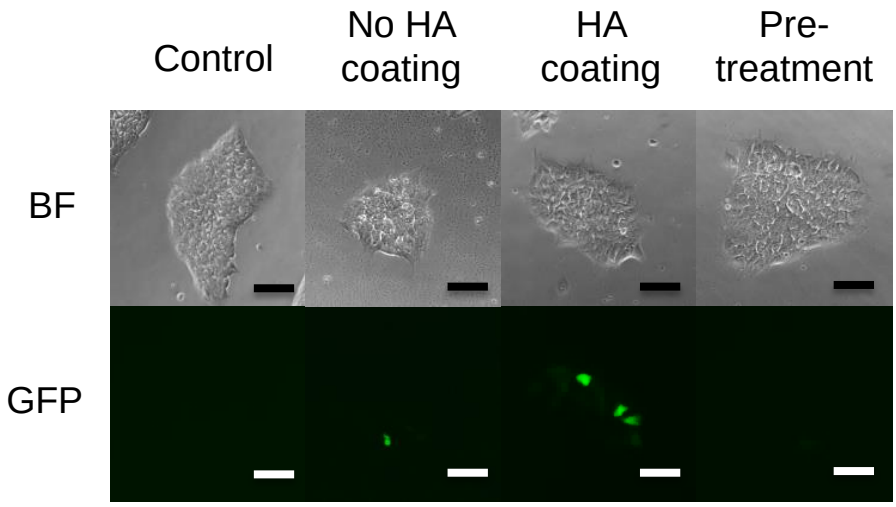

Figure 3.7: Fluorescence images of H1 hESCs 48 h post transfection with and without HA coated nanocomplexes and with 5 mg/mL free HA pretreatment. Scale bar: 250 µm

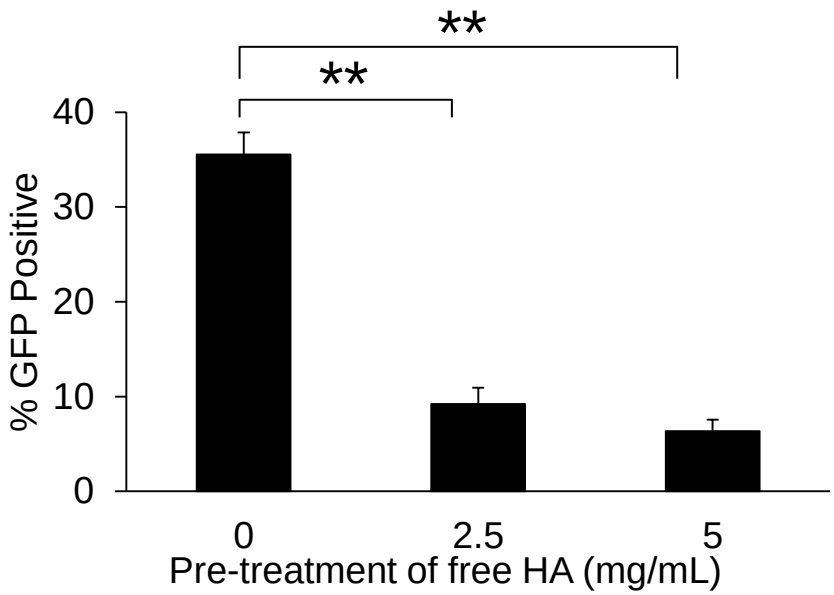

Figure 3.8: Transfection of 1:7.5:7.5 nanocomplexes in cells pretreated with 0, 2.5 or 5 mg/mL of free HA.

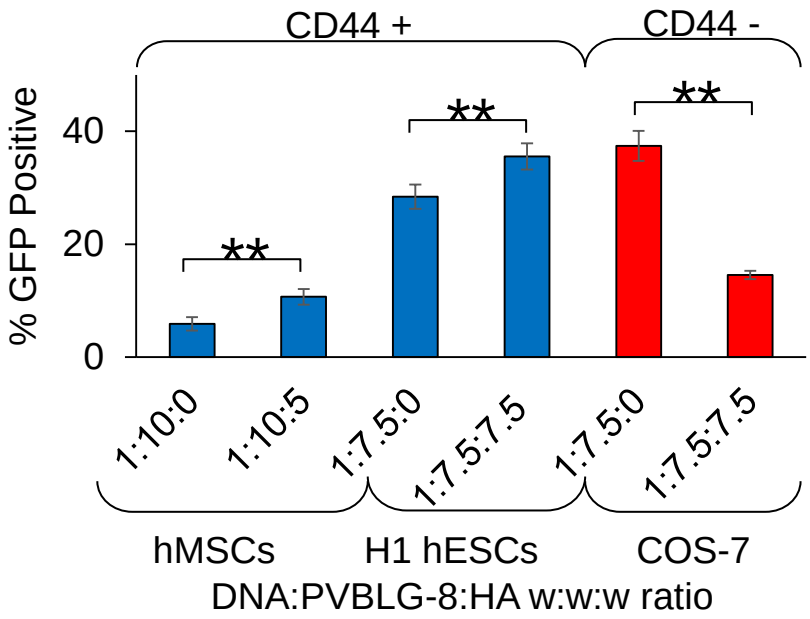

Figure 3.9: Transfection comparison between CD44+ hMSCs and hESCs, and CD44- COS-7 cells to demonstrate the effect of HA targeting.

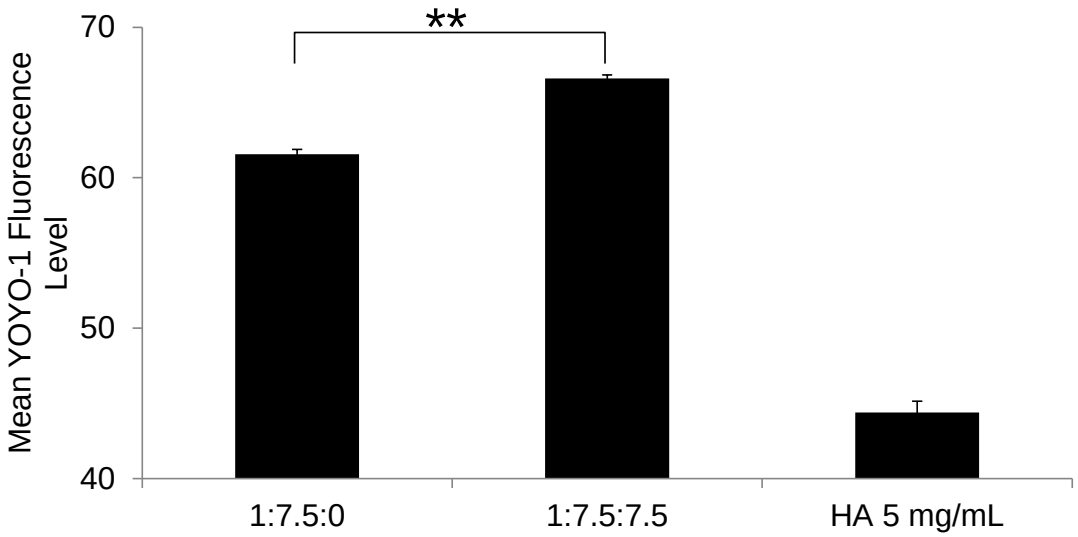

Figure 3.10: Cell uptake level of PVBLG-8/YOYO-1-DNA complexes in hESCs with varying amounts of HA coating and with the pretreatment of hESCs with free HA (n =3).

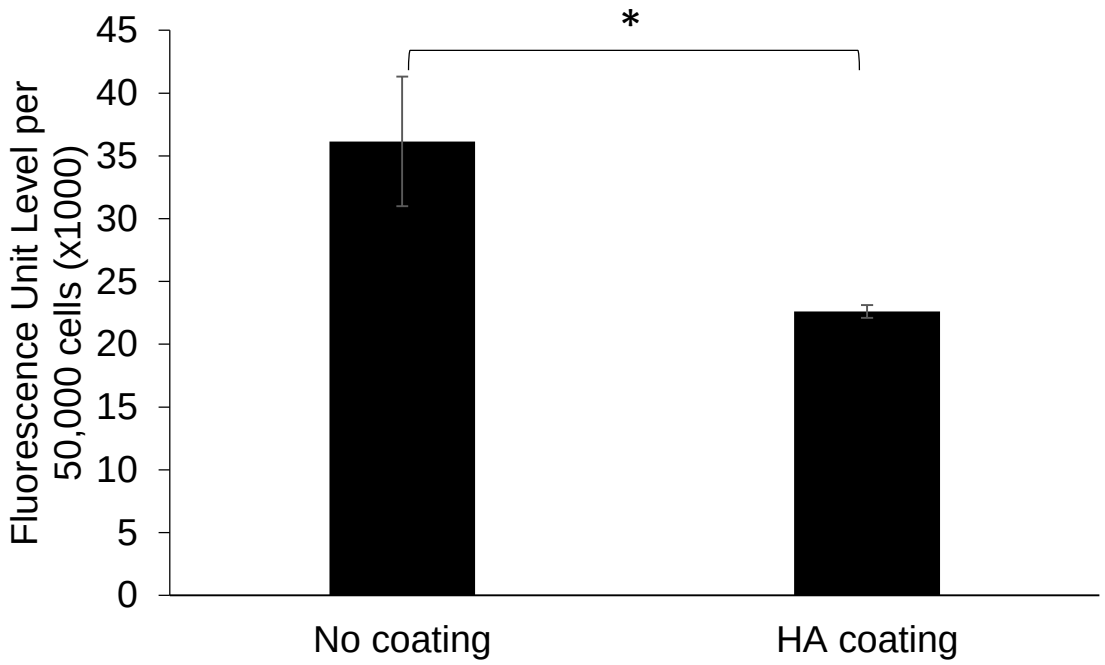

Figure 3.11: Cell uptake level of YOYO-1-DNA /PVBLG-8 complexes with and without HA coating in CD44 negative COS-7 cells at 1:7.5 weight ratios (n =3).

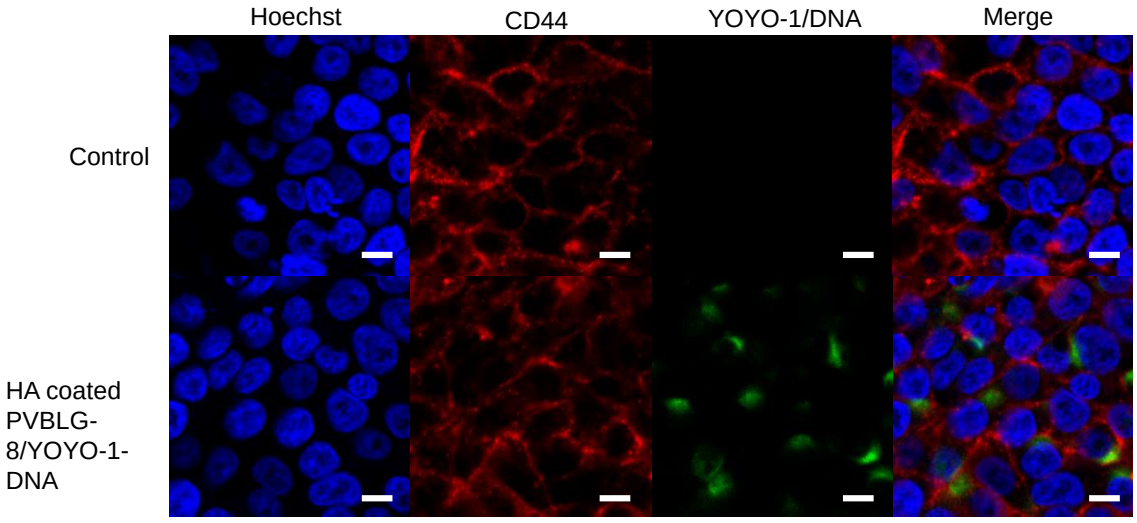

Figure 3.12: CLSM images of hESCs incubated with HA coated PVBLG-8/YOYO-1-DNA complexes at 4° C for 1 h with CD44 antibody staining. Scale bar: 10 µm

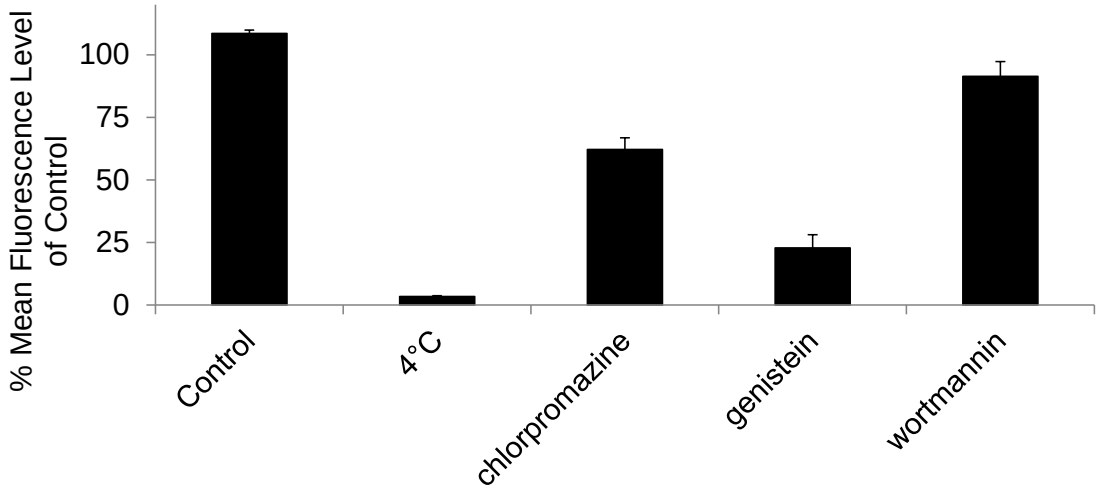

Figure 3.13: Cell uptake mechanisms HA coated PVBLG-8/YOYO-1-DNA complexes in hESCs through the pre-treatment and treatment of various endocytotis inhibitors (n=3).

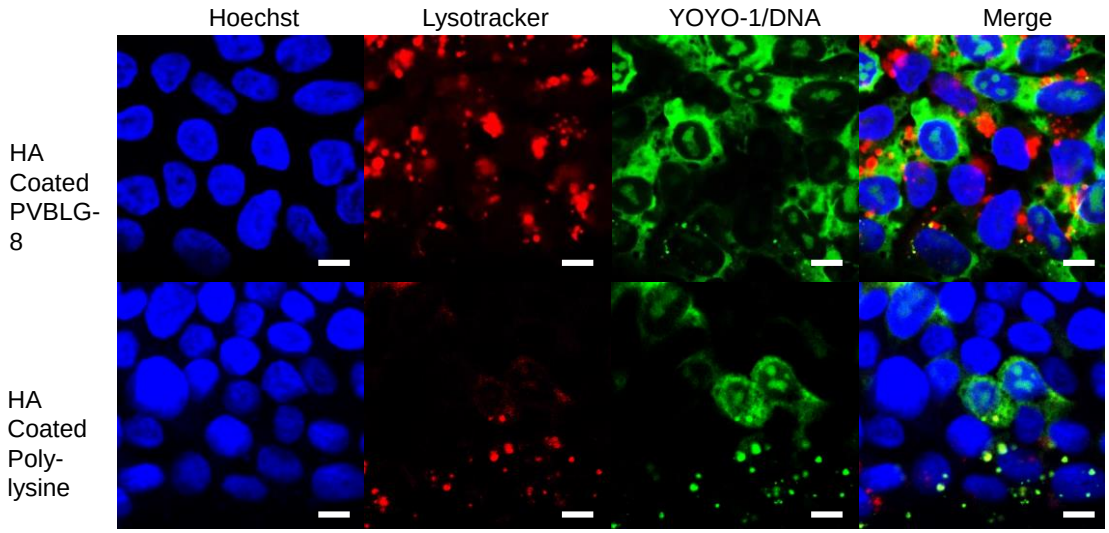

Figure 3.14: CLSM images of uptake of HA coated PVBLG-8/YOYO-1-DNA and Poly-L-lysine/YOYO-1-DNA complexes and with Lysotracker staining. Scale bar: 10 µm

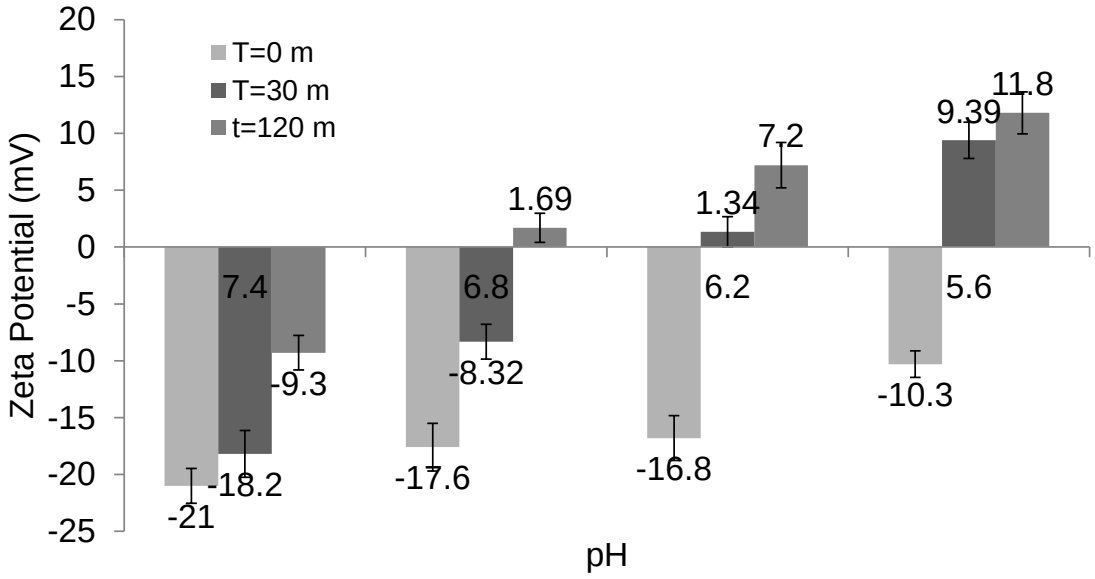

Figure 3.15: pH and HAase effect on HA coated nanocomplexes. Changes in the the zeta potential of DNA/PVBLG-8/HA nanocomplexes after treatment with 0.5 mg/mL of HAase at different pH values for different times.

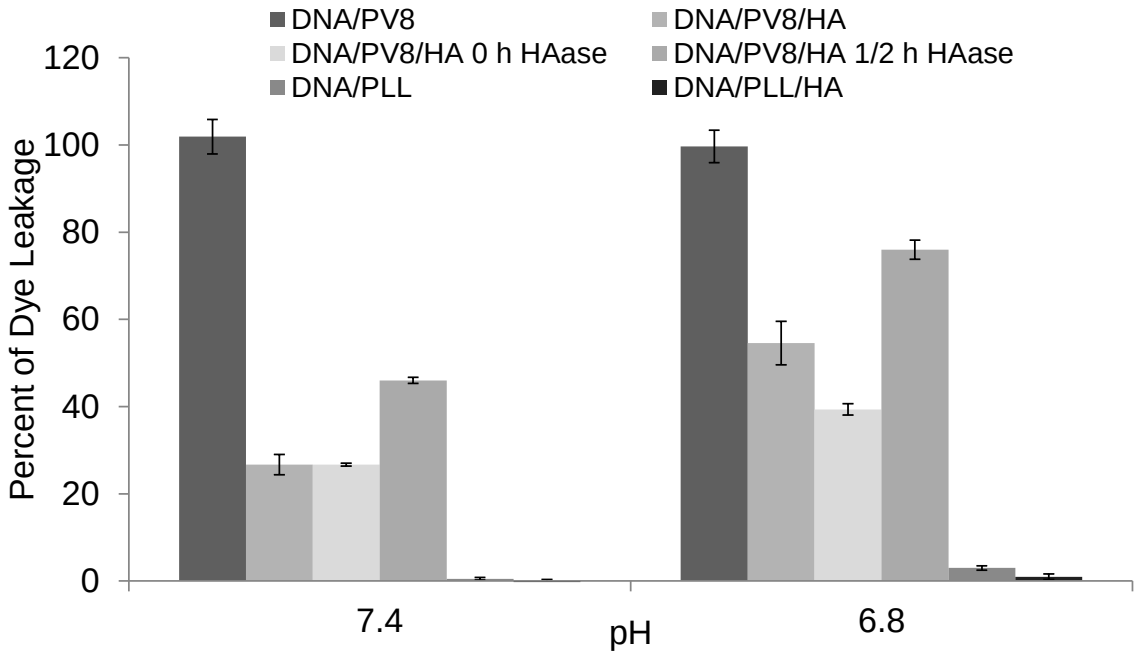

Figure 3.16: pH and HAase effect on HA coated nanocomplexes. ANTS/DPX loaded LUVET leakage study of different nanocomplexes with and without the HAase treatment at different pH values.

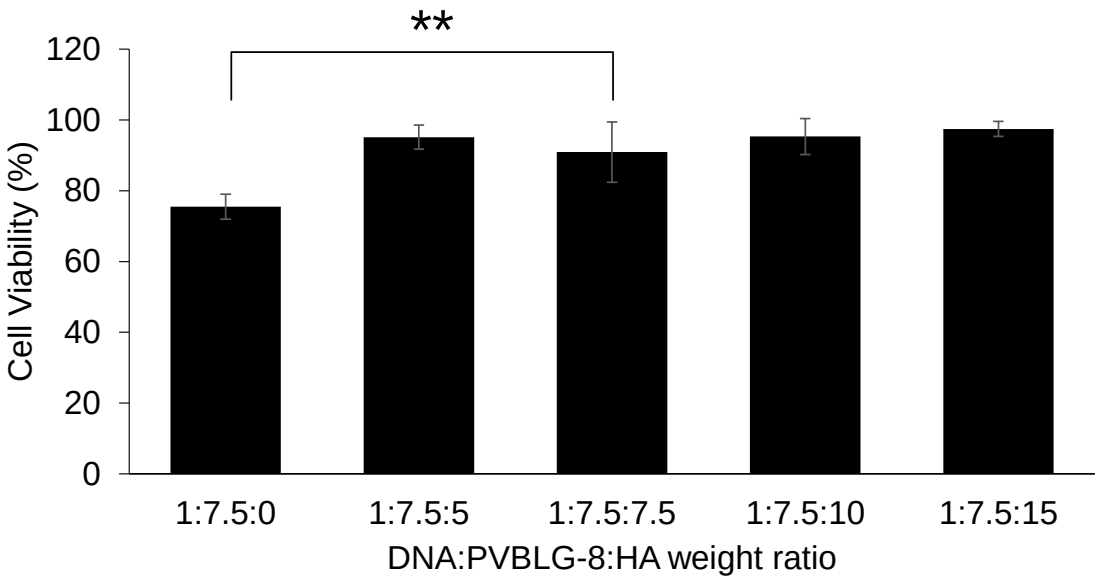

Figure 3.17: Cell viability of hESCs at varying ratios of HA coating of nanocomplexes as determined by MTT assay

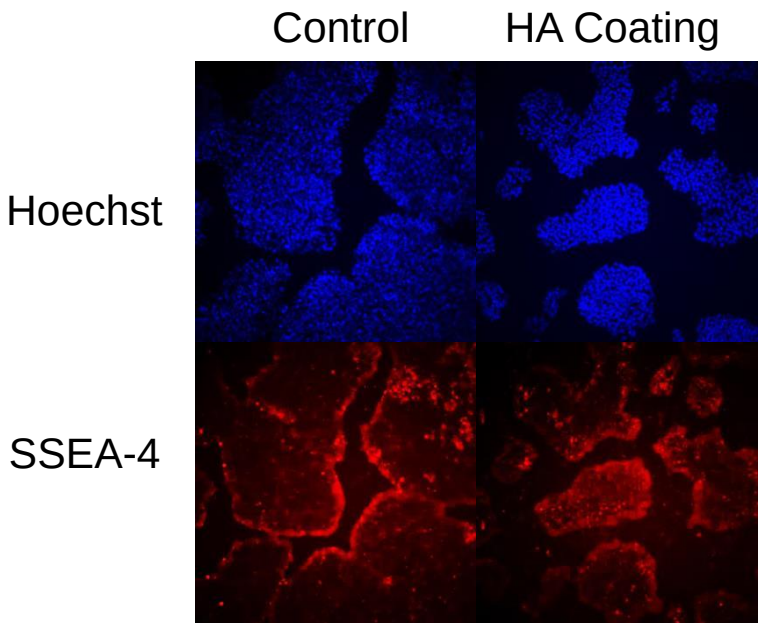

Figure 3.18: DAPI and SSEA4 staining patterns of hESCs 72 h after transfected with HA coated nanocomplexes. Scale bar: 250 µm

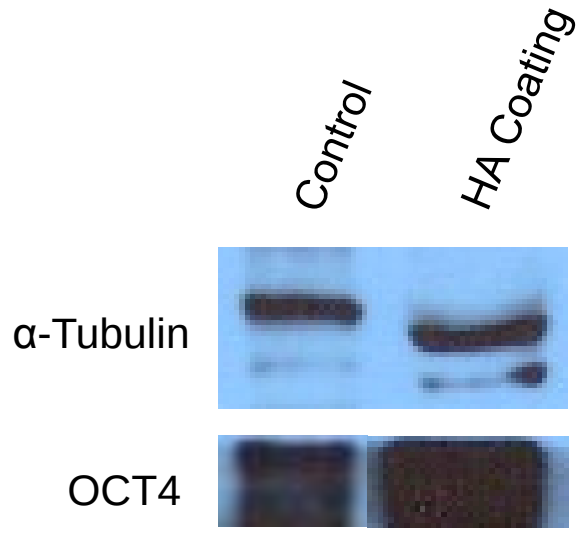

Figure 3.19: Western blot analysis on the OCT4 expression in hESCs 5 days post HA coated nanocomplexes transfection.

3.7 References

[1] Gabrielson NP, Lu H, Yin LC, Li D, Wang F, Cheng JJ. Reactive and Bioactive Cationic a-Helical Polypeptide Template for Nonviral Gene Delivery. Angewandte Chemie-International Edition 2012;51(5):1143-47.

[2] Yin L, Song Z, Kim KH, Zheng N, Tang H, Lu H, et al. Reconfiguring the architectures of cationic helical polypeptides to control non-viral gene delivery. Biomaterials 2013;34(9):2340-9.

[3] Yin LC, Song ZY, Kim KH, Zheng N, Gabrielson NP, Cheng JJ. Non-Viral Gene Delivery via Membrane-Penetrating, Mannose-Targeting Supramolecular Self-Assembled Nanocomplexes. Adv Mater 2013;25(22):3063-70.

[4] Zheng N, Yin LC, Song ZY, Ma L, Tang HY, Gabrielson NP, et al. Maximizing gene delivery efficiencies of cationic helical polypeptides via balanced membrane penetration and cellular targeting. Biomaterials 2014;35(4):1302-14.

[5] Zhang RJ, Yin LC, Cheng JJ. Effect of side chain profiles on helical polypeptide mediated non-viral gene transfection efficiency. Abstracts of Papers of the American Chemical Society 2013;246.

[6] Yen J, Zhang Y, Gabrielson NP, Yin L, Guan L, Chaudhury I, et al. Cationic, helical polypeptide-based gene delivery for IMR-90 fibroblasts and human embryonic stem cells. Biomaterials Science 2013.

[7] Yin LC, Tang HY, Kim KH, Zheng N, Song ZY, Gabrielson NP, et al. Light-Responsive Helical Polypeptides Capable of Reducing Toxicity and Unpacking DNA:

Toward Nonviral Gene Delivery. Angewandte Chemie-International Edition 2013;52(35):9182-86.

[8] Gerecht S, Burdick JA, Ferreira LS, Townsend SA, Langer R, Vunjak-Novakovic G. Hyaluronic acid hydrogel for controlled self-renewal and differentiation of human embryonic stem cells. Proceedings of the National Academy of Sciences 2007;104(27):11298-303.

[9] Cho HJ, Yoon HY, Koo H, Ko SH, Shim JS, Lee JH, et al. Self-assembled nanoparticles based on hyaluronic acid-ceramide (HA-CE) and Pluronic (R) for tumor-targeted delivery of docetaxel. Biomaterials 2011;32(29):7181-90.

[10] Cho HJ, Yoon IS, Yoon HY, Koo H, Jin YJ, Ko SH, et al. Polyethylene glycol-conjugated hyaluronic acid-ceramide self-assembled nanoparticles for targeted delivery of doxorubicin. Biomaterials 2012;33(4):1190-200.

[11] Choi KY, Chung H, Min KH, Yoon HY, Kim K, Park JH, et al. Self-assembled hyaluronic acid nanoparticles for active tumor targeting. Biomaterials 2010;31(1):106-14.

[12] Choi KY, Min KH, Na JH, Choi K, Kim K, Park JH, et al. Self-assembled hyaluronic acid nanoparticles as a potential drug carrier for cancer therapy: synthesis, characterization, and in vivo biodistribution. J Mater Chem 2009;19(24):4102-07.

[13] Choi KY, Min KH, Yoon HY, Kim K, Park JH, Kwon IC, et al. PEGylation of hyaluronic acid nanoparticles improves tumor targetability in vivo. Biomaterials 2011;32(7):1880-89.

[14] Kim EJ, Shim G, Kim K, Kwon IC, Oh YK, Shim CK. Hyaluronic acid complexed to biodegradable poly L-arginine for targeted delivery of siRNAs. J Gene Med 2009;11(9):791-803.

[15] Lu H, Wang J, Bai YG, Lang JW, Liu SY, Lin Y, et al. Ionic polypeptides with unusual helical stability. Nat Commun 2011;2:206.

[16] Bang EK, Gasparini G, Molinard G, Roux A, Sakai N, Matile S. Substrate-Initiated Synthesis of Cell-Penetrating Poly(disulfide)s. J Am Chem Soc 2013;135(6):2088-91.

[17] Smolarsky M, Teitelbaum D, Sela M, Gitler C. A simple fluorescent method to determine complement-mediated liposome immune lysis. J Immunol Methods 1977;15(3):255-65.

[18] Khalil IA, Kogure K, Akita H, Harashima H. Uptake pathways and subsequent intracellular trafficking in nonviral gene delivery. Pharmacol Rev 2006;58(1):32-45.

[19] Gratton SEA, Ropp PA, Pohlhaus PD, Luft JC, Madden VJ, Napier ME, et al. The effect of particle design on cellular internalization pathways. Proc Natl Acad Sci USA 2008;105(33):11613-18.

[20] Kneipp J, Kneipp H, Wittig B, Kneipp K. One-and two-photon excited optical pH probing for cells using surface-enhanced Raman and hyper-Raman nanosensors. Nano Lett 2007;7(9):2819-23.

[21] Mislick KA, Baldeschwieler JD. Evidence for the role of proteoglycans in cation-mediated gene transfer. Proc Natl Acad Sci USA 1996;93(22):12349-54.

[22] Ponta H, Sherman L, Herrlich PA. CD44: from adhesion molecules to signalling regulators. Nature reviews Molecular cell biology 2003;4(1):33-45.

[23] Hooper NM. Detergent-insoluble glycosphingolipid/cholesterol-rich membrane domains, lipid rafts and caveolae (review). Molecular membrane biology 1999;16(2):145-56.

[24] Dufaÿ Wojcicki A, Hillaireau H, Nascimento TL, Arpicco S, Taverna M, Ribes S, et al. Hyaluronic acid-bearing lipoplexes: physico-chemical characterization and in vitro targeting of the CD44 receptor. Journal of Controlled Release 2012;162(3):545-52.

[25] Akinc A, Thomas M, Klibanov AM, Langer R. Exploring polyethylenimine-mediated DNA transfection and the proton sponge hypothesis. J Gene Med 2005;7(5):657-63.

[26] Sonawane ND, Szoka FC, Verkman AS. Chloride accumulation and swelling in endosomes enhances DNA transfer by polyamine-DNA polyplexes. J Biol Chem 2003;278(45):44826-31.

Chapter 4:

Enhancement of gene delivery into human embryonic stem cells

4.1 Introduction

Considering the colony-forming properties of hESCs that limit non-viral gene delivery, I hypothesized that increasing cell spreading would increase cellular uptake and thus the gene transfection efficiency. Growing hESCs on stiffer substrates has shown to disperse cells and promote cell spreading[1,2], and it has also been shown in other cell types that an increase in the substrate stiffness can lead to higher transfection efficiency[3]. However, such an approach not feasible for hESCs, mainly due to the sensitive nature of hESCs to their external environment. It has been reported that hESCs grown on stiff substrates will start differentiating[4], but it indicates that cellular uptake is intrinsic to the stiffness and structure of the cells, and a decrease in membrane tension and contractility would lead to increased cellular spreading[5] and stimulate endocytosis[6].

Dissociation of hESCs into single cells or small colonies can potentially facilitate cell spreading. However, since hESCs are considered to be in the primed state, they are intolerant to single cell passaging and usually exhibit <1% clonal efficiency due to apoptosis upon cellular detachment and dissociation[7]. Rho-associated kinase (ROCK) inhibitor has been used to diminish dissociation-induced apoptosis, resulting in increased

survival of individual hESCs[7]. By pre-treatment of the hESCs with Y-27632 (10 μM) for an hour before single cell dissociation, the cloning efficiency increased to 27%. Cells treated with Y-27632 maintain their pluripotency and morphology for at least 5 passages and are able to differentiate into neural cells[7]. Therefore, with an attempt to facilitate hESC spreading without causing apoptosis, the selective ROCK inhibitor, Y-27632, was used to alter the cell's myosin fibers and mimic the cell's structure when grown on a stiffer substrate by inhibiting non-myosin IIA[8,9]. Y-27632 is also known to decrease cell-generated tension[10]. I hypothesized that Y-27632 would facilitate the spreading and flattening of hESCs colonies on plates due to decreased membrane tension, which would then increase the surface area exposure to allow for a more efficient uptake of gene delivery vectors and promote the gene transfection (Scheme 4.1). A broad spectrum of non-viral gene delivery vectors, including commercially available reagents (Lipofectamine 2000 (LPF), Fugene HD (FHD), poly-$_L$-lysine (PLL), poly-$_L$-arginine (PLR), and polyethyleneimine (PEI)), were evaluated in terms of their transfection efficiencies in the presence or absence of Y-27632. Mechanistic analysis into the effect of Y-27632 on cell spreading, cell uptake property, and pluripotency of hESCs was also performed. The treatment of hESCs with Y-27632 was revealed to significantly increase transfection efficiency of all the tested materials by 1.5 to 2 fold in hESCs, establishing an alternative use of Y-27632 as a tool for enhanced non-viral gene delivery.

4.2. Materials and Methods

4.2.1. General

Human embryonic stem cell line H1 (hESC-H1) was cultured in mTeSR 1 medium from Stem Cell Technologies (Vancouver, Canada). Fugene HD (FHD) was purchased from Promega (Madison, WI, USA). Y-27632 was purchased from Stemgent (Cambridge, MA, USA). Opti-MEM, Lipofectamine 2000 (LPF), and YOYO-1 were purchased from Invitrogen (Carlsbad, CA, USA). pEGFP-N1 was obtained from Elim Biopharmaceuticals (Hayward, CA, USA). Milli-Mark™ Anti-SSEA-4-PE was purchased from EMD Millipore (Billerica, MA, USA). PLL, PLR, and PEI were purchased from Sigma-Aldrich (St. Louis, MO, USA).

4.2.2. Instrumentation

Flow cytometry analysis was conducted on a BD LSRII color flow cytometry analyzer (Becton Dickinson, Franklin Lakes, NJ). Cells were visualized with a Zeiss Axiovert 40 CFL fluorescence microscope equipped with a 10x and 20x objective (Thornwood, NY). Fluorescence imaging was done using the GE InCell Analyzer 2000 from GE Healthcare Sciences (Piscataway, NJ, USA). Zeta potential and size analysis were conducted on a Malvern Zetasizer (Worcestershire, UK).

4.2.3 Preparation and characterization of nanocomplexes

Various non-viral vectors were used for the transfection analyses. Plasmid DNA (1 µL, 1 mg/mL) was diluted with water (50 µL). The transfection reagent, polyarginine (10

μL, 1 mg/mL), polylysine (10 μL, 1 mg/mL), or polyethylenimine (5 μL, 1 mg/mL) was diluted with water (50 μL). The two solutions were then vortexed gently and allowed to incubate for 20 min at rt, after which they were combined and allowed to incubate for another 20 min at rt.

Plasmid DNA (1 μL, 1 mg/mL) was diluted with mTeSR (50 μL). The transfection reagent, LPF (2 μL, 1 mg/mL) was diluted with mTeSR (50 μL). The two solutions were then vortexed gently and allowed to incubate for 20 min at rt, after which they were combined and allowed to incubate for another 20 min at rt.

Various non-viral vectors were used for the transfection analyses. Plasmid DNA (1 μL, 1 mg/mL) was diluted with mTeSR (50 μL). The transfection reagent, FHD (3.5 μL, 1 mg/mL) was added to the DNA solution. The solution was then vortexed gently and allowed to incubate for 20 min at rt, after which they were combined and allowed to incubate for another 20 min at rt.

Solutions of plasmid DNA (5-25 μg/mL) were prepared in water or medium. Separately, a solution of 50 μg of the vectors was prepared in 400 μL water. A solution of 50 μl LPF and FHD in 400 μL media was also prepared as a control. The DNA solution was then mixed with the vectors, LPF, or FHD solution and allowed to incubate at room

temperature for 20 min. Dynamic light scattering (DLS) and zeta potential analysis were conducted on the samples with a Malvern Zetasizer.

4.2.4 hESC Transfection with Y-27632

hESCs were seeded on Matrigel-coated 24-well plates and cultured in mTeSR medium for 24 h. For the full treatment group, Y-27632 was added into the culture medium at a final concentration of 0, 10, 30 or 50 μM for 4 h prior to the transfection. Nanocomplexes prepared from pEGFP-N1 plasmid and different transfection vectors were added dropwise into the media and cells were cultured at 37°C for 4 h. For the pre-treatment group, cells were treated with Y-27632 (50 μM) for 4 h at 37°C prior to transfection. The cells were then washed with PBS and fresh media was added prior to the addition of the nanocomplex and further incubation at 37°C for 4 h. For the post-treatment group, cells were treated with Y-27632-free medium for 4 h prior to transfection. Directly prior to transfection, the medium was replaced with Y-27632 (50 μM) containing medium, and cells were transfected with various vectors at 37°C for 4 h. In all three cases, 4 h after treatment with the nanocomplexes, the media was replaced with fresh mTeSR and cultured for 48 h before measurement of the transfection efficiency by flow cytometry. Alternatively, 10 μM of blebbistatin, a non-muscle myosin IIA inhibitor, downstream of the rho-associated protein kinase, was added to the cells prior to and during transfection.

4.2.5 Intracellular Uptake Studies

DNA (1 mg/mL) was labeled with YOYO-1 (20 μM) at one dye molecule per 50bp of DNA[11], and was allowed to form nanocomplexes with transfection reagents as described above. hESCs were plated on matrigel coated 24-well plate and cultured until they reached medium (50 cells) sized colonies. Nanocomplexes were added at 1 μg YOYO-1-DNA/well and cells were incubated at 37°C for 4 h. Cells were then harvested, re-suspended in PBS, and subjected to flow cytometry analysis to quantify the cellular uptake level of YOYO-1-DNA.

To elucidate the mechanisms underlying the cellular internalization of FHD/DNA nanocomplexes, the uptake study was performed at 4 °C or in the presence of various endocytic inhibitors. Cells were pre-treated with chlorpromazine (10 μg/mL), genistein (200 μg/mL), methyl-β-cyclodextrin (mβCD, 50 μM), dynasore (80 μM), or wortmannin (50 nM) for 30 min before addition of the nanocomplexes and throughout the uptake study at 37°C for 2 h. Results were expressed as percentage uptake level of control cells that were treated with the nanocomplexes at 37 °C for 2 h in the presence of Y-27632 (50 μM) while in the absence of endocytic inhibitors.

4.2.6 hESC spreading and transfection analysis

hESC H1 were plated on matrigel coated 96-well plates as medium sized colonies and cultured for 24 h. Y-27632 was added at various concentrations (0, 10, 20, and 50 μM)

and after 4 h incubation, the cell nuclei were stained with Hoechst 33258 and the cytoplasm was stained with CellTracker Red CMTPX per manufacturer's protocols. Five wells were imaged with 9 fields each using the GE InCell Analyzer 2000 in the Hoechst and Texas Red channel (Fig. 4.17). The images were then analyzed using the GE InCell Analyzer workstation. The nuclei were identified using top-hat segmentation in the Hoechst channel, and the cell area was analyzed and calculated through the analysis in the CMPTX channel using multiscale top-hat. The cytoplasmic area was then normalized to the number of nuclei counted.

hESC H1 were seeded on matrigel-coated 24-well plates and cultured in mTeSR medium for 24 h. Before transfection, Y-27632 was added into the culture medium at a final concentration of 0, 10, 30 or 50 μM, and incubated at 37 °C for 4 h. Nanoparticles from pEGFP-N1 and FHD were added dropwise into the culture medium and cells were further incubated at 37°C for 4 h. The medium was then replaced with fresh mTeSR medium, and cells were further cultured for 48 h. After 48 h, the cell nuclei were stained with Hoechst 33258. Forty-five fields were imaged using the GE InCell Analyzer 2000 in the Hoechst and GFP channel (Fig. 4.18). Using the InCell Analyzer Workstation, the nuclei were identified using top-hat segmentation in the Hoechst channel and the numbers of cells were then calculated. The identified nuclei were then further segmented by multiscale top-hat in the GFP signal to determine the number of cells with positive GFP

signals. The transfection efficiency was then determined by dividing the number of GFP positive cells by the total number of cells.

4.2.7 siGLO Green Delivery into hESC

Two wells of a 6 well plate of hESC H1s or WA01 OCT4 GFP KI H1 were plated into a 24 well plate coated with Matrigel a day or two before transfection. Y-27632 at 0 μM, 10 μM or 30 μM was added to the cells 4 hours before transfection. For transfection with Lipofectamine 2000 with incubation, siGlo Green (30 picomoles) was added to Optimem (50 μL) and Lipofectamine (1 μL, 1 mg/mL) was added to another tube of Optimem (50 μL). The two solutions were mixed and incubated at room temperature for 20 minutes and added directly to the cells. For the alternative method, instead of mixing the two solutions, the polymer solution was added directly to the cells first and then the solution containing the siGlo Green was added separately to the cells right after. The cells were incubated for either 48 hours and collected and analyzed with flow cytometry.

4.2.8 RITC Silica nanoparticle synthesis

Methanol (1.0 mL), DI water (0.27 mL), and concentrated ammonia (0.24 mL) were mixed. TEOS (62.5 μL, 0.28 mmol) was then added to the solvent mixture followed by the addition of a DMSO solution (20 μL) of trimethylorthosilicate (2 mg, 4.3 μmol). Fabrication of monodisperse RITC-NCs with other sizes can be similarly achieved by tuning the concentrations of TEOS, water, and ammonia. After the reaction was complete,

without isolating the NCs, a methanol solution of RITC-trimethylorthosilicate (10 mg/mL, 100 μL) was added to the silica NC solution. The mixture was stirred for 12 h in the dark. A methanol solution of mPEG-sil (10 mg/mL, 100 μL) was added. RITC-NCs were collected by centrifugation at 15k rpm, washed with ethanol (3 × 1 mL), and redispersed in DI water or 1× PBS buffer before use. [12]

4.2.9 hESC RITC-SNP Uptake

Two wells of a 6 well plate of hESC H1s or WA01 OCT4 GFP KI H1 were plated into a 24 well plate coated with Matrigel a day or two before transfection. Y-27632 at 0 μM or 3 μM was added to the cells 4 hours before transfection. The RITC-SNP (30-40 μg) was added to the wells and incubated for 2h. The cells were then washed with PBS (3x) and analyzed with flow cytometry.

4.2.10 Sample preparation and flow cytometry analysis

Prior to analysis by flow cytometry, transfected cells on the 24-well plate were washed with PBS (3 × 500 μL) to remove any residual serum, dead cells, and debris. Accutase (100 μL) was added to detach the cells from the plate, and PBS (100 μL) was then added to re-suspend the cells. An aqueous solution of paraformaldehyde (4%, 100 μL) was added to fix the cells, which were then subject to flow cytometry analysis.

4.2.11 Cell viability

For the MTT assays cytotoxicity assessment, 1 6-well well of confluent hESCs was plated into 24 wells of a matrigel coated 48-well plate one day before transfection. The cells were then pre-treated for 4 h with 0, 10, 30, and 50 µM of Y-27632 for 4 h and transfected with FHD as described previously. The cells were further incubated for 4 h at 37°C in the transfection mix before removal of the transfection reagent and replacement of fresh media. After 48 h, the cell viability was monitored by the MTT assay and was represented as percentage viability of control cells that did not receive any transfection treatment. For the MTT assay, the cells were washed with PBS and MTT solution was added. Following 4-h incubation at 37°C, MTT solubilization solution (10% Triton X-100 in acidic (0.1M HCl) isopropanol) was added to the cells and the absorbance of 570 nm light was quantified on a Perkins Elmer plate reader (Waltham, MA, USA).

4.2.12 Western blot analysis and SSEA-4 staining

After 72 h, the cells were stained with DAPI (250 µL, 3 nM) and SSEA-4–PE (250 µL, 0.02 mg/mL), a pluripotency cell marker, for 30 min at 37 °C. The cells were imaged using the GE InCell Analyzer 2000.

After 4 d treatment of 50 µM Y-27632 and FHD transfection, the cells were lysed with the RIPA buffer, mixed with Laemmli buffer supplemented with 2-Mercaptoethanol, and heated at 100 °C for 5 min to denature the proteins. After being cooled in ice, the

samples were subjected to electrophoresis on a 10% SDS PAGE Gel at 120 V for 1.5 h, and wet transferred to the nitrocellulose membrane using the AMRESCO Rapid Western Blot Kit per manufacturer's instructions. The membrane was stained with OCT4 and α-Tubulin primary antibodies and then with HRP-tagged secondary.

4.3 Results

4.3.1 Inhibition of Rho-associated kinase facilitates non-viral gene transfection

Prior to the transfection assessment, the pEGFP-N1 plasmid nanocomplexes with the gene transfection vectors were evaluated by dynamic light scattering and zetasizer to determine their complexation capacities. I confirmed that all tested materials were able to form nanocomplexes with DNA, as reported by many other prior studies. Upon complexation with DNA, the nanocomplexes of DNA with PLR, PLL and PEI gave sizes around 60-70 nm while DNA complexes with LPF and FHD following the standard protocol afforded much larger particle size (above 300 nm, Fig. 4.1). PLR, PLL, and PEI are cationic polymers with sufficiently long backbones so that they can well condense the anionic DNA into compact nanocomplexes via electrostatic interaction as well as intermolecular entanglement. In comparison, LPF and FHD are cationic lipid based materials, and their short molecular length would prevent sufficient entanglement with the DNA molecules, thus leading to relatively larger complexes.

Transfection efficiency of each material was then evaluated in the presence (50 μM) or absence of Y-27632 by monitoring the EGFP expression, attempting to probe the effect of Y-27632 on gene transfection. As shown in Fig. 4.2, PLR was unable to mediate transfection in H1 hESCs (transfection efficiency < 1%), which was consistent with previous findings in multiple cell lines[13,14]. Upon the treatment of Y-27632, all other materials significantly increased their transfection efficiency of hESCs as measured by flow cytometry. Specifically, the PLL transfection efficiency with Y-27632 increased from 3.0 ± 0.8% to 5.8 ± 0.8%. For PEI mediated transfection, the transfection efficiency increased from 7.7 ± 0.8% to 13.7 ± 1.3% in the presence of Y-27632. Similar enhancement of gene transfection efficiencies was observed with the use of Y-27632 when LPF and FHD were used as transfection agents. Their transfection efficiencies improved from 8.8 ± 0.8% to 15.3 ± 1.2% and 21.5 ± 0.9% to 37.0 ± 1.0%, respectively. These studies clearly demonstrate that Y-27632 treatment can universally increase the transfection efficiency by approximately 1.7 to 1.9 fold in non-viral gene delivery to hESCs.

4.3.2 Y-27632 treatment increases cell spreading

To further investigate the treatment effect of Y-27632, transfection studies were performed on H1 hESC colonies that were treated with varying concentrations of Y-27632 for 4 h prior to and during transfection. DNA/FHD complexes, which displayed the highest transfection efficiency among all tested systems, were selected for further studies. With no

treatment, the EGFP transfection efficiency was 14.4 ± 0.9%. With 10 μM treatment of Y-27632, the transfection efficiency increased to 17.6 ± 1.4%. When the concentration of Y-27632 was increased to 30 μM and 50 μM, the respective efficiency increased to 22.7 ± 0.8% and 26.4 ± 1.1% (Fig. 4.3-4.4). To confirm that the mechanism of increased transfection efficiency was due to the spreading and actin-myosin interactions, the cells were treated with blebbistatin, a small molecule that acts downstream of Y-27632[15], inhibits non-muscle myosin IIA, reduces actin/myosin interactions and alters the intracellular structure and morphology. Treatment of blebbistatin at 10 μM also resulted in increased transfection efficiency of DNA/FHD complex up to 17.8 ± 0.4%, indicating a strong correlation between cell structure and transfection efficiency (Fig. 4.3).

When hESC colonies were treated with Y-27632 for 4 h at varying concentrations (10, 30, and 50 μM), significant morphological changes of the cells were observed. In the absence of Y-27632, the cells maintained a two-dimensional cobble stone like colony morphology, and the cells were tight and rounded up (Fig. 4.5). At 10 μM, the colonies started to spread and lose their rounded-up structure. At 30 and 50 μM, the cells were even more spread out and elongated, further indicating that they had relaxed their original structure. This increased the surface area and decreased the surface membrane tension. To further validate the Y-27632-mediated cell spreading, the cytoplasm and nuclei of the Y-27632-treated cells were respectively labelled before cells were imaged and analysed using

the GE InCell Analyzer (Fig S4.1). Without Y-27632 treatment, the cells were calculated to have a cytoplasmic area of 445 ± 29.8 μm^2 per cell. When treated with Y-27632 at 10, 30, and 50 µM, the cytoplasmic area per cell increased to 516 ± 8.0, 563 ± 32.7 and 589 ± 18.6 μm^2, respectively (Fig. 4.6). The increased cytoplasmic area thus substantiated the promotion of cell spreading upon Y-27632 treatment. Through further analysis of the cell spreading effect on transfection efficiency, the GFP efficiency was also measured using the GE InCell Analyzer and InCell Workstation (Fig S4.2). With the increased spreading, the GFP transfection efficiency increases from about 6.3 ± 3.4% at 0 µM to 10.9 ± 4.4%, 22.8 ± 0.6% and 30.6 ± 1.7% at 10, 30, and 50 µM of Y-27632 treatment, respectively (Fig 4.6). Through the GE InCell imaging analysis of the hESCs cytoplasmic area and GFP expression, correlation between the cell spreading and GFP transfection upon the treatment of Y-27632 was noted.

4.3.3 Sequential treatment of Y-27632 and uptake inhibition study

To study the importance of morphological changes, hESCs were treated with Y-27632 in three different stages, with FHD as the model vector. When the cells were treated with Y-27632 for 4 h and removed before transfection, the transfection efficiency was 28.9%. When the cells were treated with Y-27632 only during the transfection for 4 h, the transfection efficiency decreased to 25.4%. Finally, when the cells were treated for 4 h before and during the transfection with Y-27632, the transfection efficiency increased to

31.3% (Fig. 4.7). The increase in transfection when the hESCs were pretreated with Y-27632 indicates the importance of altering the cell morphology before the transfection.

A further uptake study of the YOYO-1-DNA was conducted at various concentrations of Y-27632. In the absence of Y-27632, 67% of the cells had taken up the FHD/YOYO-1-DNA nanocomplexes. When the concentration of Y-27632 was increased from 10 to 50 μM, the uptake level continued to increase to 95%, in consistence with the transfection trend (Fig. 4.8). Such observation indicated that Y-27632 promoted the overall cellular uptake of the nanocomplexes as a result of facilitated colony spreading, which ultimately potentiated the transfection efficiency.

The internalization mechanism is often closely related to the intracellular fate and ultimately the transfection efficiency. To this end, the effect of Y-27632 on the intracellular kinetics was further probed by monitoring the cell uptake in the presence of different endocytic inhibitors. Energy dependent endocytosis was blocked at 4°C; clathrin mediated endocytosis was blocked by chlorpromazine by triggering dissociation of the clathrin lattice; caveolae was inhibited by genistein and mβCD by inhibiting tyrosine kinase and depleting cholesterol, respectively; clathrin mediated endocytosis and caveolae were inhibited by dynasore by inhibiting dynamin; macropinocytosis was inhibited by wortmannin by inhibiting phosphatidyl inositol-3-phosphate[16,17]. As shown in Fig. 4.9, through the different inhibition of endocytotic pathways, the uptake of YOYO-1-DNA did

not diminish through the use of the inhibitors. On the other hand, at 4°C, there was a decrease in uptake efficiency. This suggests that the FHD nanocomplexes entered the cells partially via energy dependent endocytosis, but not through clathrin and caveolae mediated endocytosis or macropinocytosis. Interestingly, there was an increase of uptake at 4°C from 50% to 75% in the Y-27632 treated cells. Potentially, this denotes the decreased energy requirement for endocytosis with the treatment of Y-27632.

4.3.4 Combination of Y-27632 treatment with HA coated nanocomplexes

To demonstrate the combined effect of Y-27632 treatment and HA coated DNA/PVBLG-8 nanocomplexes, the two methods were combined in their transfection into H1 hESCs. Using the optimal transfection ratios of 1:7.5 (DNA:PVBLG-8 weight ratios) and 1:7.5:7.5 (DNA:PVBLG-8:HA weight ratios), the transfection efficiency increases from 11.2% to 15.4% GFP positive for PVBLG-8 only transfection with and without Y-27632 treatment, respectively. Finally, using the HA coated nanocomplexes the transfection efficiency increased to 16.8% and 24.5% GFP positive with and without Y-27632 treatment, respectively. This indicates that coupling the two systems does significantly increase the transfection efficiency.

4.3.5 siSRNA siGLO Green uptake

Transfection of siRNA siGlo Green was performed using Lipofectamine 2000 with the treatment of Y-27362 at 0 μM, 10 μM, and 30 μM concentrations with uptake

efficiencies of 55.67%, 75.4% and 85.92%, respectively, again demonstrating the effects of transfection efficiency enhancement of Y-27632 (Fig. 4.11).

4.3.6 Nanoparticle uptake

In the initial study, 3 sizes of silica nanoparticles tagged with RITC (RITC-SNP) were synthesized using the Stober method [12], 200, 51 and 25 nm. Two sets of RITC-SNP were synthesized one with and one without PEG surface modifications. These RITC-SNP were incubated for 2 h with the cells treated with 0 μM or 30 μM Y-27632. For the 200, 50, 25 nm sized RITC-SNP with no surface modifications, the transfection efficiencies without Y-27632 treatment and incubated for 2 h were 1.75%, 1.23% and 0.65%, respectively. The transfection efficiencies for cells treated with 30 μM Y-27632 were 9.5%, 6.5% and 3.5% (Fig. 4.12). For the 200, 50, 25 nm sized RITC-SNP with no surface modifications the transfection efficiencies without Y-27632 treatment and incubated for 5 h were 70.03%, 86.54% and 86%, respectively. The transfection efficiencies for cells treated with 3x Y-27632 were 83.61%, 92.65% and 94.53% (Fig. 4.13). These trends demonstrated higher uptake with the treatment or Y-27632 in hESC, especially with the use of non-surface modified RITC-SNP.

4.3.7 Treatment of Y-27632 maintains pluripotency of hESCs

Treatment of hESCs with Y-27632 at the concentration of 50 μM significantly increases non-viral transfection efficiency. The treated cells can also revert back to their

normal hESC morphology 48 h post-treatment (Fig. 4.4). This study demonstrates that Y-27632 only transiently alters the hESC morphology to facilitate improved gene delivery. To further confirm whether the hESCs were only transiently altered by the treatment of Y-27632 and FHD transfection, extracellular stage specific embryonic antigen 4 (SSEA-4) was stained with PE conjugated antibodies and imaged 72 h post transfection with 50 μM Y-27632 treatment (Fig. 4.14). The cells stained uniformly positive for SSEA-4, indicating well-maintained pluripotency. A western blot assay of the hESCs conducted 4 days post FHD/DNA transfection with Y-27632 also indicated unaltered expression of OCT4, a gene indicator of hESC pluripotency. With the treatment of Y-27632 at all concentrations, there was no change in the OCT4 expression. However, when treated with 10, 30, and 50 μM of Y-27632 in the presence of FHD, a slight reduction in the OCT4 expression level was observed, indicating that Y-27632 itself did not affect pluripotency and the minor change of OCT4 expression could be induced by the transfection reagent. These experiments substantiated that gene transfection and Y-27632 treatment were transient and the cells were able to revert back to their natural pluripotent state after removal of Y-27632 (Fig. 4.15). The treatment of hESCs with Y-27632 also showed no cytotoxicity to the cells at any treatment concentrations (Fig. 4.16). The Y-27632 treatment at any of the concentrations for transfection demonstrated only transient alteration of the cells with well-retained pluripotency and low cytotoxicity.

4.4 Discussion

In the current study, I demonstrated that with the treatment of Y-27632, transfection efficiencies of a variety of non-viral gene delivery materials in hESC, including PLR, PLL, PEI, LPF, and FHD, were markedly augmented. Y-27632 allowed the hESC colonies to effectively transform their internal mechanical structure by inhibiting the actin-mysoin contractility and cell-to-cell adhesion, thus facilitating spreading of the cells. As such, the exposed surface area was increased and the membrane tension was decreased, ultimately leading to an increase in the internalization level of exogenous genetic materials. Using one of the most efficient commercial transfection reagents, FHD, I demonstrated a dose dependent effect of Y-27632 small molecule treatment in hESCs. An increase in the Y-27632 concentration from 0 to 50 μM correlated to a 1-fold increment in the transfection efficiency. To ensure that the increased transfection efficiency was due to the actin-myosin inhibition effect on the spreading or morphology change of the cells and not the other pathways associated with the rho-associated protein kinase pathway, the cells were also treated with 10 μM blebbistatin. Blebbistatin acts downstream of the rho-associated protein kinase, and directly inhibits non-muscle myosin IIA. This inhibition directly decreases the affinity of myosin with actin, indicating that the Y-27632's role in the cell morphological change is responsible for the increased gene transfection.

From the treatment of varying concentrations of Y-27632, the cell's morphology changes from a rounded up structure to an elongated flat morphology and disassociation from the colony. This flattening and spreading of the cells increased the cell surface area

that was exposed to exogenous nanocomplexes, and thus the nanocomplexes were more readily taken up by the cells. A higher Y-27632 concentration resulted in enhanced cell spreading and ultimately increased transfection efficiency. The important role of Y-27632 in increasing cell adhesion and survival also helped the cells to maintain physiological functions, thus contributing to the transfection process[1]. In addition, through the spreading and elongation of the cells, the cell membrane could have also decreased membrane tension, allowing for a higher rate of endocytosis [5,6]. With decreased membrane tension, the energy required for endocytosis is lowered [6], which is shown in the 4°C FHD nanocomplex uptake experiment, in which the uptake efficiency increased with the treatment of Y-27632.

It is important that the cells be transiently altered before transfection, so that the spreading of the cells and decrease of the membrane tension could allow for efficient nanocomplex uptake. In our detailed study on the adding sequence of Y-27632, pretreated cells showed significantly higher transfection efficiency than post-treated cells, indicating the importance of morphological change prior to the transfection process. The altered morphology primes the cells by increasing the cytoplasmic area and facilitating the uptake of the nanocomplexes during transfection. In consistence with our findings that cells in smaller colonies afforded higher transfection efficiencies (data not shown), it was further demonstrated that Y-27632-mediated cell spreading and larger cell surface area is attributed to the decreased surface tension and de-clumping of the cell colonies.

Not only does the pre-treatment with Y-27632 enhance DNA plasmid and siRNA nanocomplexes, but it also can enhance the uptake of other nanoparticles, like unmodified silica nanoparticles at a varying sizes. As expected, there is a correlation between the uptake efficiency and nanoparticle size. For smaller nanoparticles (20-25 nm), the higher the uptake efficiency, while larger nanoparticles (200 nm) have much lower uptake efficiency. When increasing time of incubation of the nanoparticles, there is a drastic increase of nanoparticle uptake. Yet in both cases, the treatment of Y-27632 increases does significantly increase the uptake efficiency, indicating that the system works for the uptake of all kinds of nanoparticles.

I have also demonstrated that the system of transient change of cell morphology with the smart and targeting system can overall significantly increase gene transfection efficiency. With the treatment of Y-27632 there is an increase in the transfection of PVBLG-8 nanocomplexes, but with also increased cytotoxicity (data not shown). Then with the further addition of the HA coating, the transfection efficiency is significantly increased, indicating that Y-27632 treatment does not affect caveolae and receptor mediated endocytosis pathways, indicating that the system can be coupled together. But further optimization is required to bring the two systems together effectively to reach the optimal transfection efficiency applicable to stem cell engineering applications.

As previously reported [7], the use of Y-27632 does not permanently affect the pluripotency and hESC cell state. In accordance with this finding, the cells recovered to their natural, tight, two-dimensional colony morphology 72 h after removal of Y-27632. Expression of SSEA-4 and OCT4 were also observed, suggesting reversible alteration of cell physiology and maintenance of cell pluripotency.

4.5 Conclusion

I studied and adapted a new approach to increase the non-viral gene delivery to hESCs by transiently altering the colony structure to increase their susceptibility for uptake of nanocomplexes. Treatment of hESCs with Y-27632 prior to and during transfections effectively increases cell spreading and decreases cell membrane tension, which increases cell uptake and thus potentiates the gene transfection. The hESC colonies were able to return to their original morphology and maintain their pluripotency within hours after removal of Y-27632. While most of the current studies in non-viral gene delivery focus on the material design, this study opens a new window to control gene transfection in hESCs on the cellular side. Therefore it provides a promising approach for manipulation of pluripotent stem cells through transient gene therapy, overcoming a big hurdle against controlling and studying pluripotent stem cell differentiation and development toward various biomedical applications. With the increase in the gene transfection efficiency, an increase in differentiation efficiency of hESCs can be expected, which would reduce the need for enrichment and sorting of desired cells. This new system has also been shown that

it can be coupled with the HA targeting nanocomplex system, which can be further optimized to bring non-viral gene delivery into hESCs to levels that can be used instead of viral systems for stem cell engineering applications. The preliminary findings of the current study also unravel the possibility of manipulating the cellular states and properties in future designs of intracellular delivery vehicles into hESCs. A lot of stem cell engineering research is heavily reliant on viral gene delivery systems, including reprogramming, differentiation, gene targeting/editing, and mechanistic studies, but are then limited due to safety concerns. But with these advances towards safe and effective non-viral gene delivery, these stem cell engineering applications are one step closer to clinical therapies.

4.6 Figures

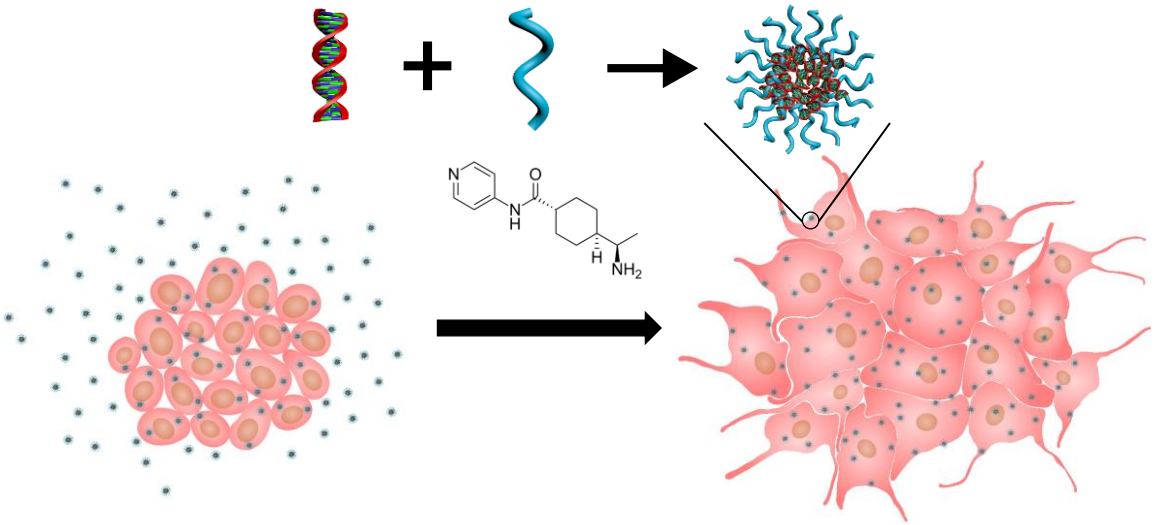

Scheme 4.1: Y-27632 enhances the transfection efficiencies of various polyplexes or lipoplexes in hESCs via increased membrane exposure through transient spreading of the cells.

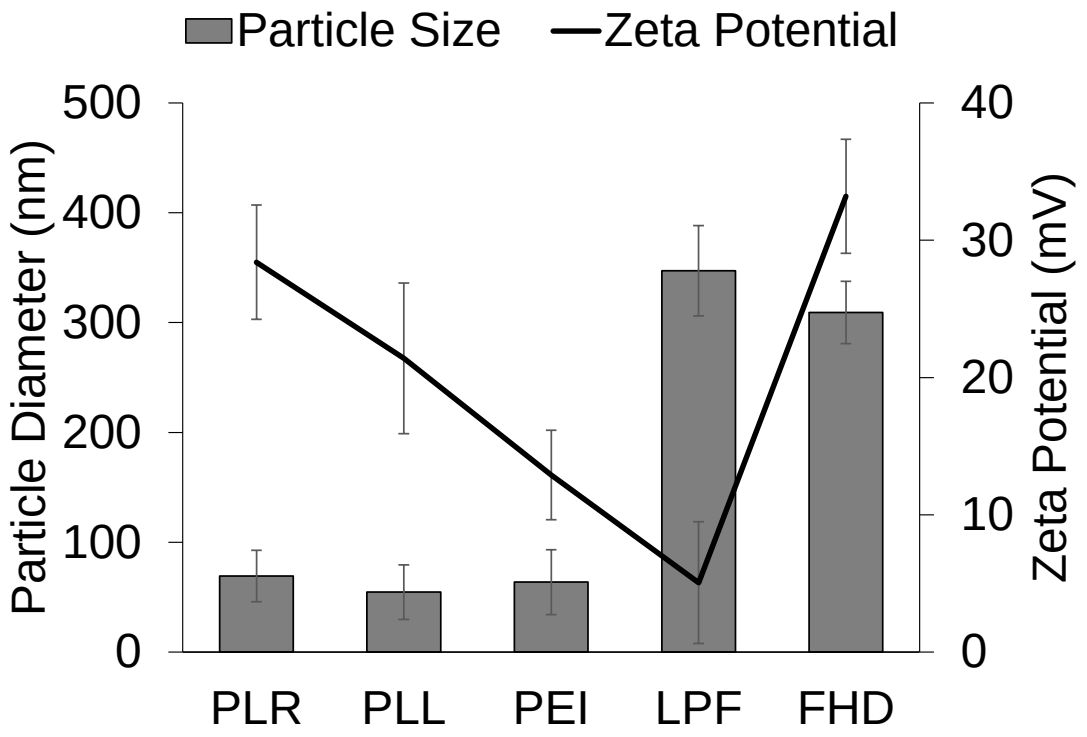

Figure 4.1: Size and zeta potential of various nanocomplexes (w:w): PLR (1:10), PLL (1:10), PEI (1:5), LPF (1:2), and FHD (1:3.5)

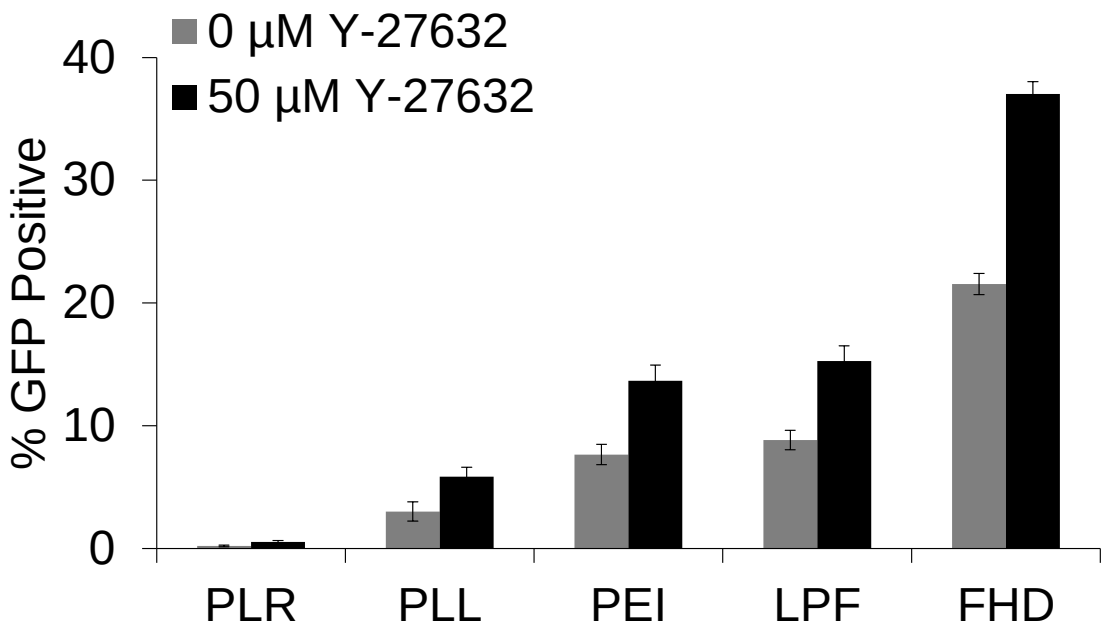

Figure 4.2: Transfection efficiencies of various reagents in hESCs in the presence of absence of Y-27632 (50 µM). Cells were pre-treated with Y-27632 cells for 4 h before removal of Y-27632 and addition of various complexes.

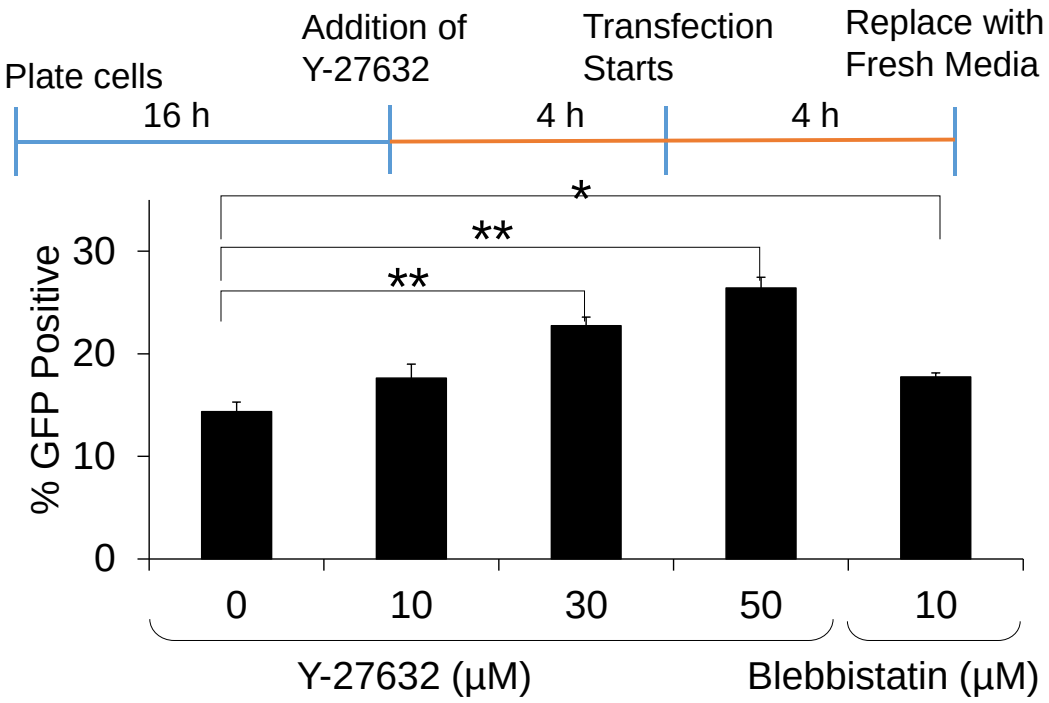

Figure 4.3: Transfection scheme and transfection efficiencies of Fugene HD/DNA complexes in H1 hESCs in the presence of Y-27632 or Blebbistatin at various concentrations. (* $p < 0.05$, ** $p < 0.01$)

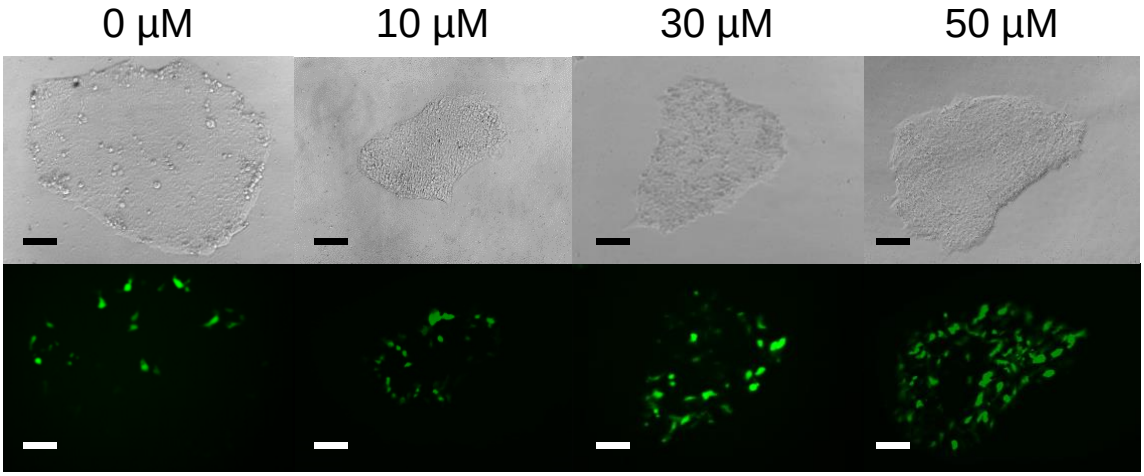

Figure 4.4: Fluorescence images of H1 hESCs 48 h post transfection with FHD/pEGFP complexes. Cells were pre-treated with 0 µM, 10 µM, 30 µM, and 50 µM Y-27632 for 4 h before transfection and during the 48-h post incubation. Scale bar: 250 µm

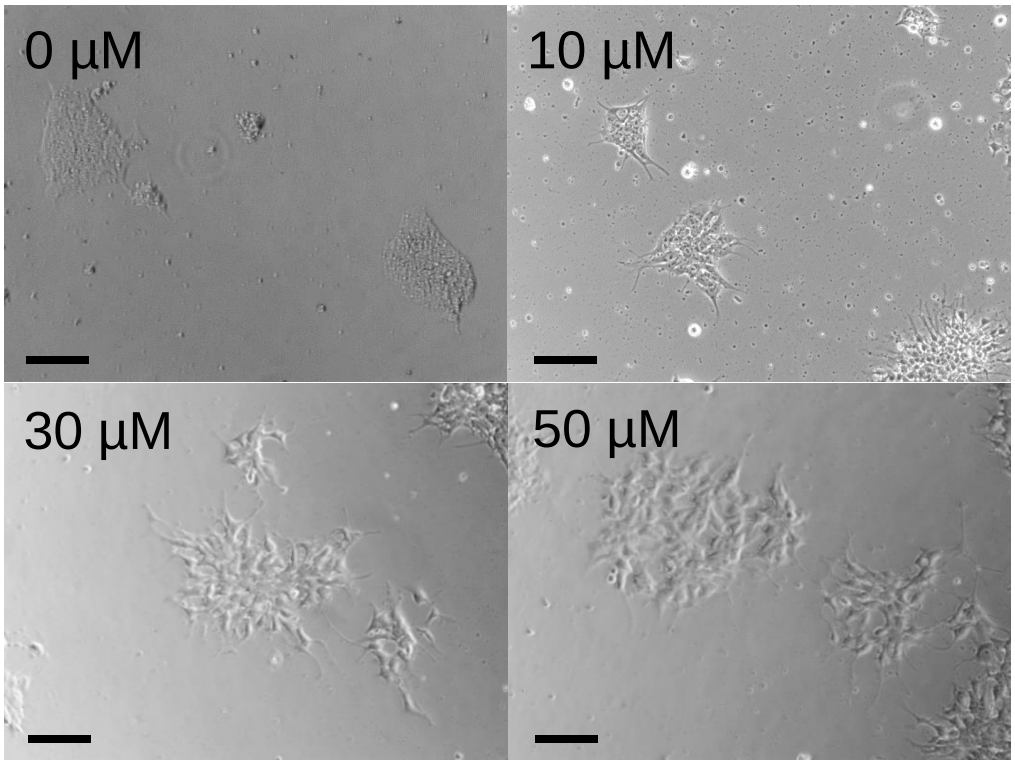

Figure 4.5: Bright-field imaging showing the morphological change of hESCs after 4-h treatment with Y-27632 at various concentrations. Scale bar: 250 µm

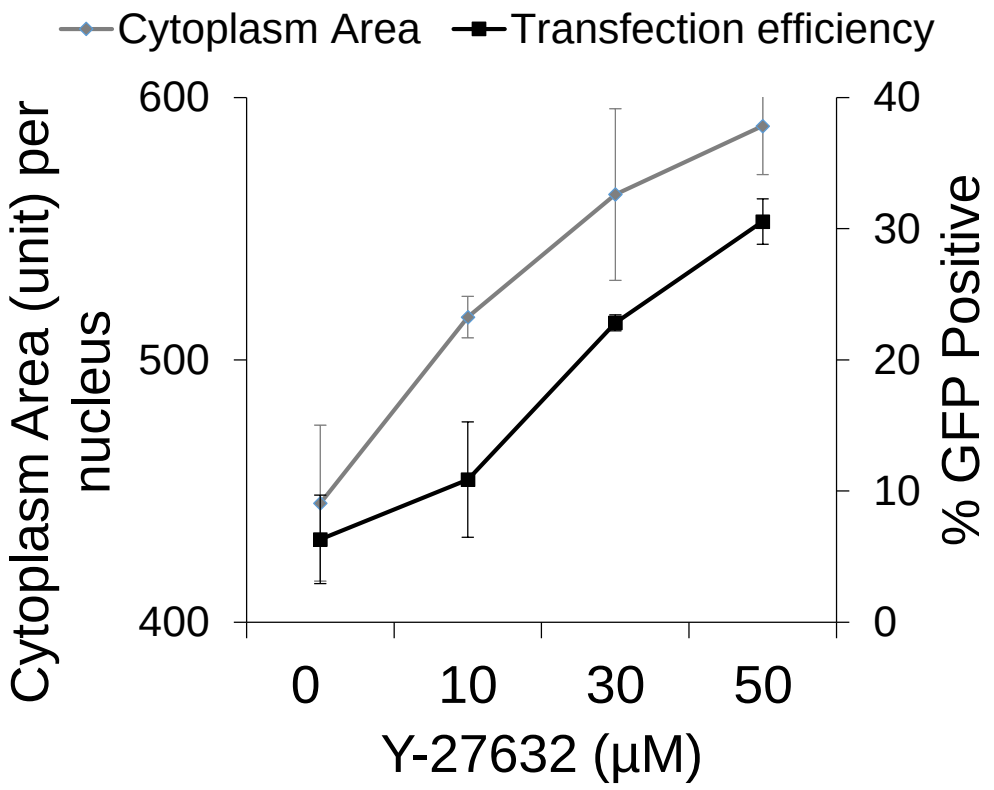

Figure 4.6: Alteration of the cytoplasm area (unit) per nucleus of hESCs following treatment with Y-27632 of various concentrations. Images were taken and analyzed with the GE InCell Analyzer. (n=5)

EGFP Transfection Efficiency Dependence on the Presence of Y-27632 either before and/or during the Transfection Step

Pre-incubation (4 h)	Transfection (4 h)	% GFP Positive
---	---	19.6 ± 0.8
---	50 µM	25.4 ± 1.9
50 µM	---	28.9 ± 1.8
50 µM	50 µM	31.3 ± 3.6

Figure 4.7: Transfection efficiency of FHD in hESCs in the presence of Y-27632. Y-27632 was applied to the cells for 4 h before transfection, during the 48-h transfection period, or a combination thereof.

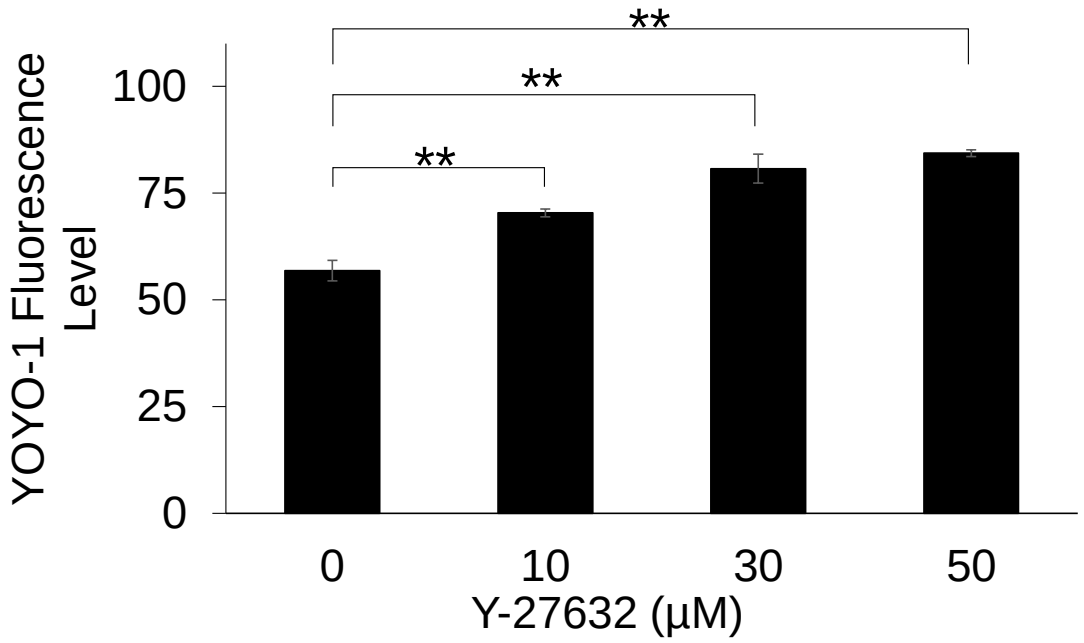

Figure 4.8: Cell uptake level of FHD/YOYO-1-DNA complexes in hESCs in the presence of various concentrations of Y-27632 (n =3). (* $p < 0.05$, ** $p < 0.01$)

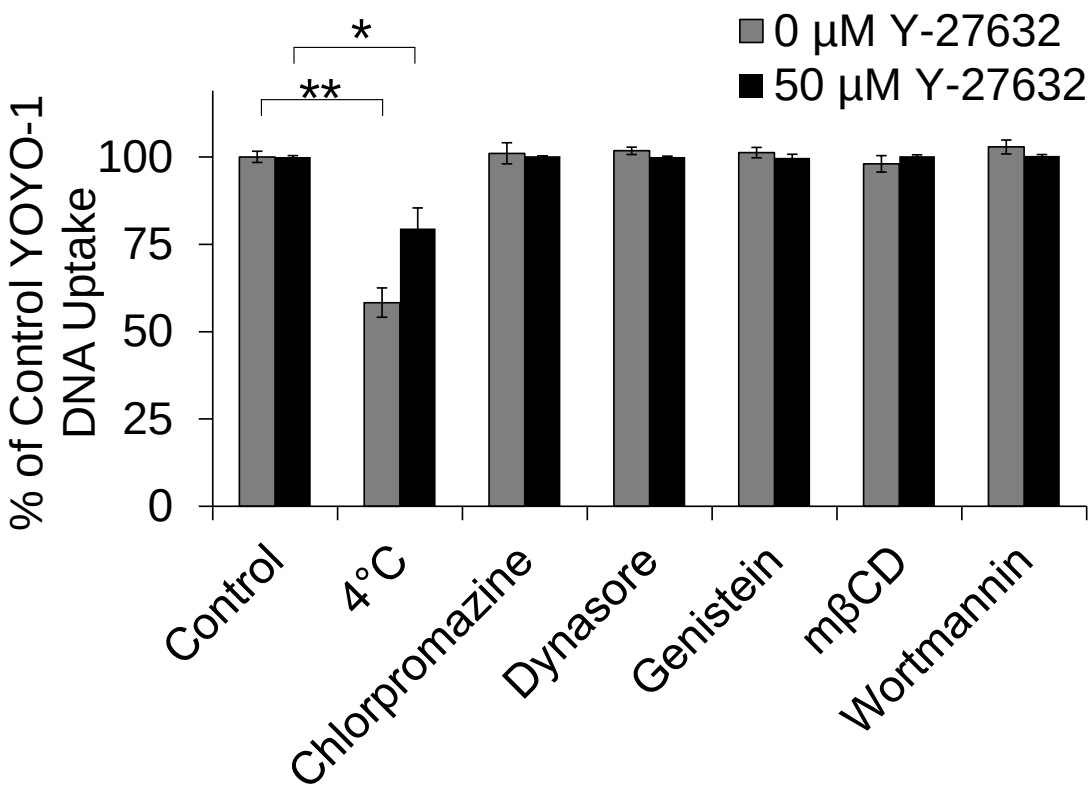

Figure 4.9: Cell uptake mechanisms of FHD/YOYO-1-DNA complexes in hESCs in the presence or absence of Y-27632. Results were expressed as percent uptake level of control cells without low temperature (4 ^{o}C) or endocytic inhibitor treatment (n=3).

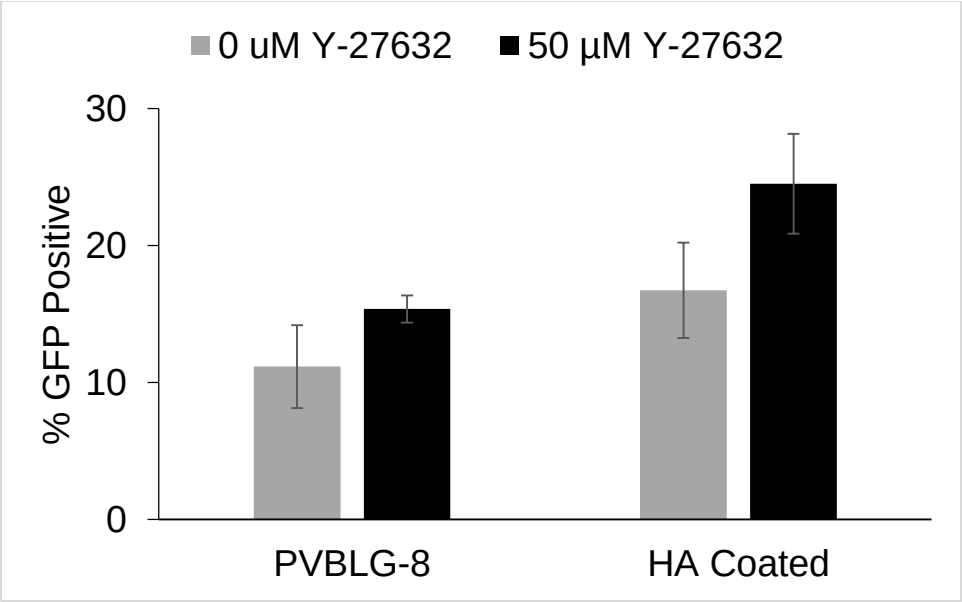

Figure 4.10: Transfection efficiencies of PVBLG-8 (1:7.5 DNA:PVBLG-8 w:w ratio) and HA coated DNA/PVBLG-8 nanocomplexes (1:7.5:7.5 DNA:PVBLG-8:HA w:w:w ratio) in hESCs in the presence of absence of Y-27632 (50 µM). Cells were pre-treated with Y-27632 cells for 4 h before removal of Y-27632 and addition nanocomplexes.

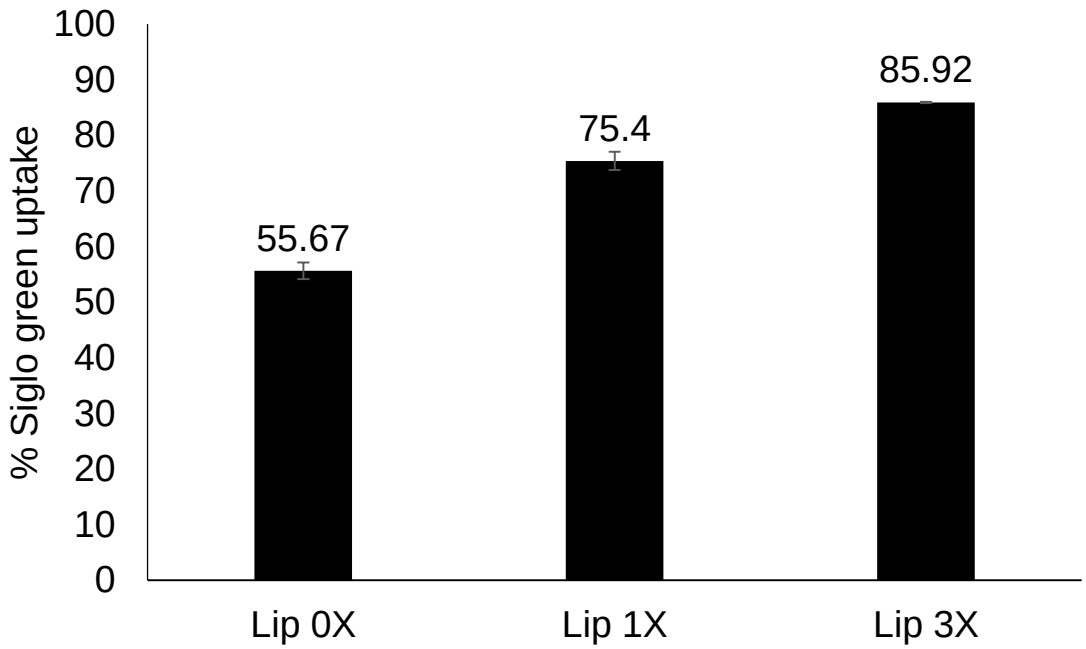

Figure 4.11: Flow Cytometry of siGlo Green (siRNA analog) using Lipofectamine, after 3 h Y-27632 incubation.

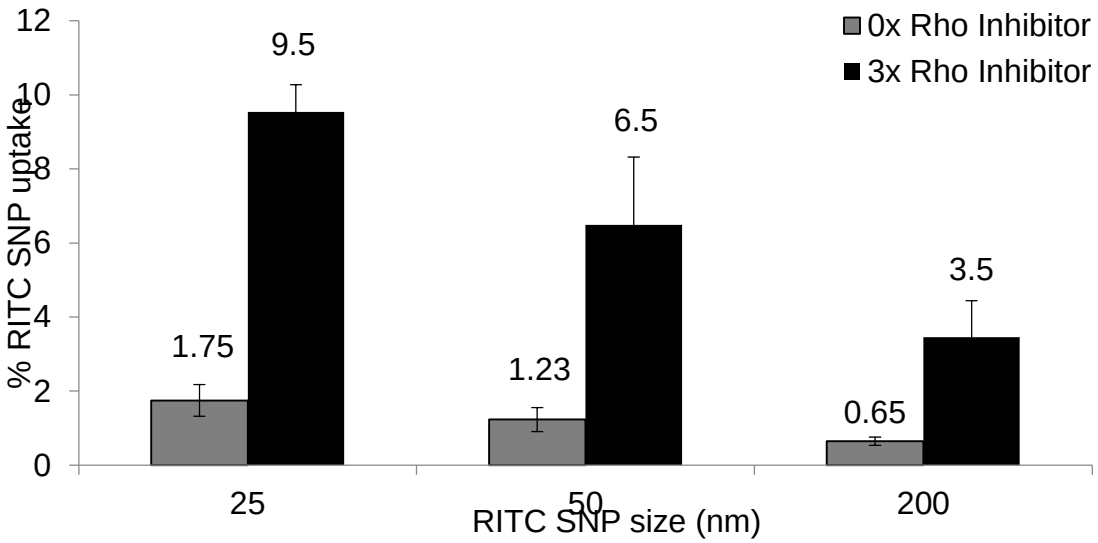

Figure 4.12: Flow Cytometry data analysis of hESC with and without treatment of Y-27632 with different sizes of SNP tagged with RITC without surface modification after 2 h incubation.

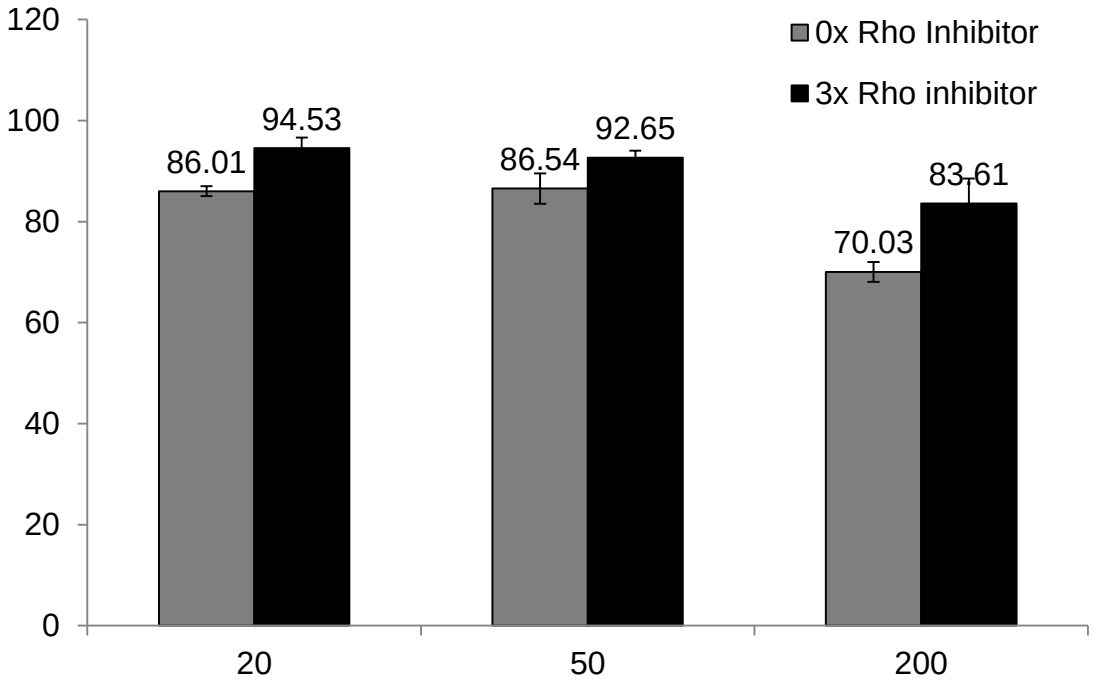

Figure 4.13: Flow Cytometry data analysis of hESC with and without treatment of Y-27632 with different sizes of SNP tagged with RITC without surface modification after 5 h incubation.

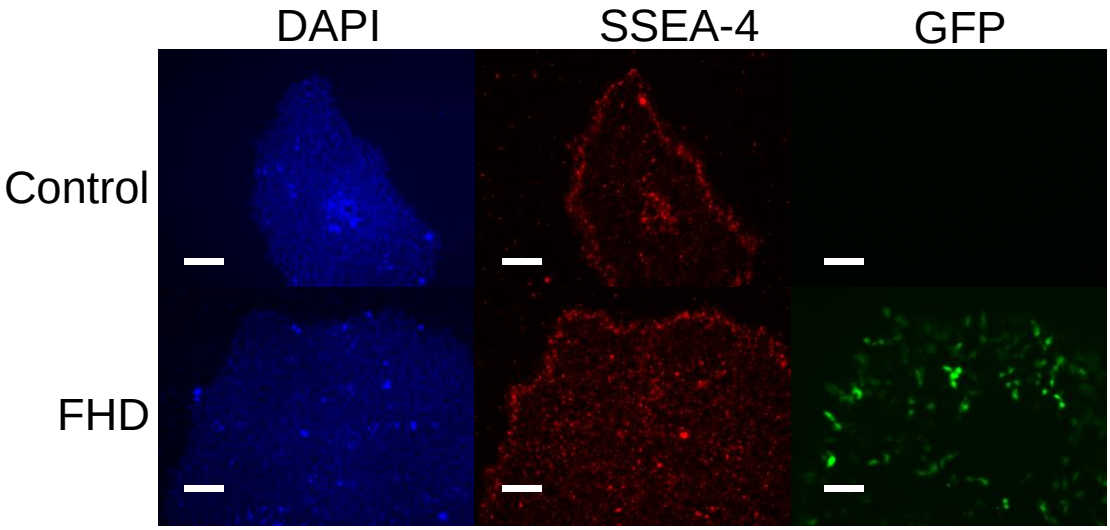

Figure 4.14: Y-27632 does not compromise the pluripotency of hESCs. DAPI and SSEA4 staining patterns of hESCs without Y-27632 treatment (control group) or transfected with FHD in the presence of 50 μM Y-27632 (FHD group). Scale bar: 250 μm

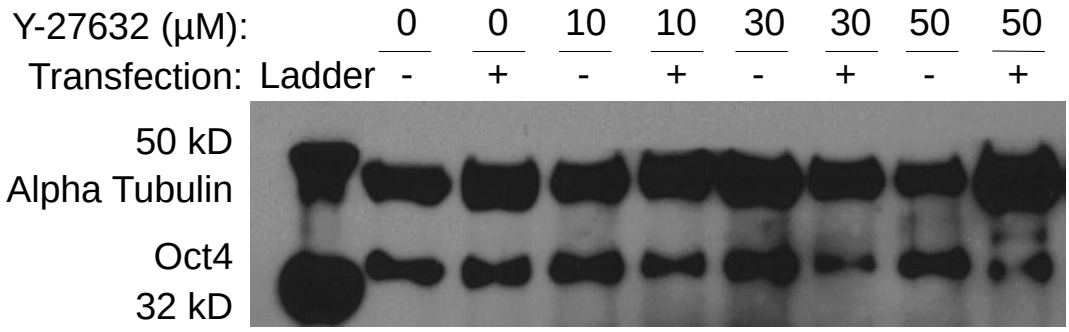

Figure 4.15: Western blot analysis on the OCT4 expression in hESCs 5 days post FHD transfection and treatment of Y-27632 at various concentrations.

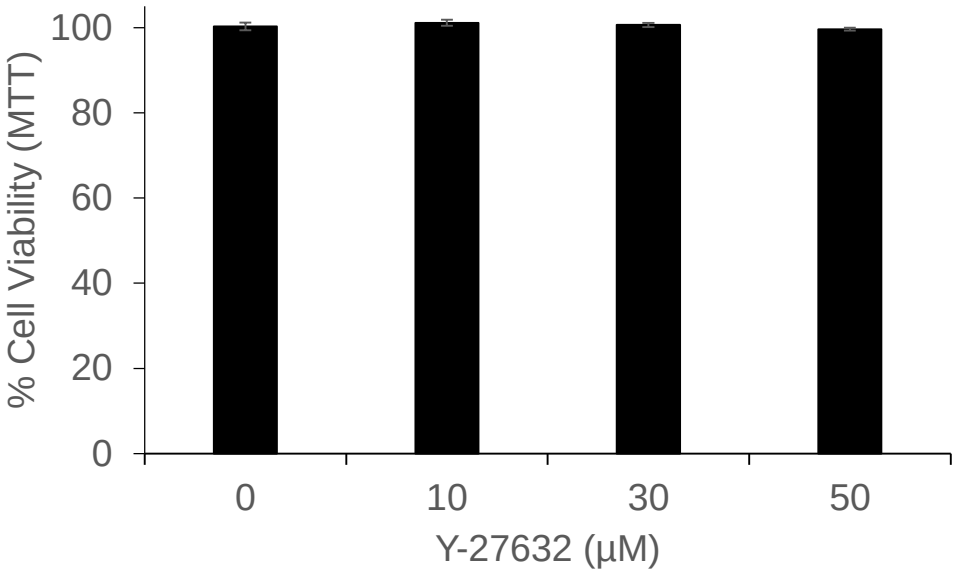

Figure 4.16: Cytotoxicity of H1 hESCs 48 h after transfection with FHD at various concentrations MTT cell viability assay of the FHD transfection with varying concentrations (0-50 µM) of Y-27632 treatment in H1 hESCs after 48 h.

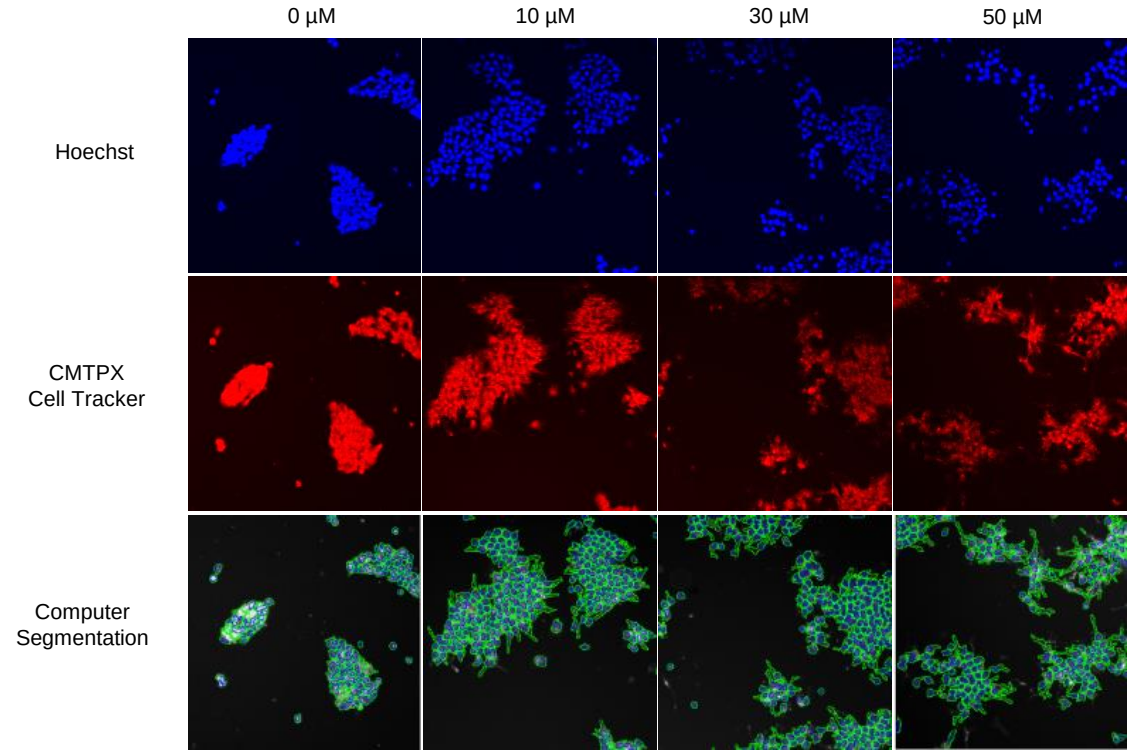

Figure 4.17: Representative images of the alteration of the hESC cytoplasmic area following treatment with Y-27632 of various concentrations (0, 10, 30 and 50 µM). First row represents the Hoechst channel and the second row represents CMTPX cell tracking channel. The third row represent the software generated segmentation used for analysis. The blue outline represents the identified nuclei and the green outline is the identified CMTPX stain of the cellular cytoplasm from which the cell area was calculated.

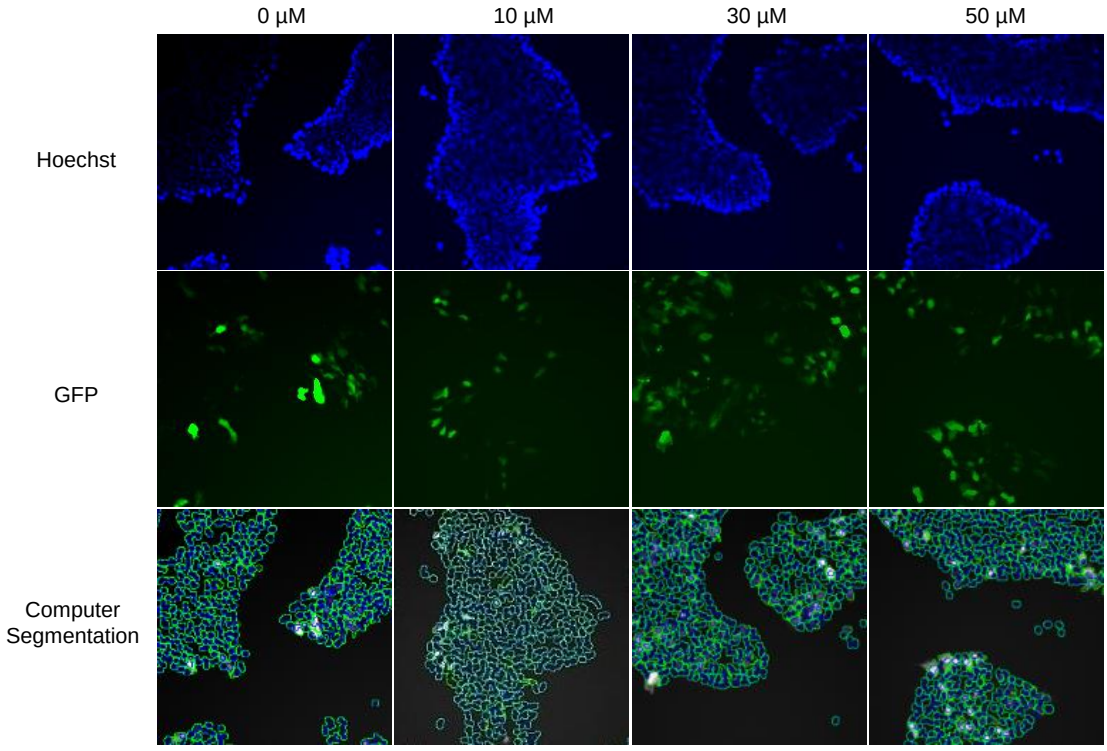

Figure 4.18: Representative images of the transfection of hESCs after alteration of the cytoplasm area with the treatment of Y-27632 at various concentrations (0, 10, 30 and 50 µM). First row represents the Hoechst channel and the second row represents the GFP channel. The third row represent the software generated segmentation used for analysis. Blue outline represents the identified nuclei and green outline is the determined cell cytoplasm as extrapolated by the nuclei and GFP channel.

4.7 References

[1] Harb N, Archer TK, Sato N. The Rho-Rock-Myosin Signaling Axis Determines Cell-Cell Integrity of Self-Renewing Pluripotent Stem Cells. Plos One 2008;3(8).

[2] Lakins JN, Chin AR, Weaver VM. Exploring the link between human embryonic stem cell organization and fate using tension-calibrated extracellular matrix functionalized polyacrylamide gels. Progenitor Cells: Springer; 2012. p. 317-50.

[3] Kong HJ, Liu JD, Riddle K, Matsumoto T, Leach K, Mooney DJ. Non-viral gene delivery regulated by stiffness of cell adhesion substrates. Nature Materials 2005;4(6):460-64.

[4] Zoldan J, Karagiannis ED, Lee CY, Anderson DG, Langer R, Levenberg S. The influence of scaffold elasticity on germ layer specification of human embryonic stem cells. Biomaterials 2011;32(36):9612-21.

[5] Raucher D, Sheetz MP. Cell spreading and lamellipodial extension rate is regulated by membrane tension. J Cell Biol 2000;148(1):127-36.

[6] Dai J, Sheetz MP. Regulation of endocytosis, exocytosis, and shape by membrane tension. Cold Spring Harbor Symp Quant Biol 1995;60:567-71.

[7] Watanabe K, Ueno M, Kamiya D, Nishiyama A, Matsumura M, Wataya T, et al. A ROCK inhibitor permits survival of dissociated human embryonic stem cells. Nat Biotechnol 2007;25(6):681-86.

[8] Kaunas R, Nguyen P, Usami S, Chien S. Cooperative effects of Rho and mechanical stretch on stress fiber organization. Proc Natl Acad Sci USA 2005;102(44):15895-900.

[9] McBeath R, Pirone DM, Nelson CM, Bhadriraju K, Chen CS. Cell shape, cytoskeletal tension, and RhoA regulate stem cell lineage commitment. Dev Cell 2004;6(4):483-95.

[10] Narumiya S, Ishizaki T, Uehata M. Use and properties of ROCK-specific inhibitor Y-27632. Regulators and Effectors of Small Gtpases, Pt D 2000;325:273-84.

[11] Gabrielson NP, Cheng JJ. Multiplexed supramolecular self-assembly for non-viral gene delivery. Biomaterials 2010;31(34):9117-27.

[12] Tang L, Fan TM, Borst LB, Cheng J. Synthesis and Biological Response of Size-Specific, Monodisperse Drug–Silica Nanoconjugates. ACS nano 2012;6(5):3954-66.

[13] Yin L, Song Z, Kim KH, Zheng N, Tang H, Lu H, et al. Reconfiguring the architectures of cationic helical polypeptides to control non-viral gene delivery. Biomaterials 2013;34(9):2340-9.

[14] Tang HY, Yin LC, Kim KH, Cheng JJ. Helical poly(arginine) mimics with superior cell-penetrating and molecular transporting properties. Chemical Science 2013;4(10):3839-44.

[15] Ohgushi M, Matsumura M, Eiraku M, Murakami K, Aramaki T, Nishiyama A, et al. Molecular pathway and cell state responsible for dissociation-induced apoptosis in human pluripotent stem cells. Cell Stem Cell 2010;7(2):225-39.

[16] Khalil IA, Kogure K, Akita H, Harashima H. Uptake pathways and subsequent intracellular trafficking in nonviral gene delivery. Pharmacol Rev 2006;58(1):32-45.

[17] Gratton SEA, Ropp PA, Pohlhaus PD, Luft JC, Madden VJ, Napier ME, et al. The effect of particle design on cellular internalization pathways. Proc Natl Acad Sci USA 2008;105(33):11613-18.